THESE

pour obtenir le grade de

DOCTEUR ES-SCIENCE DE L'UNIVERSITE HASSIBA BENBOUALI DE CHLEF

Faculté de Technologie, Département de Génie des Procédés

Spécialité " Génie des Procédés"

Option " Génie Chimique"

Présentée par

OUAGUED Malika

ETUDE DE LA PRODUCTION D'HYDROGENE PAR VOIE SOLAIRE THERMIQUE EN ALGÉRIE

"STUDY OF HYDROGEN PRODUCTION BY A THERMAL SOLAR WAY IN ALGERIA"

Jury

Pr. OUAGUED Abdallah	UHBC de Chlef	Président
Dr. KHELLAF Abdallah	CDER, Alger	Directeur de thése
Pr. LOUKARFI Larbi	UHBC de Chlef	Co-Directeur de thèse
Pr. ZAHLOUL Hamou	UHBC de Chlef	Examinateur
Pr. HANINI Salah	Université de Médéa	Examinateur
Dr. BOUDRIES Rafika	CDER, Alger	Examinateur

Année Universitaire: 2013/2014

Abstract

Algeria is blessed with a very important renewable, and more particularly solar, energy potential. This potential opens for Algeria real opportunities to cope with the increasing energy demand and the growing environmental problems linked to the use of fossil fuel. In order to develop and to promote concrete actions in the areas of renewable energy and energy efficiency, Algeria has introduced a national daring program for the period extending from 2011 to 2030. In this program, solar energy, and more particularly solar thermal energy plays an important role. In this thesis, the potential of hydrogen production by thermochemical cycle in Algeria, using solar radiation as heat sources, is estimated under the climate conditions of the country. The study analyzes an integrated copper-chlorine (Cu-Cl) thermochemical cycle with solar parabolic trough system for hydrogen production.

In order to determine the most promising solar sites in Algeria, monthly mean daily direct solar radiation have been estimated and compared for different locations corresponding to different climatic regions. Different tilted and tracking collectors are considered so as to determine the most efficient system for the parabolic trough collector (PTC).

In order to evaluate the performance of a tracking solar parabolic trough collector, a heat transfer model is developed. The receiver, heat collector element (HCE), is divided into several segments and the principle of heat balance is applied in each segment over a section of the solar receiver. Different oils are considered in order to determine the thermal performances of the heat transfer fluids (HTFs). Then, the HTF temperature and heat gain evolutions are compared under the topographical and climatic conditions.

Simulation model is also developed in this thesis to analyze thermodynamically the Cu–Cl cycle. Energy and exergy of the process, based on four steps cycle, are examined. The systems operating parameters, such as, heat gain from the solar system are varied to investigate their effects on hydrogen production rate. A comparative study is also carried out to compare the effects of different Algerian climatic locations on the hydrogen production rate.

Keywords: Direct normal solar irradiance, solar parabolic trough collector, thermal oil performance, Algerian climatic conditions, copper-chlorine thermochemical cycle, hydrogen production.

Résumé

L'Algérie a non seulement une des réserves de gaz les plus étendues du monde, mais a également des ressources énergétiques renouvelables énormes. L'Algérie a développé sa propre stratégie nationale pour l'exploitation des énergies renouvelables. Les objectifs sont d'assurer le changement des hydrocarbures vers un développement durable sans danger pour la santé et sans pollution pour l'environnement. La situation géographique de l'Algérie et les conditions climatiques, tel que le soleil abondant durant toute l'année, sont des avantages pour l'usage étendu de l'énergie solaire. Le but principal de cette thèse est le recours à l'énergie solaire thermique afin de fournir l'énergie nécessaire au procédé de production d'hydrogène par cycle thermochimique. Ce procédé à base de Cuivre-Chlore (Cu-Cl) est proposé en intégrant la technologie de concentrateurs solaires cylindro-paraboliques comme source d'énergie thermique pour application dans les conditions climatiques algériennes.

On a prévoié tout d'abord l'estimation de l'irradiation solaire normale directe pour plusieurs sites représentatifs du territoire algérien, et ce, afin de permettre l'identification des sites les plus appropriés disponibles. Les facteurs géographiques et météorologiques aux endroits indiqués et leurs caractéristiques sont prises comme entrées dans le modèle solaire, basé sur un ciel clair. L'irradiation solaire directe normale est utilisée pour estimer le potentiel du concentrateur solaire pour différentes inclinaisons et orientations et pour différents poursuiteurs solaires.

Ensuite, un modèle numérique est présenté pour étudier les performances thermiques du collecteur cylindro-parabolique dans les conditions climatiques algériennes. Différents paramètres comme le profil de température, le gain de chaleur, les pertes de chaleur et le rendement thermique sont étudiés par un modèle de transfert de chaleur approprié. Des huiles thermiques ont été employées en tant que fluide caloporteur dans l'absorbeur du collecteur cylindro-parabolique pour comparer leur profil de température.

Une analyse thermodynamique des différentes réactions chimiques ayant lieu dans le cycle Cu-Cl est aussi décrite dans cette thèse pour déterminer son efficacité énergétique et exergétique. Une étude paramétrique est menée afin d'évaluer l'effet du gain de chaleur à partir du champ solaire cylindro-parabolique sur le taux de production d'hydrogène. Une étude comparative est également effectuée pour analyser les effets de différents sites climatiques algériens sur le taux de production d'hydrogène.

Mots Clés: Irradiation solaire normale directe, concentrateur solaire cylindro-parabolique, huiles thermiques, Conditions climatiques algériennes, cycle thermochimique Cuivre-Chlore, production d'hydrogène.

الملخص

مع تزايد استهلاك الطاقة في الجزائر و نضوب احتياطي النفط والغاز الطبيعي، فقد أصبح البحث عن بدائل للوقود أمراً حتمياً. تعي الجزائر و المجتمع الدولي الأزمة الناجمة عن استخدام الوقود الأحفوري، وتركز على تطوير تقنيات الانبعاثات الخالية من الكربون باستخدام مصادر للطاقة المتجددة. تعتبر الطاقة الشمسية من المصادر المتجددة للطاقة تحت الاعتبار لتوفرها بكثرة، وفي حالة استغلالها بكفاءة، ستلبي حاجة العالم للطاقة في المستقبل.

يعد الهيدروجين من أخف وأنظف أنواع الغازات، و احد الخيارات الرئيسة لاستعماله كوسيلة لخزن الطاقة واستخدامه كمصدر غير ملوث للبيئة كمساند أو بديل عن الوقود التقليدي الهيدروكاربوني . وبرغم ذلك، يستنفد استخراج الهيدروجين من الماء الكثير من الطاقة والتكاليف .وفي الوقت الحالي، يتم إنتاج غاز الهيدروجين باستخدام الوقود الأحفوري الذي ينتج عنه انبعاثات ثاني أوكسيد الكربون الضارة. من أجل تطوير تقنيات تستخدم الهيدروجين كمصدر للطاقة النظيفة، أجريت هذه الاطروحة لدراسة إنتاج الهيدروجين عن طريق دورة كيميائية حرارية نحاس-كلور باستخدام الطاقة الشمسية المركزة كمصدر حراري في الجزائر.

تضمنت هذه الدراسة بناء نموذج رياضي لمنظومة شمسية لإنتاج الهيدروجين لتخمين معدل الإشعاع الشمسي المتعامد المباشر اليومي الساقط على اسطح مثبتة افقية و مائلة او اسطح متحركة. أجريت الدراسات على المنظومة في ساعات النهار لأيام عشوائية مميزة بسماء صافية في مختلف المناطق المناخية في الجزائر.

تم تطوير نموذج اخر لدراسة الأداء الحراري لملتقط الاشعة الشمسية المركزة هندسيا في شكل اسطوانة مكافئية وذلك قصد تحديد المواقع الملائمة. تمت دراسة معايير مختلفة كدرجات الحرارة، الحرارة المكتسبة، الحرارة الضائعة والمردود الحراري للملتقط الشمسي للأشعة المركزة . وقد استخدمت مختلف الزيوت الحرارية كسوائل لامتصاص الحرارة داخل انبوب التسخين لمقارنة درجات الحرارة والحرارة المكتسبة لهته الزيوت.

النموذج الثالث في هذه الأطروحة يهدف الى دراسة و تحليل الدورة الكيميائية الحرارية نحاس-كلور لانتاج الهيدروجين باستعمال الطاقة المحصل عليها بواسطة صفيف مجمعات شمسية ذات الشكل الاسطواني المكافئ. يتم فحص المردود الطاقوي على أساس دورة من أربع خطوات. تمت دراسة معايير مختلفة كالحرارة المكتسبة من المنظومة الشمسية و آثارها على معدل إنتاج الهيدروجين .وتم أيضا دراسة مقارنة لتأثير مختلف المواقع المناخية الجزائرية على معدل إنتاج الهيدروجين.

الكلمات المفتاحية :معدل الإشعاع الشمسي المتعامد المباشر, مجمع شمسي اسطواني مكافئ, زيوت حرارية, الظروف المناخية الجزائية, دورة كيميائية حرارية نحاس-كلور, انتاج الهيدروجين

Acknowledgments

After thanks to God, I am grateful to my family particularly to my parents and to my fiancé who have given me the force to carry on this thesis. Thank you for supporting me and believing in me.

This work was conducted in the department “Process Engineering” of University Hassiba Benbouali of Chlef. I thank this institution for its confidence and support.

I express my sincere gratitude to my supervisors Mr. Abdallah Khellaf, Director of Research at CDER Algiers, and Mr. Larbi Loukarfi, Professor at UHBC of Chlef (Mechanical Engineering Department), for their great patience, help and discussions. They were always willing to help and answer to any question. I really appreciated their competence and availability.

I wish to show my gratitude to Mr. Abdallah Ouagued, Professor at UHBC of Chlef, for being president of the jury of my thesis.

I would like to thank Mr. Hamou Zahloul, Professor at UHBC of Chlef for his help and for being examiner of my thesis.

I would like to thank Mr. Salah Hanini, Professor at theUniversity of Medea, for accepting for the second time to be part of my thesis examiners.

I would like to thank Mrs. Rafika Boudries, Doctorate CDER Algiers, for being examiner of my thesis.

It has been very pleasant for me to work with the members of our research laboratory, Laboratory of theoretical physics and material physics, who have been of friendly help to me.

I want also to express my appreciation to all the future doctors and actual doctors of the department “Process Engineering”, the department "Engineering Sciences" and the department "Material Sciences", and I would like to thank them for their support.

Many friends have helped me directly or indirectly to realize this thesis, making it better than it otherwise would have been.

Thanks to all that I have not mentioned here but they have supported me in their manners.

Malika

Table of Contents

List of Figures

List of Tables

Nomenclature

A_c	Collector aperture, (m^2)
A_a	Receiver tube cross-section area, (m^2)
A_f	Fluid flow cross-section area, (m^2)
A_v	Glass envelope tube cross-section area, (m^2)
C_a	Absorber specific heat, (J/kg.K)
C_{air}	Air specific heat at T_{amb}, (J/kg.K).
C_f	HTF specific heat in segment "*i*" , (J/kg.K)
C_v	Glass envelope specific heat, (J/kg.K)
D_{ae}	Outside diameter of absorber pipe, (m)
D_{ai}	Inside diameter of absorber pipe, (m)
D_{ve}	Outside diameter of glass envelope (m)
D_{vi}	Inside diameter of glass envelope, (m)
f	Friction factor for the inner surface of the absorber pipe
F_f	HTF flow rate, (m^3/s)
h_a	Convection heat transfer coefficient of annulus gas at T_{moy1}, (W/m^2K)
h_f	Convection heat transfer coefficient of the HTF, (W/m^2K)
h_v	Convection heat transfer coefficient of ambient air , (W/m^2K)
I_{ba}	Direct normal irradiance per unit of collector area, (W/m^2)
k_{air}	Thermal conductivity of the ambient air at temperature T_{moy2}, (W/m.K)
k_f	Thermal conductivity of the HTF at temperature T_f^i, (W/m.K)
k_{std}	Thermal conductivity, (W/m.K);
L	Receiver length, (m)
m_a^i	Absorber mass in segment "*i*", (kg)
m_f^i	HTF mass at inlet of receiver segment "*i*" , (kg)
m_v^i	Glass envelope mass in segment "*i*", (kg)
Nu_{air}	Nuselt number at T_{moy2}
Nu_f	Nuselt number at T_f^i
$Pr_{air}^{'}$	Air Prandtl number at T_{amb};
$Pr_{air}^{''}$	Air Prandtl number at T_v^i;
Pr_f	Prandtl number at T_f^i;
Q_{aconv}^i	Convection heat transfer rate for receiver segment "*i*" between the surface of the absorber to the surface of the envelope, (W)

Q_{arad}^{i}	Radiation heat transfer rate for receiver segment "*i*" between the surface of the absorber to the surface of the glass envelope, (W)
Q_{asol}	Direct incident solar irradiance absorption rate into the receiver segment "*i*", (W)
Q_{fconv}^{i}	Convection heat transfer rate between the heat transfer fluid and wall of the absorber pipe in the segment '*i*', (W)
Q_{vconv}^{i}	Convection heat transfer rate between the surface of the envelope to the atmosphere for receiver segment "*i*", (W)
Q_{vrad}^{i}	Radiation heat transfer rate between the outer surface of the envelope to the sky receiver segment "*i*", (W)
Q_{vsol}	Direct incident solar irradiance absorption rate into the envelope of receiver segment "*i*", (W)
Q_{sol}	Direct incident solar irradiance per unit length of receiver, (W/m)
Q_z	Heat rate coming to the segment '*i*', (W)
$Q_{z+\Delta z}$	Heat rate leaving from the segment '*i*', (W)
Re_f	Reynolds number at Tf^{i};
t	Time, (s)
T_a^i	Absorber pipe temperature in segment '*i*', (K)
T_{amb}	Ambient temperature, (K)
T_f^i	HTF temperature inlet of receiver segment "*i*", (K)
T_f^{i-1}	HTF temperature in the segment "*i-1*", (K)
T_{moy1}	Average temperature, $(T_{moy1}=(T_a+T_v)/2)$, (K)
T_{moy2}	Average temperature, $(T_{moy2}=(T_v^{i}+T_{amb})/2)$, K
T_{sky}	Estimated effective sky temperature, (K)
T_v^i	Glass envelope temperature in segment "*i*", (K)
v_{air}	wind speed, (m/s)
v_f	HTF rate, (m/s)
w	Collector width, (m)

Greek letters

α_a	Absorptance of the absorber selective coating
α_v	Glass envelope absorptance
ρ_a	Density of the absorber selective coating, (kg/m^3)

ρ_{air}	Air density at T_{amb}, (kg/m^3)
ρ_f	HTF density at average temperature of receiver segment "*i*" at Tf^i, (kg/m^3)
ρ_v	Density of glass envelope, (kg/m^3)
η_a	Effective optical efficiency of the absorber
η_{col}	Collector efficiency
η_v	Effective optical efficiency of the glass envelope
τ_v	Glass envelope transmittance
Δz	Receiver segment length, (m)
λ	mean-free-path between collisions of a molecule, (cm)
δ	molecular diameter of annulus gas, (cm)
γ	ratio of specific heats for the annulus gas
σ	Stefan-Boltzmann constant, (5.6697 W/m^{2}K^4)
μ_{air}	dynamic viscosity of the air at Tamb, (kg/m.s);
μ_f	HTF dynamic viscosity at average temperature of receiver segment "*i*" at Tf^i, (kg/m.s)

Introduction

The world energy economy has the largest influence on the decisions that people and governments make. Current global consumption rates are depleting the planets ability to sustain our way of life. Increased demand means increased prices in every sector of the world economy. Renewable energy is the key to a future, with no dangerous climate change [1]. By the middle of 21st century, renewable sources of energy could account for three-fifths of the world's electricity market and two-fifths of the market for fuels used directly [2]. However, the world still has a major dependency on fossil energy in the form of oil, natural gas and coal with consumption of about 85 million barrels of oil and 104 trillion cubic feet of natural gas per day [3-5]. In 2008, around 81.3% of the world's primary energy was supplied from Oil, Gas and Coal products; resulting in around 29,381 million ton of Carbon dioxide (CO_2) which is a major source of the global warming problem [6]. By 2050, global Carbon dioxide emissions would be reduced to 75% of their 1985 levels provided that energy efficiency and renewable are both pursued aggressively [2].

Besides the environmental impact of the extensive use of fossil fuels, the unstable oil prices the world witnesses since the seventies has a great influence on the investment in the energy market and consequently on the development plans worldwide. The limited resources of Oil and Gas and their unstable prices as well as their environmental impact have made the search for alternative energy resources reliable and without consequence on the environment [7].

Unlike fossil fuels, hydrogen is a sustainable and clean energy carrier. It is widely expected to be the world's next-generation fuel. Hydrogen has a high specific energy and a relatively higher flexibility in use in comparison with electricity. It is then a good energy vector [4]. It is suitable for use in a fuel cell to generate electricity directly, and its specific energy is 2.5 times higher than that of any other conventional fuel [8,9].

With an annual world consumption of about 50 billion kilograms, hydrogen demand is expected to rise dramatically over the next few decades [5]. Hydrogen is a secondary source of energy which is produced from a hydrogen rich material such as hydrocarbons, ammonia and water [10]. The effectiveness of hydrogen in addressing the challenges posed by the use of fossil fuels lies in its production method. Solar energy is considered to be an attractive alternative heat source for hydrogen production that is highly abundant, sustainable and environmentally friendly resource.

1. Energy in Algeria

Algeria not only has one of the world's most extensive gas reserves, but also has huge renewable energy resources. Algeria has developed its own national strategy for renewable energy development [11]. The objectives are to ensure a change from hydrocarbons to a sustainable energy without environmental damage. Fortunately, the geographic location of Algeria have several advantages for the extensive use of solar energy. Located in the Sun Belt region, Algeria has suitable climatic conditions such as the abundant sunshine throughout the year, low humidity and precipitation, water availability, and plenty of unused flat land close to road networks and transmission grids [11].

According to the German Aerospace Agency (DLR) study based on satellite imaging, Algeria, with 1.787.000 km^2, has the largest longterm land potential for the concentrating solar thermal plant in the Mediterranean basin. More than 2,000,000 km^2 of land receive yearly a sunshine exposure equivalent to 2500 kWh/m^2. The mean yearly sunshine duration varies from a low value of 2650h on the coastal line to 3500h in the south [11,12].

In Algeria, the traditional water reserves are annually 19.3 billion cubic meters. The availability of surface water is 12.4 billion cubic meters annually with 95% of these resources located in the north. The availability of groundwater is 6.9 billion cubic meters annually with 73% of these resources located in the south [13].

The access to appropriate electric power transmission lines and natural gas pipeline is another crucial factor for the use of solar energy. Natural gas pipeline networks are a crucial factor for solar–gas hybrid systems. Studies have shown that the transport of a mixture of natural gas and hydrogen, especially produced by thermal solar technology, is possible through the existing natural gas networks without pipeline modification as long as the mass fraction of hydrogen remains sufficiently low [14]. Furthermore, the proximity of concentrating solar power plant CSP to the transmission lines facilitate the operation to provide firm power to the grid [11].

Algeria has an extensive electricity transmission network, not only covering the densely populated coastal areas, but also due to the emplacement of its oil and gas industry reaching far into the largely unpopulated center of the country. The owner of the grid is the state utility Sonelgaz [11]. Recently, the electricity transmission network amounts to a rate of 98% with over 225,309 km of power lines in which more than 80% are in the north of the country [15].

The Pipeline Transportation Activity provides for the delivery of hydrocarbons (crude oil, natural gas, LPG and condensate) through a pipelines network of almost 16,200 km. The pipe transportation system counts 12 gas pipelines with a combined length of 7459km, with a transportation capacity of 131 Bm^3/year, 39 Bm^3 of which are intended for exports. Since the commissioning of the transcontinental gas pipelines, Enrico Matei (connecting Algeria to Italy via Tunisia) and Pedro Duran Farrel (linking Algeria to Spain via Morocco), new construction projects are being implemented, particularly in order to meet the European market's growing demand [16]. The use of this pipelines network to export mixture natural gas-hydrogen is a real challenge for the future economy of Algeria.

2. Objectives and methodology

The main overall objectives of this research are to propose design for using solar thermal energy within the hydrogen production by thermochemical cycles technique. Furthermore, the performances of solar parabolic trough technology combined with Copper-Chlorine cycle for hydrogen production are studied under Algerian conditions. Thermochemical cycles technique for water splitting has several advantages over other hydrogen production processes. These advantages could make it a competitive future option for hydrogen production, which is a key component of a hydrogen economy. Using solar energy sources suggest that thermochemical hydrogen production could become commercial, and help meet the foreseen future hydrogen demand. The reasons for choosing Cu-Cl cycle lie in the fact that the peak temperature of the cycle is much lower than the temperature needed for water thermolysis. This cycle provides also flexibility on the choice of the high temperature heat source it can be coupled with. As such, it has then a much lower overall capital requirement.

The parabolic trough technology is an appropriate technology to be used with hydrogen production by thermochemical cycle. The reasons for choosing parabolic trough technology to be used could be summarized as follow:

-It is a proven commercially in the field for more than 20 years.
- It is an accepted technology by the World Bank.
- It is based on reliable systems.
- it can be installed in large capacity units.

The first objective of this thesis is to estimate the direct normal solar irradiance which is of great importance in the development of concentrating solar plant technologies. The direct

normal solar irradiance (DNI) allows the identification of the most suitable sites available for deploying the parabolic trough technology in Algeria. It is generally assumed that concentrating solar power systems are economic only for locations with DNI above 1800 kWh/m^2/year with an average daily DNI above 5 kWh/m^2/day [11,17,18].

Improving the understanding of parabolic trough technology is another objective of this research. Numerical models are performed to predict thermal performance of parabolic trough collector under Algerian conditions. In this model, the climatic and topographical conditions specific to the area have been taken into account by exploiting the direct solar radiation.

The other objective of this research is to develop simulation models to analyze the Cu–Cl cycle using solar PTC as heat source under Algerian conditions. Thermodynamic analysis, accounting for relevant chemical reactions, is proposed to describe different steps of the Cu–Cl cycle for hydrogen production.

The proposed implementation of this project is in Algeria and similar climatic regions. A FORTRAN code has been developed to analyze the proposed design and to investigate the system performances. As the system is a combination of different components, the code consists of some subroutines to solve each individual component of the system.

3. Description of model design

The proposed design of the system is shown in figure I.1. It is an integration between a conventional combined Cu-Cl thermochemical cycle for hydrogen production and solar field, based on a parabolic trough solar collector. When solar radiation is available, the solar field starts supplying energy to the thermal cycle from sunrise to sunset. In the integrated system, parabolic trough solar systems are used to supply the required heat to Cu-Cl thermochemical water splitting. The parabolic trough mirrors are used to reflect the solar light to the receiver. The sun tracking control system drives the solar collectors to track the sun position. The heat transfer fluid flows through the absorber receiver and heats up to high temperature. This high temperature heat transfer fluid then enters the high temperature heat exchanger where it releases heat to the water returning from Cu-Cl cycle. The super heated steam exiting the high temperature heat exchanger is supplied to the Cu-Cl cycle in order to meet the heat requirement of the cycle. After releasing heat at different stages in the Cu-Cl cycle, water is supplied back to the high temperature heat exchanger. The solar field is equipped with tow tank direct storage system. With the storage system, heat gain from the PTC can be stored for

later use when the sun sets or is blocked by clouds. The heat transfer fluid is stored in two tanks, one at high temperature and the other at low temperature. The thermal oil from the low-temperature tank flows through the solar collector or receiver, where solar energy heats it to a high temperature, and it then flows to the high-temperature tank for storage. Fluid from the high-temperature tank flows through the high temperature heat exchanger, where it generates superheated steam for Cu-Cl cycle. The fluid exits the heat exchanger at a low temperature and returns to the low-temperature tank.

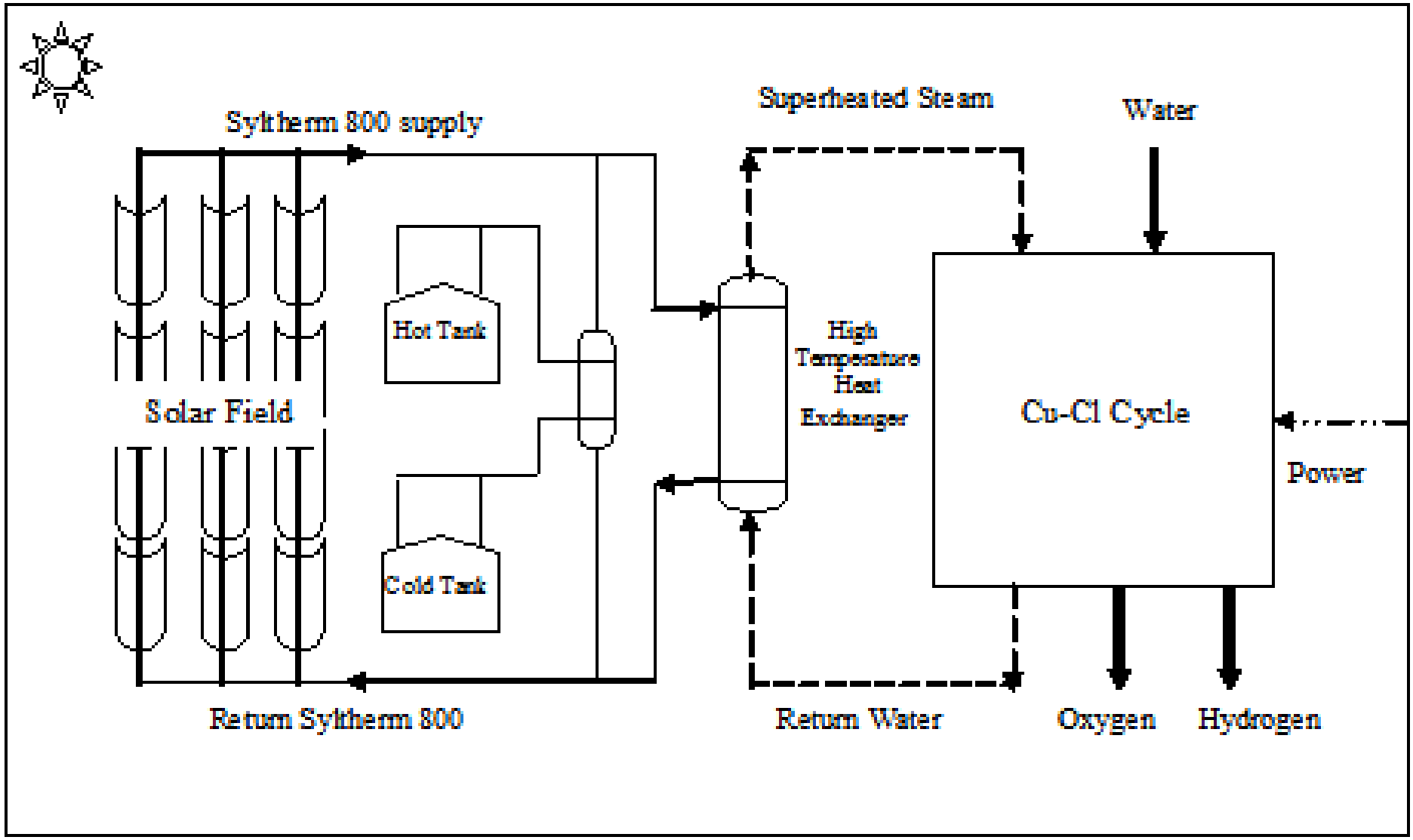

Figure 1. Schematic diagram of the integrated system.

4. Scope of thesis

First, Background topics relevant to this research are discussed and a literature survey is presented in Chapter II. Literature is reviewed to get a holistic understanding of the methods of concentrating solar energy and hydrogen production. Comparisons of the most popular solar thermal technology and the thermochemical cycles for hydrogen production are done based on published information. A discussion of the parabolic trough technology and the copper-chlorine thermochemical cycle are presented along with summaries of results reported in the literature

Second, the geographical and meteorological factors at the given locations and the plant set-up characteristics are identified in Chapter III. The environmental conditions, including sun's position, ambient temperature and wind, are taken as model inputs. Based on clear sky model, these inputs has been used to estimate the direct solar radiation at different locations representative of different climatic conditions in Algeria. Direct Normal Irradiance is used to estimate the potential for concentrating solar collector for different tilted and tracking systems.

Third, the energy performance of the parabolic trough collector is evaluated through a simulation of the successive energy conversions from solar radiation in Chapter IV. Heat transfer model of tracking solar parabolic trough collector is detailed. Temperature profile, heat gain, heat losses and thermal efficiencies are estimated by this model. Influence of the climatic conditions and solar radiation on the performances of the parabolic trough plant is simulated over specific days and interpolated throughout the year. Different thermal oils have been employed as heat transfer fluid in the receiver of parabolic trough collector to compare their temperature profile and their thermal energy cost.

Fourth, simulation model to analyze the Cu–Cl cycle is performed in Chapter V. Thermodynamic analysis accounting for relevant chemical reactions and including the determination of energy and exergy efficiencies is described. A parametric study is conducted to investigate the effect of heat gain from the parabolic trough technology on the hydrogen production rate. Furthermore, rate production of hydrogen by the Cu–Cl cycle is analyzed and compared for performances improvement of the system for different climatic regions in Algeria.

Finally, the findings of the study are discussed in Chapter VI. A review of the comparisons and the findings are discussed and the main conclusions and recommendations are presented.

Chapter I. Background

I.1. Clean energy

Energy development is increasingly dominated by major global concerns over population, air pollution, coastal pollution, fresh water pollution, deforestation, biodiversity loss and global climate deterioration [19].

A sustainable energy vision of the future centers on the need to reduce global green house gas emissions, ensure security of energy supply, and create a new industrial and technological energy base [19,20].

Renewable energy has grown rapidly in recent years [21]. Renewable resources have produced 16.5% of the world primary energy in 2005 [21]. The share of world electricity has been 18% mostly from hydro resources [22]. Renewable sources may be the only candidates for satisfying most of the criteria of the sustainable backstop supply technology, except perhaps for the aspect of financial affordability when compared to the present low prices of fossil and nuclear power. For example, photovoltaic power from the sunlight is unlimited, but expensive to collect and convert, and additional steps are required to bridge intermittent supplies. Several other renewable power resources experience similar challenges [19,23].

Hydrogen may play an important role as an energy carrier of the future [24-28]. It may be used as a fuel in almost every application where fossil fuels are being used today. Hydrogen combustion will be held without harmful emissions with an exception of NOx emissions. In addition, hydrogen may be converted into useful forms of energy more efficiently than fossil fuels. And despite public perception, hydrogen is as safe as other common fuels [19,29]. However, hydrogen is not an energy source. It does not occur in nature in its elemental or molecular form. Therefore, hydrogen must be produced.

I.2. Hydrogen

Hydrogen is currently promoted as a possible future energy carrier. It can be converted with high efficiency to electricity in a fuel cell without any pollutant emission to air except water vapor. In addition, hydrogen has advantageous properties as an energy carrier including being convenient to use, transport and store, and being produced from a widely available raw material as water. Environmental harm does not occur when hydrogen is used, provided it is

produced from environmentally benign energy sources [30,31]. Hydrogen has many qualities [32]:

- It is the most abundant atom on earth, as a constituent of water;
- It is the most energetic molecule: 120 MJ/kg, i.e. twice as much as natural gas;
- It is neither polluting nor toxic;
- Its combustion produces no pollutant (only water);
- It is the lightest of all gases, which a positive term factor in terms of security (it diffuses at high speed in the air)
- It has numerous production modes, adapted to all forms of primary energy (electrolysis, thermal water decomposition, reforming);
- Its transport is easy and environment-friendly (in particular through pipes);
- Its modes transformation are varied (fuel cell, thermal engine, turbine, combustion).

The annual world consumption of hydrogen is about 50 billion kilograms, which is used primarily for ammonia production and conversion of heavier crude oils to lighter liquid fuels [19,33]. The hydrogen demand has grown rapidly because of a decrease in availability of light crude oils which do not require extra hydrogen for conversion to gasoline. The increase in using heavy crude oils requires large amounts of hydrogen for conversion to gasoline. If the cost goals for automotive fuel cells are reached, the transportation sector may ultimately be fueled by hydrogen. This implies a growth in hydrogen consumption of one to two orders of magnitude over a period of several decades [19,34].

The transition to the hydrogen economy will not be simple or straightforward, its course will be dictated on one hand by our ability to overcome the major economical and technical hurdles spread across the whole spectrum of the hydrogen economy namely production, storage & distribution and use; and on the other hand by advancements in competing technologies that are not hydrogen dependent.

Extensive research on ways to meet potential hydrogen demands is being conducted, mainly focusing on effective ways to produce hydrogen. Sources of energy are needed from which hydrogen can be produced in large quantities, in an environmentally benign manner and at low cost. Several methods to produce H_2 are under development [31]. Some of the processes which can be used to produce hydrogen include electrolysis, steam reforming of fossil hydrocarbons, biomass gasification, partial oxidation of hydrocarbons, algae

liquefaction, thermochemical processes coupled with clean or renewable energy technologies, etc. Most of the production methods mentioned are either not technically feasible or economically uncompetitive on a large scale [4,35,36]. However, a major portion of the world's hydrogen production is dependent on fossil fuels. The predominant existing process for large-scale hydrogen production is steam methane reforming (SMR) [37]. SMR is an energy-intensive endothermic low-pressure process requiring high-temperature heat input. The input natural gas is used as the reduced chemical source of H_2 and burned to produce heat to drive the process at temperatures of up to 900°C [19,38]. SMR is a carbon-based technology that emits carbon dioxide. This paradigm shift will require a large-scale sustainable method of hydrogen production, wherein some role of ‘‘green energy’’, will have importance. ‘‘Green’’ hydrogen production would not emit greenhouse gases that contribute to climate change [39,40].

The electrolysis of water to produce hydrogen is a mature technology that is used today to produce hydrogen [19]. Electrolysis is not currently competitive for the large-scale production of hydrogen, except where low-cost electricity is available [33]. Using electrolysis for large-scale H_2 production over the long term depends upon the evolution of the electric grid, the capital costs of electrolysis, and other factors [33]. Current capital costs are estimated to be near 600 $/kW, while some predict future capital costs may approach 300 $/kW [33]. Conventional alkaline electrolyzers have efficiencies of 70–85%, and proton-exchange-membrane electrolyzers are projected to have efficiencies of 80–90%. There is a significant trade-off between capital costs and efficiency [38]. Electrolysis may be viable provided there is successful development of efficient, low-cost electrolysis systems and associated local H_2 storage and distribution systems [19]. There are challenges to setting up mainstream electrolyzer use for hydrogen production, primarily high capital costs of the systems, the cost of electricity, and the efficiencies of the systems. The PV electricity costs approximately 30 $/kWh, perhaps ten times what is needed to make electrolysis cost competitive, and the cost of electrolyzers themselves must be significantly reduced to enable large-scale implementation [41,42]. Because the amount the system efficiency can be increased is limited (current target is 78%), increased efficiency will not reduce the cost as much as a significant reduction in electricity price. For example, if forecourt systems can use industrial priced electricity as opposed to commercial priced electricity (7.89 $ vs. 4.83 $ per kWh), hydrogen prices can be reduced by 31% [42].

The most promising route is splitting water, which is a natural carrier of hydrogen. It takes energy to split the water molecule and release hydrogen, but that energy is later recovered during oxidation to produce water. To eliminate fossil fuels from this cycle, the energy to split water must come from non−carbon sources, such as the electron−hole pairs excited in a semiconductor by solar radiation, the heat from a nuclear reactor or solar collector, or an electric voltage generated by renewable sources such as hydropower or wind [33].

Thermochemical cycles are alternative and potentially more efficient methods to produce hydrogen from water splitting [36, 43]. Thermochemical cycles are processes that primarily make use of heat and a series of intermediate chemical reactions to break down water into hydrogen and oxygen [36]. More than 200 thermochemical cycles have been proposed for hydrogen production, but over the years many have been discarded for reasons ranging from difficulty in feasibility to low efficiency [44]. Some of the most popular thermochemical cycles under study include the Hybrid Sulphur process, Sulphur Iodine cycle, Copper oxide-Copper sulphate cycle, Copper-chlorine cycle, Hybrid chlorine cycle and the Magnesium iodide cycle. Some of the key criteria in literature for selection of a thermochemical cycle for commercialization include cycle efficiency, capital requirements and peak temperature [44]. A basic comparison of the five most popular cycles is shown in Table I.1 [35,45-49].

Table I.1. Thermochemical cycle comparison [35,45-49].

Cycle	**Efficiency %**	**Capital Requirement ($millions)**	**Peak Temperature (°C)**
Hybrid Sulphur	36.6	400	870
Hybrid Chlorine	36	800	850
Hybrid CuO-$CuSO_4$	52.4	360	870
Sulphur-Iodine	52	660	870
Copper-Chlorine	52	370	550

From Table 1.1, the hybrid copper- chlorine cycle has a relatively high efficiency and slightly higher capital requirement. The peak temperature of the copper-chlorine is much lower and has more flexibility on the high temperature heat source it can be coupled with, and as such has a lower overall capital requirement [35].

I.3. Copper-Chlorine thermochemical cycle

The copper–chlorine (Cu-Cl) cycle has been identified by Atomic Energy of Canada Limited (AECL) and Argonne National Laboratory as one of the most promising low temperature cycles [50-54]. The Cu-Cl cycle splits water into hydrogen and oxygen using intermediate copper and chlorine compounds [55,56]. By comparison to other cycles that normally require temperatures above 1100 K, It is a promising cycle because of its relatively low temperature requirement (800 K) [54]. The Cu-Cl cycle could be linked with thermal solar plant to decompose water into its constituents, oxygen and hydrogen as a net result, using a net input of water and heat. The process involves a series of closed-loop chemical reactions that do not contribute to any greenhouse gas emissions to the environment.

Simulation packages of Cu-Cl cycle are useful tools to provide the system designer or operator with design, optimization and operation information before building a thermochemical cycle pilot plant [57]. There are three types of the Cu-Cl cycle, based on the number of main chemical reactions: the five-step cycle, the four-step cycle and the three-step cycle. These three types are shown in Tables I.2, Table I.3 and Table I.4, respectively [57].

Table I.2. The five steps in the Cu-Cl cycle with their corresponding reactions [57].

Step	Reaction	Temperature range °C
S1	$2CuCl_2(s) + H_2O(g) \rightarrow CuOCuCl_2(s) + 2HCl(g)$	400
S2	$CuOCuCl_2(s) \rightarrow 2CuCl(l) + \frac{1}{2}O_2(g)$	500
S3	$4CuCl(s) + H_2O \rightarrow 2CuCl_2(aq) + 2Cu(s)$	25-80
S4	$CuCl_2(aq) \rightarrow CuCl_2(s)$	>100
S5	$2Cu(s) + 2HCl(g) \rightarrow 2CuCl(l) + H_2(g)$	430-475

Table I.3. The four steps in the Cu-Cl cycle with their corresponding reactions [51,57].

Step	Reaction	Temperature range °C
S1	$2CuCl(aq) + 2HCl(aq) \rightarrow 2CuCl_2(aq) + H_2(g)$	<100 (electrolysis)
S2	$CuCl_2(aq) \rightarrow CuCl_2(s)$	<100
S3	$2CuCl_2(s) + H_2O(g) \rightarrow Cu_2OCl_2(s) + 2HCl(g)$	400
S4	$Cu_2OCl_2(s) \rightarrow 2CuCl(l) + \frac{1}{2}O_2$	500

Table I.4. The three steps in the Cu-Cl cycle with their corresponding reactions [48,57].

Step	Reaction	Temperature range °C
S1	$2CuCl_2(aq) + H_2O(g) \rightarrow 2CuCl(l) + 2HCl(g) + \frac{1}{2}O_2(g) + H_2O(g)$	400-600
S2	$4CuCl(s) \rightarrow 2Cu(s) + CuCl_2(aq)$	20-80
S3	$2Cu(s) + 2HCl(g) \rightarrow 2CuCl(l) + H_2(g)$	430-475

The copper–chlorine cycle has received increasing attention since 2008. Naterer et al. [39] have examined the heat requirements of the copper–chlorine cycle steps, in efforts to recover as much heat as possible and minimize the net heat supply to the cycle. The electrochemical reaction, copper (Cu) production step, has been described with its operational and environmental conditions, and analyzed thermodynamically by Orhan et al. [30]. The Results have shown that at a reaction temperature of 45 ◦C and a reference-environment temperature of 25 ◦C, the exergy efficiency of electrochemical reaction has been found to be 99% and to decrease with increasing reference environment and/or reaction temperatures. Haseli et al. [37] have presented the transport phenomena of a non-catalytic reaction of cupric chloride particles with superheated steam in a fluidized bed for nuclear-based hydrogen production. Numerical results have shown that, the conversion of steam decreases with superficial velocity, whereas the conversion of solid particles increases.

The role of the Cu–Cl cycle for thermochemical water decomposition, potentially driven by heat from a nuclear power generation station, in producing hydrogen in a sustainable way has been investigated by Orhan et al. [58]. The energy efficiency of the cycle has been found to be 45% and the exergy efficiency 10%. Several variations of copper-chlorine cycles with different numbers of steps and methods of grouping have been compared, and major features of the cycles with different numbers of steps have been discussed by Wang et al. [19,48]. Wang et al. state that the different forms are a result of combining different reaction steps into one reaction [35,48]. The O_2 production and the HCl production steps of Cu-Cl cycle have been described by Orhan et al. [59,60]. The operational and environmental conditions of the two reactions were also defined, and a comprehensive thermodynamic analysis was performed.

Daggupati et al. [56] have examined a solid conversion process during hydrolysis and decomposition of cupric chloride. Reaction rate constants and the time required for complete solid conversion are determined by a shrinking-core model. The Results have shown that at a

temperature of 375 °C, complete conversion of $CuCl_2$ can be achieved by controlling the excess steam, the operating pressure and the inert gas supply. Orhan et al**.** [61] have analyzed a coupling of the Cu–Cl cycle with a desalination plant for hydrogen production from nuclear energy and seawater. Desalination technologies have been reviewed to determine the most appropriate option for the Cu–Cl cycle and a thermodynamic analysis has been presented for various configurations of this coupled system. Exergy-related parameters have also been inverstigated by Orhan et al. [62] to minimize the cost of a Cu–Cl cycle. The Results have shown that the cost rate of exergy destruction varies between 1$ and 15$ per kilogram of hydrogen and the exergy economic factor between 0.5 and 0.02 as the cost of hydrogen rises from 20$ to 140$ per GJ of hydrogen energy. Energy and exergy analyses of the geothermal-based hydrogen production via a new four-step copper-chlorine cycle have been conducted by Balta et al. [63]. As a result, overall energy and exergy efficiencies of the cycle have been found to be 21.67% and 19.35%, respectively, for a reference case. Naterer et al. [64] have described hydrogen production with Canada's Super-Critical Water Reactor, SCWR. Advances towards an integrated lab-scale Cu-Cl cycle have been discussed, including experimentation, modeling, simulation, advanced materials, thermochemistry, safety, reliability and economics.

The impact of exit streams containing byproducts of incomplete reactions in an integrated thermochemical copper-chlorine cycle has been studied by Marin et al. [65]. They have also examined the implications of incomplete hydrolysis reactions on the kinetics and thermodynamics of the oxygen reactor in the Cu-Cl cycle. Daggupati and al. [54] have developed a predictive model of convective heat transfer and conversion of cupric chloride particles in a fluidized bed reactor of a copper–chlorine cycle. The maximum conversion of steam at 400°C was found to be 3.75% and it requires excess steam of 12.8 moles per unit mole of cupric chloride solid for complete conversion of solid. Orhan et al**.** [66] have analyzed several Cu-Cl cycles by examining various design schemes for an overall system and its components, in order to identify potential performance improvements.

Rong Xu et al. [67] have proposed a solar receiver-reactor with integrated energy collection and storage driving the endothermic oxygen production step of the copper-chlorine cycle. A pinch methodology has been used by Ghandehariun et al. [68] to determine the minimum energy requirement for the overall Cu-Cl cycle. Pope and al. [69] have examined the chemical equilibrium and gaseous product fraction of a multiphase gas-solid flow involving hydrolysis of copper (II) chloride and steam in a packed bed reactor. Ratlamwala et

al. [70] have analyzed an integrated Cu–Cl thermochemical cycle, Kalina cycle and electrolyzer for hydrogen production. The system operating parameters have been varied to investigate their effects on the energy and exergy efficiencies of the integrated system, rate of hydrogen production, and rate of oxygen production. A new photochemical cell has been developed and analyzed for copper disproportionation within the Cu-Cl cycle by Zamfirescu et al. [71]. The study has examined the feasibility and the expected efficiency of the photochemical disproportionation cell. Simulation models have been developed by Orhan et al. [57] to analyze, design and optimize the Cu–Cl cycles using the Aspen PlusTM chemical process simulation package. New system configurations for the Cu–Cl cycle have been developed for performance improvement. The Results have shown that the thermal efficiency of the five-step thermochemical process has been 44%, of the four-step process has been 43% and of the three-step process has been 41%, based on the lower heating value of hydrogen.

Recently, Ratlamwala et al. [72] have analyzed two integrated systems for hydrogen production, namely: (a) integrated solar heliostat, Cu–Cl cycle and Kalina cycle system and (b) integrated solar heliostat, Cu–Cl cycle, Kalina cycle and electrolyzer system. The results have indicated that system (a) performs better than system (b) from the energy and the exergy perspectives. Thermodynamic analysis of a renewable-based multi-generation energy production system have been developed by Ozturk et al. [73]. This solar-based multi-generation system consists of four main sub-systems: Rankine cycle, organic Rankine cycle, absorption cooling and heating, and hydrogen production and utilization. The solar-based multi-generation system which has an exergy efficiency of 57.35%, is most efficient than using these sub-systems separately. Dincer et al. [74] focuses on a comparative study of five renewable energy based hydrogen production systems namely: (a) Cu–Cl integrated with Kalina cycle, (b) hybrid sulfur (HyS) cycle integrated with isobutane cycle, (c) quintuple flash power plant integrated with electrolyzer, (d) heliostat field integrated with steam cycle, Organic Rankine Cycle (ORC) and electrolyzer, and (d) solar photo-voltaic/thermal (PV/T) integrated with triple effect absorption cooling system and electrolyzer. The obtained results shown that system (a) performs the best with energy and exergy efficiencies, sustainability index, and energy demand of the system. Yildiz et al. [75] have investigated a solar-assisted biomass gasification system for hydrogen production and assessed its performance thermodynamically using actual literature data. Also, environmental impact of these systems has been evaluated through calculating the specific greenhouse gas (GHG) emissions.

Solar energy can be supplied extensively for large-scale capacities of hydrogen production. It can be used for hydrogen production by using heat from the solar plant for thermochemical processes [5]. Thermochemical "water splitting" requires an intermediate heat exchanger between the solar field and hydrogen plant, which transfers heat from the heat transfer fluid to the thermochemical cycle [33].

I.4. Solar Energy

The solar energy incident on the Earth surface is about 10.000 times the world energy demand [76]. The use of the southern Mediterranean countries areas for solar energy harvesting would by far suffice to supply the energy needs of those countries and of all the northern European industrialized countries. The solar light entering the earth surface carry with it an ample amount of energy which can be harnessed to produce energy under the form either heat, electricity or both depending on solar thermal, solar photovoltaic (PV), or solar photo-voltaic/thermal (PV/T) technologies is installed, respectively. However, for centralized or large scale heat or electrical power production, high temperature solar thermal technologies are preferred [72,73].

At the beginning of 2012, the solar thermal power plants in operation worldwide achieved a total capacity of 2.103 MWel, while new plants were under construction for 2.662 MWel of additional capacity [5]. Besides, more than 13.000 MWel were under planning, which means with signed agreement or within short-term national programs. Despite this high growth rate, the sector is still at an early stage of commercial development in comparison with other renewable technologies such as photovoltaic (70 GWel) and wind (250 GWel). Therefore the continuous assessment and optimization of both the energy and the economic performances of solar thermal power plants are required. In a simplified statement, solar thermal power plants have to convert with high efficiency solar radiation into electricity at a cost equivalent or lower than the cost of electricity production by conventional power plant [77]. In a study carried by Greenpeace [76], it has been found that the use of concentrating solar power (CSP) can prevent the emission of 154 million tons of CO_2 by 2020. Just one 50 MW_{el} parabolic trough power plant can cut the annual heavy oil consumption by 30 million liters and thus eliminate 90.000 tons of CO_2 emissions [76].

The solar thermal technologies are mainly based on four concentrating solar power (CSP) technologies presented in figure I.1 [78], namely:

- Parabolic dish collectors (PDC)
- Linear Fresnel collectors (LFC)
- Central tower systems (CRS)
- Parabolic trough collectors (PTC)

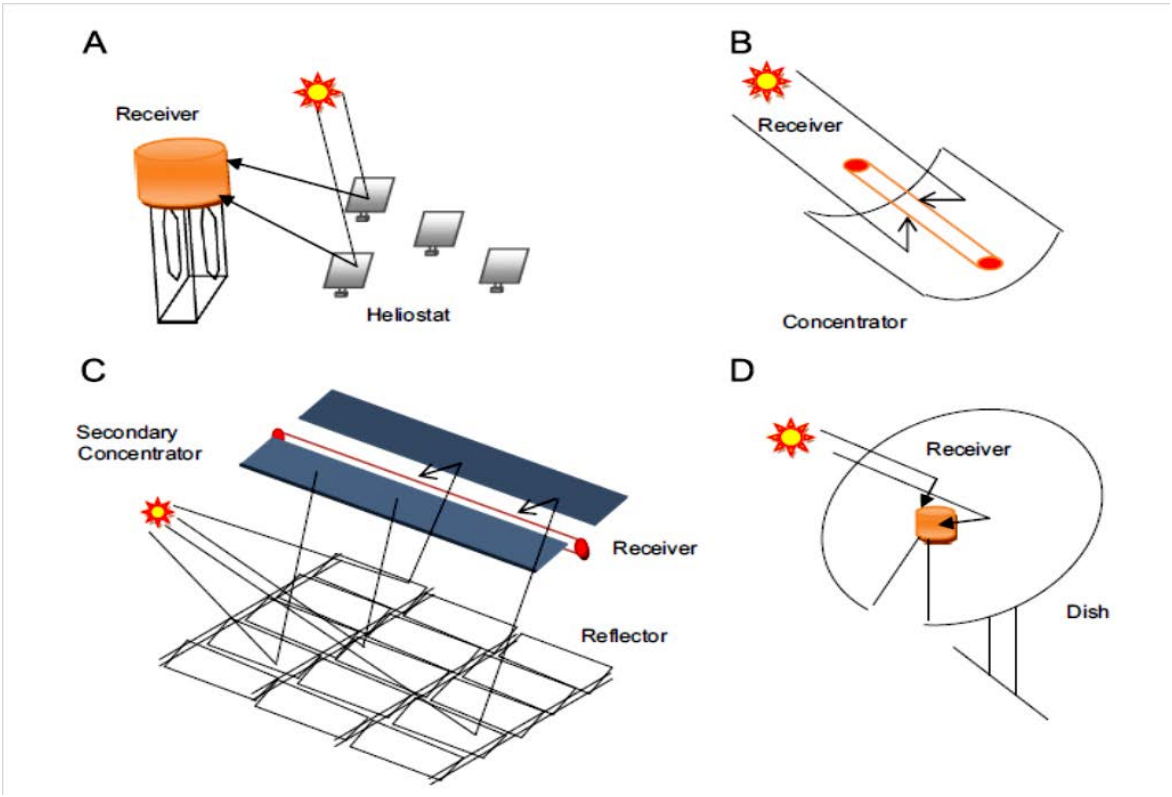

Figure I. 1. Basic concept of the four CSP families: (A) center receiver, (B) parabolic trough, (C) linear Fresnel, (D) dish [78].

One of the most important limits for choosing the most suitable technique for any proposed application is the operating temperature [79]. Figure II.2 shows the different applications for CSP systems [79, 80]. The increasing order of deployment worldwide of CSP technologies in 2011 is given in table I.5.

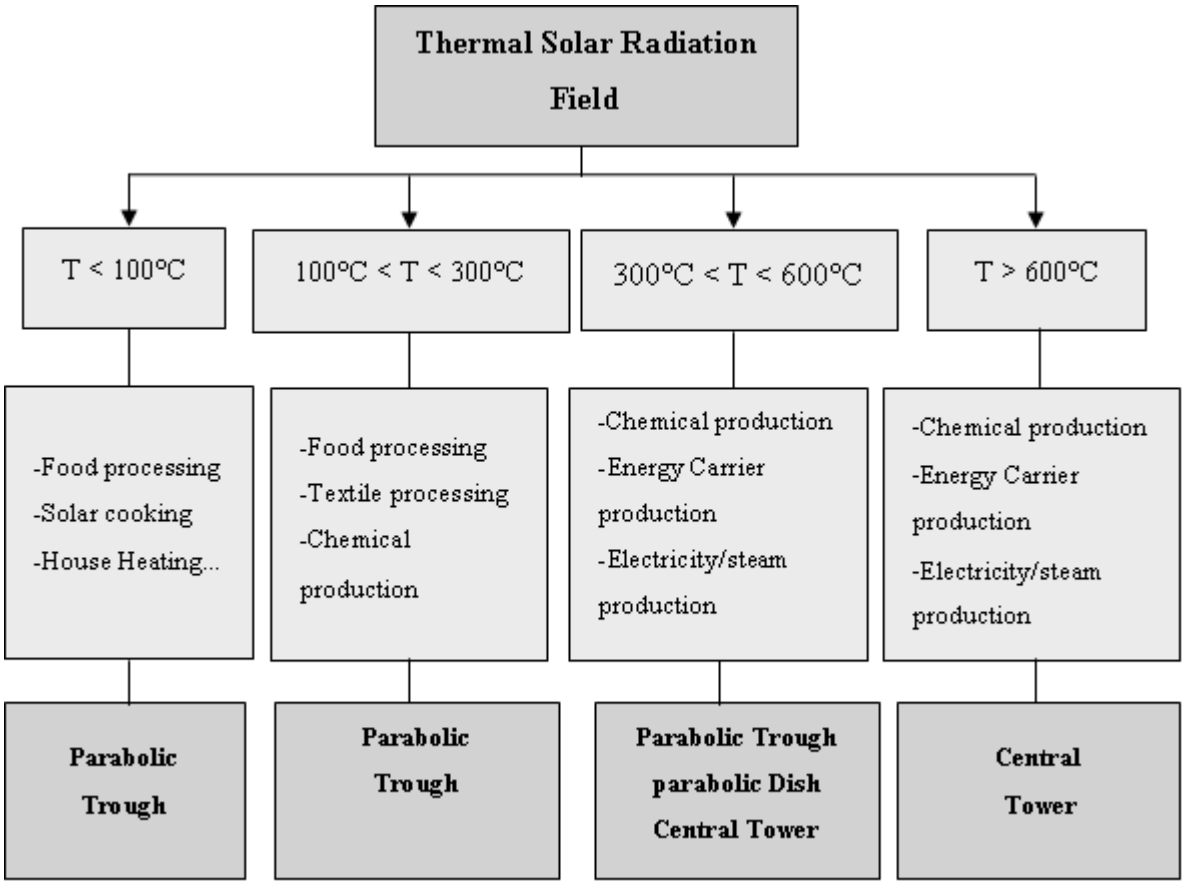

Figure I.2. CSP applications.

Table I.5. The deployment worldwide of CSP technologies in 2011, [77].

Technology	In operation (MWel)	Under construction (MWel)
Parabolic dish collectors	1	-
Linear Fresnel collectors	10	30
Central tower systems	55	502
Parabolic trough collectors	1.630	2.130

The solar tower system provides a high ratio of solar radiation concentration of up to 600°C which allows solar towers to achieve 1200 °C for air heating applications [79]. As shown in figure I.1-A, the solar tower system consists of heliostat reflectors located around the solar receiver. The reflectors track the sun's position to ensure directing the sunlight to a receiver [79]. A heat transfer medium is used in the receiver to absorb the concentrated solar energy. The absorbed heat is then supplied to a thermal system. The heat transfer fluid in the

central receiver can be water, air, molten salt or oils [81]. The solar tower is one of the proven CSP technologies in the field. Examples of the operated solar towers are solar one and solar two in the USA. Their capacity is 10 MWe each. Work in the field has shown that the central tower technology has the potential to be used in a wide range of applications of gas turbines, combined cycles, and some industrial processes [82,83].

The basic concept of parabolic dish-engine, as shown in figure I.1-D, is to use a parabolic dish to concentrate solar radiation on an engine-generator set in the focal point of the reflector [79]. The engine can be a Stirling engine or a gas turbine. In terms of efficiency, the parabolic dish is the most efficient technology of all solar technologies; its peak efficiency can be as high as 29% [84]. The typical diameter of the parabolic dish varies from 5 to 15 m with a power output of 5 to 25 kW [85]. This technology is suitable for decentralized power supply and remote locations. The barriers to apply this technology are its cost and proof of the long-term reliability.

The linear Fresnel system consists of an array of linear reflectors to concentrate the solar radiation on a central absorber, as shown in figure I.1-C. The absorber tube, which is oriented along the focal line of the reflectors, receives the concentrated solar radiation and converts the solar energy to heat. Heat transfer fluid is used to absorb this energy to be used in the proposed application. This type of collector offers good possibilities for solar energy use and it is suitable for small- and large-scale applications. Some prototypes have been tested. For example, in Germany a prototype of 50 kWe has been tested in 2005. Its operation temperature was 200 °C, its dimensions were 16 m long × 4 m high and it consisted of 11 primary reflectors. Linear Fresnel technology was used in the summer of 2006 for the first time in a real industrial application to run an ammonia-water-chiller. One of the advantages of this collector is that it does not need complex construction materials [79].

The difference between parabolic trough system and the linear Fresnel system is that parabolic trough system uses a parabolic shaped reflector, as shown in figure I.1-B. The concentration ratio can be 80 or more [86]. The collected energy then absorbed by heat transfer fluid runs inside the absorbed tube. Parabolic trough technology supplies energy at a temperature of up to 400 °C. The heat transfer fluid which is used to absorb the heat can be either water or synthetic oils [79].

I.5. Parabolic trough collectors (PTC)

Solar PTC is a proven technology that has reached industrial maturity and that is viable for commercial scale solar power generation in the Sunbelt countries [87-89]. The commercialization of this technology has taken a major step forward in the mid 1980s and early 1990s with the development of the SEGS plants in California by Luz International Ltd. More than 1.2 billion $ in private capital has been raised in debt and equity financing for the nine SEGS plants. Whereas a conventional power plant depends on fuel that is purchased as a continuous string of payments during the lifetime of the plant, a solar power plant needs to finance its “fuel costs” through capital investment at the beginning of the project. In a typical parabolic trough SEGS-type plant, the solar field represents 50% of the total investment costs. However, once a solar plant is built the “solar fuel” is free, resulting in less uncertainty in the cost of power over the life of the project. Besides reducing the dependence on the hydrocarbon limited resources, solar PTC offers the opportunity to increase the country energy mix and to contribute to the local development through job creation during construction and beyond [76,89].

Since only direct solar radiation can be concentrated [90] parabolic trough systems use a sun tracking system to ensure maximum efficiency of the concentrating process. The rotational axis is normally at the vertex line of the parabolic trough or in a parallel position slightly below it [91].

Theoretically, the parabolic troughs in the solar field of a CSP plant can have any orientation with one or two tracking systems. Sun tracking is always possible. However, there is a preferred orientation, which is the north-south alignment [91]. For parabolic trough collectors the most applied control system is in a north-south oriented rotation axis, where collectors are aligned on the north-south axis and collectors rotate from east to west tracking the sun’s position. The control system continuously drives the collectors from east at sunrise to west at sunset. Small motors are used to drive this tracking system. Figure II.3 shows one axis tracking parabolic trough with axis oriented North/South [79,92].

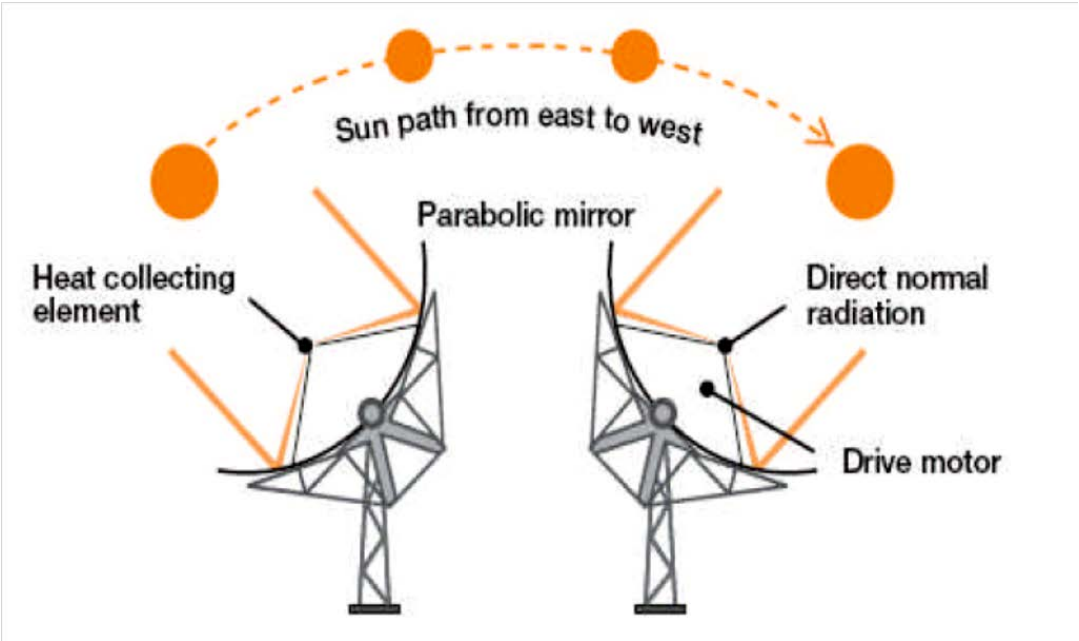

Figure I.3. One axis tracking parabolic trough with axis oriented North/South [79,92].

Solar trough systems vary in configurations and operating systems. They can be installed in solar mode only where only heat from the solar field is used to operate the thermal cycle. However, these systems require a thermal storage facility to ensure operation stability. Hybrid systems use different approaches. In this case the fossil fuel boiler (commonly natural gas fired) is used to supply the required energy for the thermal cycle. Other techniques have also been introduced, such as solar desalination. The solar field consists of rows of parabolic trough collectors [79].

In solar, only mode configuration and operation, the only energy resource to run the thermal plant is the solar field. There is no backup or assistance from fossil fuels boilers. However, a thermal storage system is needed in this regime [79]. In this mode the solar field starts running from sunrise to supply heat. For about 2-3 hours of solar radiation peak, the solar field is in addition operated to supply some energy to the storage system. When solar energy is not sufficient, the storage system starts to supply some energy to the thermal cycle. After sunset, the plant runs completely on the storage system [93]. Figure I.4 shows a solar thermal power plant with a thermal storage system [79,93].

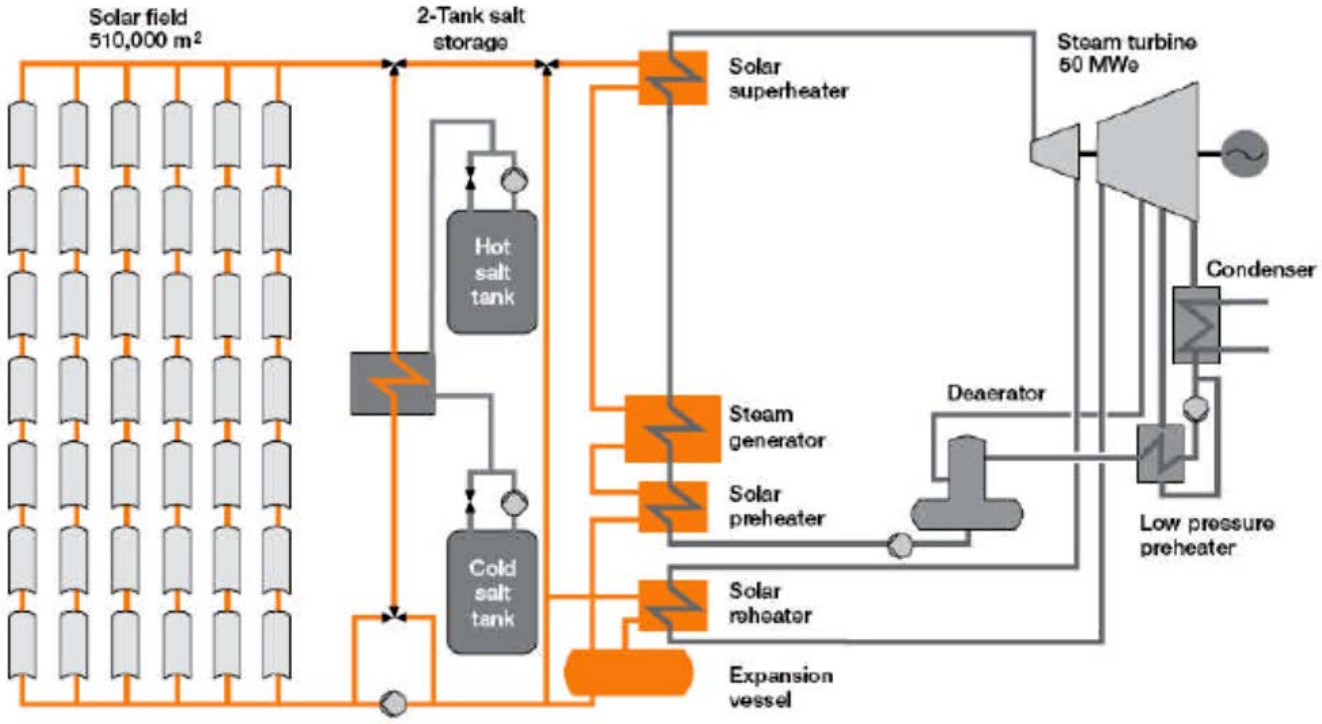

Figure I. 4. Solar thermal power plant with a thermal storage system [79,93].

The hybrid solar power generation system concept uses a backup fossil fuel boiler which is used in parallel with the solar field to guarantee reliable operation at night-time or when no solar radiation is available. Many configurations have been introduced as hybrid systems. One fossil fuel boiler or more is used to supply the required energy for the thermal cycle [94]. Figure I.5 shows hybrid trough solar power plant [79,95].

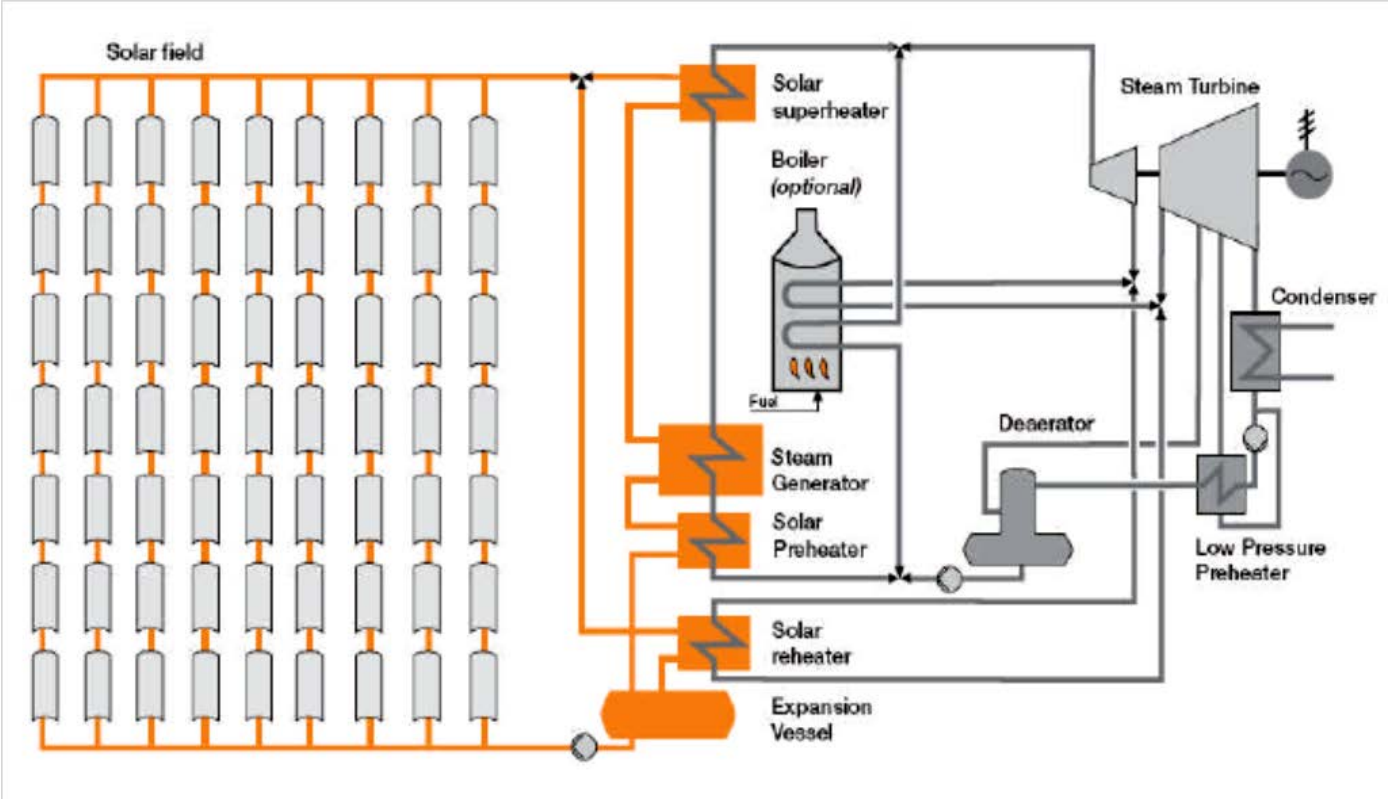

Figure I.5. Solar trough system with fossil fuel backup [79,95].

The collector, the parabolic trough, is a trough the cross-section of which has the shape of a part of a parabola. More exactly, it is a symmetrical section of a parabola that is covered by the mirrors around its vertex. The main requirements for appropriate mirror materials are their reflective properties. The reflectivity must be high. The most common parabolic mirrors today consist of silver coated glass mirrors. Radiation that enters in a plane parallel to the mirror is reflected in such a way that it passes through the focal line or receiver. Receivers have the task to convert the radiation that is projected onto them into heat and heat transfer fluids have to transport the heat to the pipes. Important are high radiation absorption and low heat losses. The receiver has to be constructed in such a way that high radiation absorption and low thermal losses are realized. Low thermal losses refer to low radiative losses as well as low convective and conductive losses [91]. Figure I.6 shows the structure of a parabolic trough receiver [91,96].

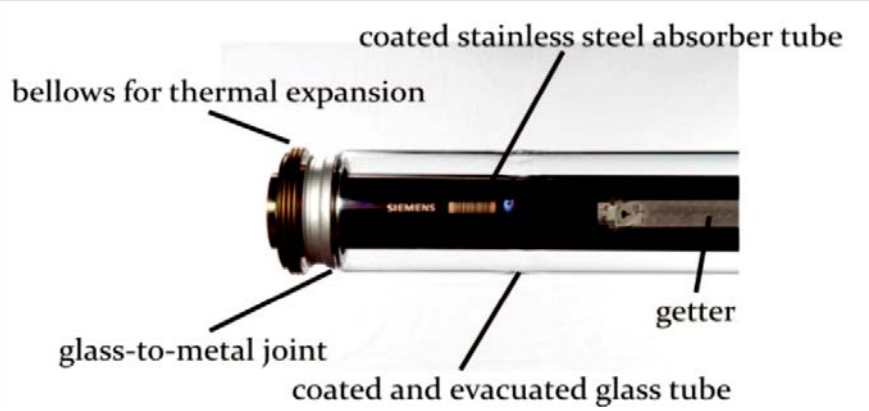

Figure I.6. Structure of a parabolic trough receiver [91,96].

PTC heat transfer analyzes have received increasing attention since 1980. Clark [97] has presented an identification of the principal design factors that influence the technical performance of a parabolic trough concentrator. These factors include reflectivity of the mirror system, the mirror-receiver tube intercept factor, the incident angle modifier and the absorptivity-transmissivity product of the receiver tube and cover tube. The temperature profile in the absorber tube of a direct steam generating PTC has been estimated by Heidemann et al. [98]. To this end, a computer program has been developed to calculate the two-dimensional transient temperature field using a modular nodal point library. Using different type of receiver selective coating and different receiver configuration, Dudley et al. [99] have tested LS-2 PTC to determine the collector efficiency and the thermal losses. LS-2 is the second-generation PTC installed in SEGS solar plant. Thomas and Thomas [100] have presented a design data for the computation of thermal losses in the receiver of a PTC for specific absorber tube diameters, various ambient temperatures, wind velocity and absorber temperatures. A numerical model has been used by Kalogirou et al. [101] to quantify the steam produced PTC system. Performance tests of the model have indicated that the modeling program was accurate to within 1.2% which has been considered very adequate. Odeh et al. [102] have carried out a numerical study to evaluate the performance of PTC direct steam generation solar collector. The model has been based on absorber wall temperature rather than fluid bulk temperature. Forristall R. [103] has described the development, the validation, and the use of a heat transfer model implemented in Engineering Equation Solver (EES). Numerical simulations of thermal and fluid-dynamic behavior of a single-pass and double-pass solar parabolic trough collector have been carried out by García-Valladares and Velázquez [104]. Their results have shown that the double-pass can enhance the thermal efficiency compared with the single-pass. Kumar and Reddy [105] have analyzed a 3-D numerical simulation of the porous disc line receiver for PTC. The analysis has been carried

out based on renormalization-group (RNG) turbulent model by using Therminol-VP1 as working fluid. Cheng et al. [106] have presented a 3-D numerical simulation of heat transfer characteristics in the receiver tube by combining the Monte Carlo Ray Trace Method (MCRT) and the FLUENT software. Gong et al. [107] have established a 1-D theoretical model using Matlab software to compute the receiver's major heat loss through glass envelope in Sanle-3 HCE (China's first high temperature vacuum receiver). A coupled simulation method based on MCRT and Finite Volume Method (FVM) has been presented by He et al. [108] to solve the complex coupled heat transfer problem of radiation, heat conduction and convection in PTC system. The heat transfer and fluid flow performance in the LS-2 collector tube has been investigated to validate the coupled simulation model. Vasquez Padella et al. [109] have studied a 1-D numerical heat transfer analysis of a PTC. The receiver and envelope have been divided into several segments and mass and energy balance have been applied in each segment. The results obtained have shown good agreement with experimental data. Cheng et al. [110] have used the same method as He et al. [108] to analyze the total photo-thermal conversion process of an experimental LS-2 PTC system. The numerical results have been compared to the experimental data and good agreement has been obtained. Solar repowering of the Soma-A thermal power plant in Turkey has been investigated using simulations by ZekiYılmazog˘lu et al. [111]. According to their results, solar repowering of Soma-A thermal power plant with parabolic trough type collectors can result in 14% power increment at full load operation of the boiler and 14% CO_2 decrement at part load operation of the boiler. Kalogirou [112] has presented a detailed thermal model of a PTC using the EES and validated with known performance of existing collectors. Wang et al. [113] have investigated the effect of inserting metal foams in receiver tube of parabolic trough collector on heat transfer. Dongqiang et al. [114] have examined overall heat loss, end loss and thermal emittance of the coating of a newly designed receiver of PTC in order to evaluate its thermal characterization. A heat loss comparison between Solel UVAC3, Schott 2008 PTR-70, and Himin PTR-2011 showed that the new receiver had very good thermal performance and distinctly decreased heat loss in the parabolic trough solar field.

Chapter II: Estimation of Direct Normal Solar Irradiance in Algeria

II.1. Introduction

A reasonably accurate knowledge of the solar radiation is necessary for solar energy applications such as solar thermal and photovoltaic applications. Due to the nature of concentrating solar power plant, only the direct normal irradiance (DNI) can be used [17]. Estimating the DNI is of great importance in the development of concentrating solar power plant technologies. The DNI allows the identification of the most suitable sites available for deploying the concentrating solar power plants. The analysis of a solar energy system design is typically initiated by predicting its performance over a "typical" "clear" day. There are a number of clear-day mathematical solar irradiance models that may be used to predict the expected maximum hour-by-hour direct solar irradiance [115,116]. Hottel [1976] presented a model, with good accuracy and simple use, to estimate the clear-day transmittance of direct solar radiation through clear sky. Hottel's clear-day model of direct normal solar irradiance is based on atmospheric transmittance calculations for four different climate zones in the globe using the 1962 U.S. Standard Atmosphere [117,118]. Using Hottel's model for different tracking systems and orientations, the purpose of this chapter is to estimate the direct solar irradiance available to collectors in Algeria.

II.2. Solar radiation

Solar radiation is a radiation of electromagnetic nature, emitted during the thermonuclear reaction taking place in the sun. This reaction is a fusion reaction. Two hydrogen atoms combine to form helium. During this reaction, there is release of nuclear particles and energy under the form of electromagnetic radiation. As the amount of hydrogen on the sun is finite, the reaction stops as soon as there is not enough hydrogen to fuel the reaction. So, for the purposes of solar radiation calculations it is safe to assume that the intensity of emitted radiation from the sun is constant. This assumption led to the development of an important parameter, the Solar Constant [119,120]. As defined by Duffie and Beckman [121], "the Solar Constant, I_{sc}, is the energy from the sun, per unit time, received on a unit of area of surface perpendicular to the direction of propagation of the radiation, at the Earth's mean distance from the sun, outside the atmosphere". This constant has been experimentally measured many times, and its value is taken as 1367 W/m^2 [119-125].

The electromagnetic radiation travels through space without alteration. But solar radiation flux onto the Earth varies at different times of the year due to the elliptical pattern of the Earth's orbit and consequential changes in distance from the sun. The solar radiation flux for a given day of the year is represented by the following equation [120,121,125]:

$$I_0 = Isc \cdot \left[1 + 0{,}034 \cdot \cos\left(\frac{360 \cdot N}{365 \cdot 25} \right) \right] \qquad \text{(II.1)}$$

Where I_0 is the extraterrestrial solar irradiance, outside the earth's atmosphere measured on the plane normal to the irradiance on the N^{th} day of the year

The above equation refers to extraterrestrial radiation measured just outside of the Earth's atmosphere. But once solar radiation reaches the earth atmosphere, it interacts with the atmosphere particles. Following these interactions, the sun radiation will reduce through reflection, absorption, and scattering of light.

The typical measurement of radiation is irradiance, I, which is the amount of solar radiation per unit time, per unit area of the surface (W/m^2). The global irradiance observed from the ground breaks down into three main components [119,126]:

- the direct or beam irradiance *Ibn*,
- the diffuse irradiance *Id*,
- and the reflected irradiance *Ir*.

The direct irradiance represents a component of global solar radiation that comes directly to the earth in a bright and clear day and is observed at the sun's position in the sky. The direct solar radiation is a dominant component of global solar radiation for clear days. Except the direct solar radiation every surface receives a part of solar radiation that comes to it indirectly. It is called the diffuse irradiance. It results from scattered rays in the atmosphere and comes from the entire sky hemisphere. Near towns and cities, as the consequence of air pollution and ground configuration, the diffuse sky radiation comes even to 22% of the complete radiation. During the cloudy days almost complete radiation is diffuse. The surfaces that make an angle with a horizontal flat receives radiation that reflects from surroundings. The reflected irradiance is the consequence of a more or less reflecting environment (sand, water, snow, buildings, etc.). Since concentrating solar systems only harness the direct normal component *Ibn*, the diffuse and reflected radiation components are left aside here [119,126,127].

II.3. Solar angles and solar times

Any user of solar energy is interested in the quantity of radiation which can be received and transformed into useful energy at a given time or given time interval at a given geographical place or area [128]. The performance of any solar absorbing surface is affected by the direction of the incoming beam radiation, or more specifically, the angle at which the incident beam radiation hits the surface [119]. The relative position of the sun and earth is conveniently represented by means of the celestial sphere around the earth. The equatorial plane intersects the celestial sphere in the celestial equator, and the polar axis in the celestial poles. The angle between the line joining the centers of the sun and the earth and its projection on the equatorial plane is called the solar declination angle. The daily rotation of the earth is depicted by the rotation of the celestial sphere about the polar axis, and the instantaneous position of the sun is described by the hour angle. For observers on the earth's surface at a location with geographical latitude, a convenient coordinate system is defined by a vertical line at the site which intersects the celestial sphere in two points, the zenith and the nadir, and subtends the latitude angle with the polar axis (Figure II.1) [117].

Any location on the surface of the earth then can be defined by the intersection of a longitude angle and a latitude angle [118]. The longitude is an angular distance east or west on the earth's surface, measured by the angle contained between the meridian of a particular place and some prime meridian. Locations east of the Greenwich Meridian (where the longitude is zero) have positive longitude angles and those to the west have negative longitude angles. The latitude angle is the angle between a line drawn from a point on the earth's surface to the center of the earth, and the earth's equatorial plane. Locations south of the equator have negative latitude angles and those to the north have positive latitude angles [7].

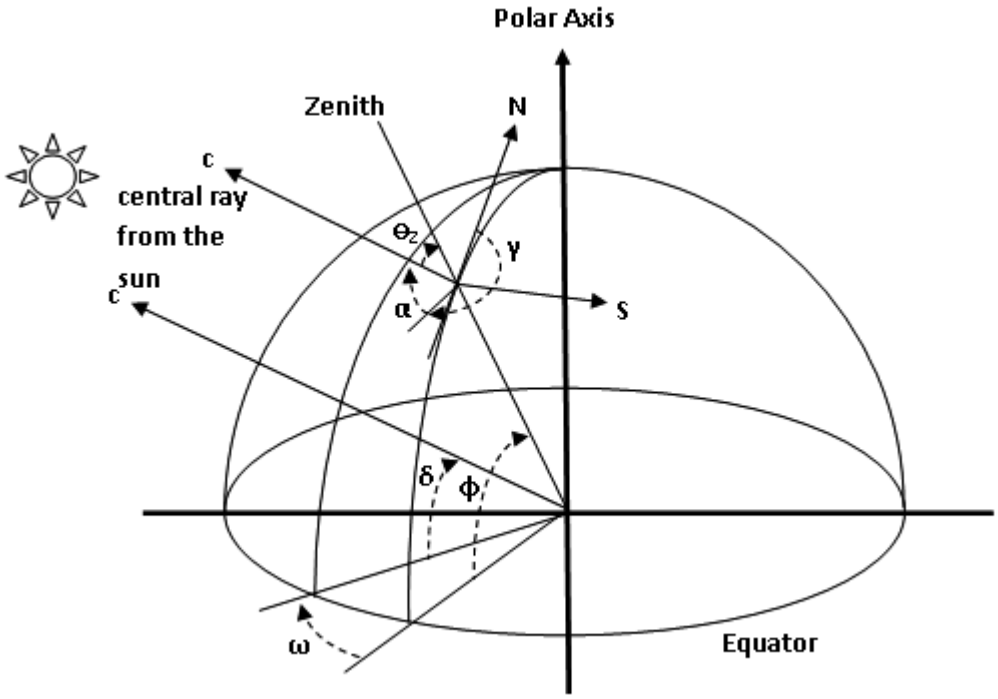

Figure. II.1: Schematic representation of the solar angles

II.3.1. Solar time

The movements of the sun as seen from the earth are obviously a function of time of day. All time values used in the calculations of solar angles are represented by Solar Time *(ST)* called also Local Apparent Time. This parameter is an adjustment to standard time that coincides with the movement of the sun across the sky, such that solar noon occurs when the sun crosses the North South meridian line. This is the moment when the sun has its greatest elevation. Sunrise and sunset are symmetrical about noon in solar time. The sunrise and sunset times in solar time are independent of longitude. The standard equation for solar time is as follows [129]:

$$\begin{aligned} ST &= MT - \left(EOT/60\right) \quad for \quad EOT \prec 0 \\ TS &= MT + \left(EOT/60\right) \quad for \quad EOT \succ 0 \end{aligned} \tag{II.2}$$

Where *EOT* is the difference between mean solar time and true solar time called the equation of time given by Lamm [129]. The resulting value is in minutes and is positive when the apparent solar time is ahead of mean solar time and negative when the apparent solar time is behind the mean solar time:

$$EOT = 60 \cdot \sum_{k=0}^{5} \left[A_k \cdot cos\left(\frac{360 \cdot k \cdot n}{365{,}25} \right) + B_k \cdot sin\left(\frac{360 \cdot k \cdot n}{365{,}25} \right) \right] \quad \text{(II.3)}$$

Where:

Table II.1. Coefficients for Equation (II.3), [129].

k	***A_k (hr)***	***B_k (hr)***
0	2,0870. 10^{-4}	0
1	9,2869. 10^{-3}	-1,2229. 10^{-1}
2	- 5,2258. 10^{-2}	-1,5698. 10^{-1}
3	- 1,3077. 10^{-3}	- 5,1602. 10^{-3}
4	- 2,1867. 10^{-3}	- 2,9823. 10^{-3}
5	- 1,5100. 10^{-4}	- 2,3463. 10^{-4}

n: number of days into a leap year cycle, with *n = 1* being January 1 of each leap year, and *n =1461* corresponding to December 31 of the 4th year of the leap year cycle.

MT is the mean solar time or civil time, defined for convenience to cover wide geographical areas. Sunrise and sunset times in MT depend on both latitude, which determines the daylength and also on longitude. The reference longitude for Universal Time is Greenwich (GMT Greenwich Mean Time), where the longitude is zero. Due to small motions of the earth about its North South polar axis, there are small differences between MT and ST at Greenwich. The conversion between mean solar time and Universal time requires knowledge of the location and take the form:

$$MT = UT + (long / 15) \quad \text{(II.4)}$$

With:

long: longitude angle of the location, (deg).

UT: Universal time, (h). Local Algerian Time is one hour ahead of Universal Time or GMT.

II.3.2. The Hour Angle

The hour angle ω is the angular distance between the meridian of the observer and the meridian whose plane contains the sun. An expression to calculate the hour angle from solar time is [130]:

$$\omega = 15 \cdot (TS - 12) \quad \text{(II.5)}$$

With:

ω: hour angle (deg).

II.3.3. The declination angle

If a line is drawn between the centre of the earth and that of the sun, the angle between this line and the earth's equatorial plane is called the declination angle δ. The declination angle varies from + 23°27’ at the summer solstice to -23°27’ at the winter solstice and zero at the equinoxes. δ is calculated by the equation of Cooper 1969 [121, 122,131]:

$$\delta = 23{,}45 \cdot \sin\left[360 \cdot \frac{284 + N}{365}\right] \quad \text{(II.6)}$$

II.3.4. Solar altitude angle

The solar altitude angle α is defined as the angle between the central ray from the sun, and a horizontal plane containing the observer. The value $\alpha = 0$ corresponding at sunset and sunrise, the solar altitude angle varies from +90° (zenith) to -90° (nadir) is represented by the expression [121,122,131]:

$$\alpha = \sin^{-1}\left(\sin\delta \cdot \sin\varphi + \cos\delta \cdot \cos\omega \cdot \cos\varphi\right) \quad \text{(II.7)}$$

With:

α: solar altitude angle, (deg)

φ: the latitude angle, expressed in degree, of the location;

II.3.5. Solar Azimuth angle

The solar azimuth angle A is the angle, measured clockwise on the horizontal plane, from the north-pointing coordinate axis to the projection of the sun’s central ray. This angle varies from $-180 \leq A \leq 180°$ [123]. It is given by:

$$A' = \cos^{-1}\left(\frac{\sin\delta \cdot \cos\varphi + \cos\delta \cdot \cos\omega \cdot \sin\varphi}{\cos\alpha}\right) \quad \text{(II.8)}$$

Where:

$$\begin{aligned} A &= 360° - A' \quad for \quad \sin\omega \succ 0 \\ A &= A' \quad for \quad \sin\omega \leq 0 \end{aligned} \quad \text{(II.9)}$$

With:

A: solar azimuth angle, (deg)

II.3.6. Solar zenith angle

As an alternative, the sun's altitude may be described in terms of the solar zenith angle θ_z which is simply the complement of the solar altitude angle [124]:

$$\theta_z = 90^\circ - \alpha \tag{II.10}$$

θ_z: solar zenith angle, (deg)

II.3.7. Maximum hours of daylight, times of sunrise and sunset

To predict the time of sunrise and sunset and the length of day, we can use the expression of the solar altitude angle. The hour angle for sunset (and sunrise) may be obtained from Equation (II.8) by substituting the condition that the solar altitude at sunset equals the angle to the horizon. If the local horizon is flat, the solar altitude is zero at sunset and the hour angle at sunset becomes [121,122,131]:

$$\omega_s = cos^{-1}(-tan\,\delta \cdot tan\,\phi) \tag{II.11}$$

With:

ω_s: hour angle at sunset, (deg)

Sunrise time and sunset time are given by equations:

$$t_{sr} = 12 - \frac{\omega_s}{15} \tag{II.12}$$

$$t_{st} = 12 + \frac{\omega_s}{15} \tag{II.13}$$

The maximum hours of daylight may be calculated as [121]:

$$S_0 = \frac{2 \cdot \omega_s}{15} \tag{II.14}$$

With:

S_0: hours of daylight at day, (h)

II.3.8. Angle of incidence

In the design of solar energy systems, it is most important to be able to predict the angle between the sun's rays and a vector normal (perpendicular) to the aperture or surface of the collector. This angle is called the angle of incidence. Knowing this angle is of critical importance to the solar designer, since the maximum amount of solar radiation energy that could reach a collector is reduced by the cosine of this angle [124, 132,133].

We develop the equations to calculate the angle of incidence for fixed axis, single axis tracking and also two axis (full) tracking apertures.

II.3.8.1. Fixed apertures (no-tracking)

The angle of incidence for an arbitrarily oriented surface or aperture that does not track may be described in figure II.2:

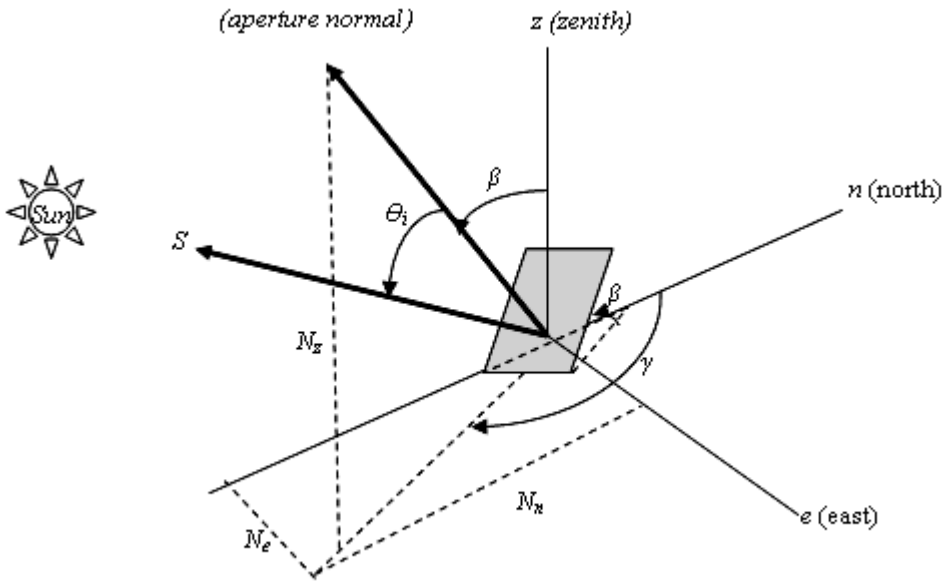

Figure II.2. Fixed collector arbitrarily oriented.

The expression of the angle of incidence in term of the orientation of the collector and the solar altitude and azimuth angles is:

$$\theta_i = cos^{-1}\left(sin\,\alpha \cdot cos\,\beta + cos\,\alpha \cdot sin\,\beta \cdot cos(\gamma - A)\right) \qquad \text{(II.15)}$$

With:

θ_i *:* angle of incidence, (deg)

β: aperture tilt angle from the horizon, (deg) :

γ : tilt angle of the aperture axe from the North, (deg) ;

Special cases of Equation (III.15) are:

a- For tilted aperture facing south: (γ=180°)

$$\theta_i = cos^{-1}\left(sin\,\alpha \cdot cos\,\beta + cos\,\alpha \cdot sin\,\beta \cdot cos\,A\right) \quad \text{(II.16)}$$

b- For horizontal apertures: (β=0°)

$$\theta_i = cos^{-1}\left(sin\,\alpha\right) \quad \text{(II.17)}$$

c- For vertical apertures:(β=90°)

$$\theta_i = cos^{-1}\left(cos\,\alpha \cdot cos(\,\gamma - A\,)\right) \quad \text{(II.18)}$$

II.3.8.2 Tracking apertures

Certain types of concentrating collector are designed to operate with tracking rotation about only one or two axis. The other important angle for the tracking apertures is the tracking angle measures rotation about the tracking axis.

II.3.8.2.1. Single-axis tracking apertures

Here, a tracking drive system rotates the collector about an axis of rotation until the sun central ray and the aperture normal are coplanar as described in figure II.3.

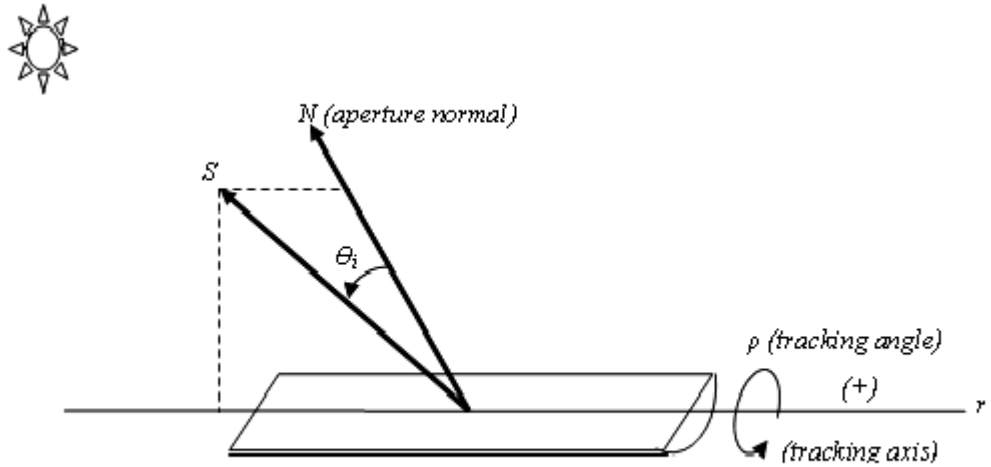

Figure II.3. Tracking drive system rotates the collector about one axis

We develop equations for the angle of incidence and the tracking angle, first for cases where the tracking axis is arbitrarily oriented but still parallel to the surface of the earth, and then for cases where the tracking axis is inclined relative to the surface of the earth [132-134].

a- Horizontal tracking axis oriented in North- South:

$$\rho = tan^{-1}\left(sin\, A / tan\, \alpha\right) \tag{II.19}$$

$$\theta_i = cos^{-1}\left(1-(cos\,\alpha)^2 \cdot (cos\, A)^2\right)^{0,5} \tag{II.20}$$

Where ρ is the tracking angle, (deg). The tracking angle is a measure of the rotation about the tracking axis.

b- Horizontal tracking axis oriented in East-West:

$$\rho = tan^{-1}\left(-cos\, A / tan\, \alpha\right) \tag{II.21}$$

$$\theta_i = cos^{-1}\left(1-(cos\,\alpha)^2 \cdot (cos\, A)^2\right)^{0,5} \tag{II.22}$$

c- Tilted tracking axis toward the south at the local latitude angle:

When the one axis tracking is tilted from the horizontal by the latitude angle pointing due south as shown in figure II.4, the axis of tracking becomes parallel to the rotation of the

earth about its axis pointing towards the polar star. The tracking angle and the incidence angle are equal to:

$$\rho = \omega$$
$$\theta_i = \delta \quad \text{(II.23)}$$

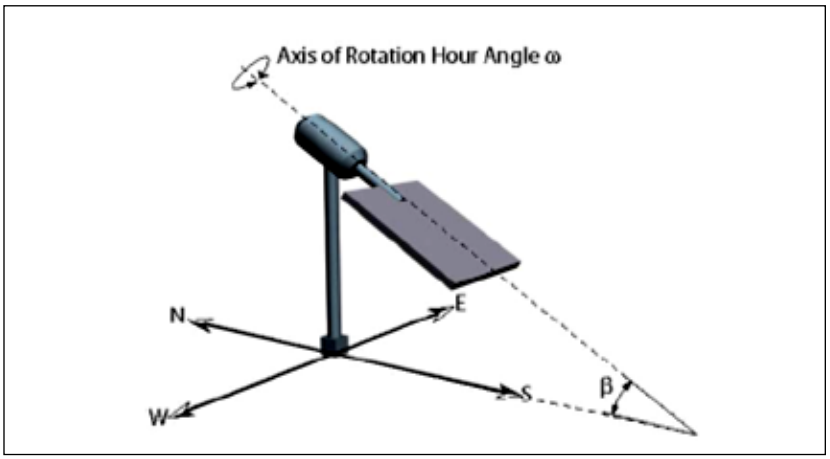

Figure II.4. One axis sun tracking systems with tilt angle equal to the latitude angle [130].

II.3.8.2.2. Two-axis tracking apertures

With two-axis tracking, a collector aperture will always be normal to the sun. Therefore the cosine effect does not come into play and:

$$cos\,\theta_i = 1 \quad \text{(II.24)}$$

For aiming an aperture toward the sun at all times, rotation about two axes is always required as shown in figure II.5. Two types of tracking mechanism are commonly in use for this purpose: azimuth / elevation tracking systems (also called az-el systems) and polar or equatorial tracking systems [118,124,130,135,136]:

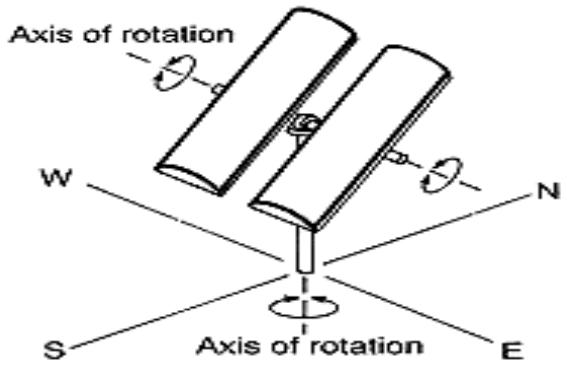

Figure II.5. Two axis sun tracking systems.

a- Polar (Equatorial) tracking

In this type of tracking, one axis is tilted by the local latitude angle of the location, and the tracking angle at this axis rotates with an angle equal to the hour angle:

$$\rho_1 = \omega \tag{II.25}$$

Moreover, the tracking angle of the second axis (which is perpendicular to the hour angle rotation axis) rotates with a tracking angle equal to the declination angle:

$$\rho_2 = \delta \tag{II.26}$$

The hourly variation of declination angle is considered very slow; hence the tracking at this axis can be adjusted once or a few times during the day. Figure II.6 shows a two axis equatorial sun tracking system with tilt angle equal to the latitude angle.

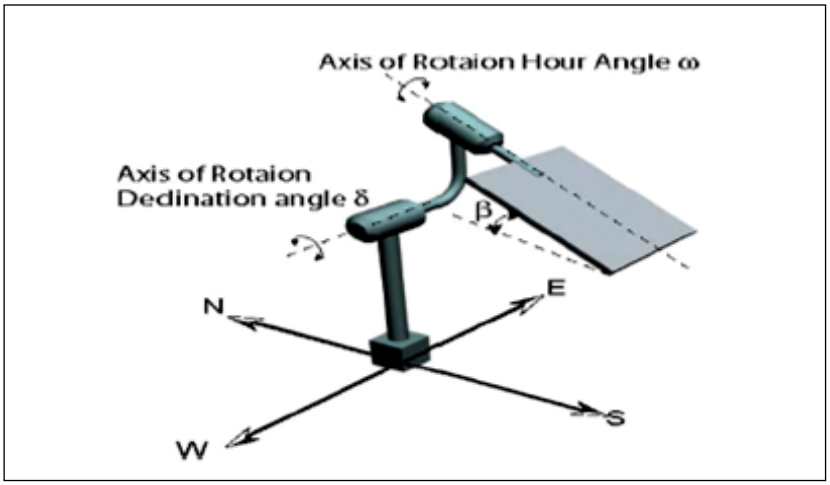

Figure II.6. Two axis equatorial sun tracking system with tilt angle equal to latitude angle [130].

b- Azimuth/Elevation tracking

The design of the azimuth/elevation tracking includes one axis rotating about the zenith axis (perpendicular axis) with a tracking angle equivalent to the azimuth angle:

$$\rho_1 = A \tag{II.27}$$

While the other axis is parallel to the surface of the earth and is rotating with a tracking angle equal to the altitude angle:

$$\rho_2 = \alpha \tag{II.28}$$

In the azimuth/elevation tracking, the two motors are required to work all day long near the zenith, and ρ1 is increasing quickly to follow the sun in the middle of the sky. Figure II.7 shows a two axis azimuth/elevation sun tracking system.

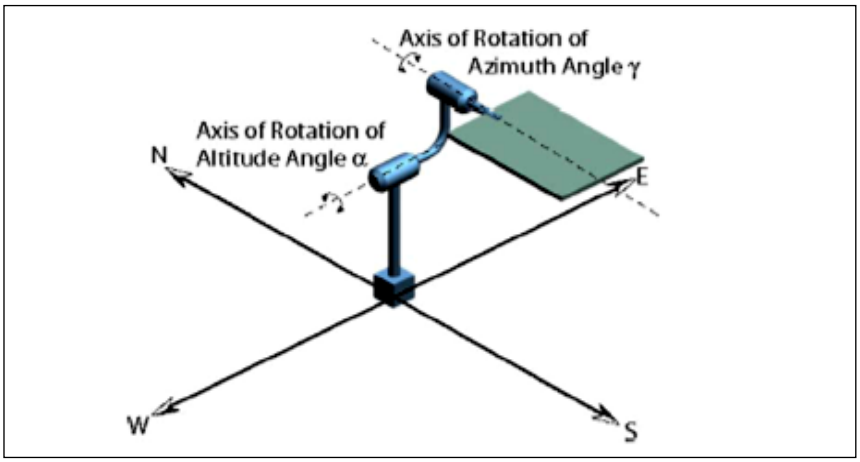

Figure II.7. Two axis azimuth/elevation sun tracking system with tilt angle equal to latitude angle [130].

II.4. Direct normal solar irradiance

For concentrating solar collector, the solar designer is only interested in the direct irradiance incident on the aperture. The Direct normal solar irradiance, the rate at which solar energy is incident on the aperture per unit aperture area, may be calculated from the beam radiation *Ibn* and the angle of incidence using the relation [120,121,125,137,138]:

$$Iba = Ibn \cdot cos\left(\theta_i\right) \qquad \text{(II.29)}$$

II.4.1. beam radiation

Hottel, (1976) [125], has presented a method for estimating the beam radiation *Ibn* (W/m^2) transmitted through clear atmospheres which takes into account zenith angle and altitude for a standard atmosphere and four climate types [120,125,137,138]. The beam irradiance is given by:

$$Ibn = I_0 \cdot \tau b \qquad \text{(II.30)}$$

With:

τb: the atmosphere transmittance of beam radiation. τb is given by [120,125,137,138]:

$$\tau b = a_0 + a_1 \cdot exp\left(-k / \cos\theta_z\right) \quad \text{(II.31)}$$

The constant ao, a1 and k for the standard atmosphere with 23 km visibility are given for altitudes *Al* less than 2.5 km by [125]:

$$\begin{aligned} a_0^* &= 0{,}4237 - 0{,}00821 \cdot (6 - Al)^2 \\ a_1^* &= 0{,}5055 - 0{,}005958 \cdot (6{,}5 - Al)^2 \\ k^* &= 0{,}2711 - 0{,}01858 \cdot (2{,}5 - Al)^2 \end{aligned} \quad \text{(II.32)}$$

Where:

$$\begin{aligned} a_0 &= a_0^* \cdot r_0; \\ a_1 &= a_1^* \cdot r_1; \\ k &= k^* \cdot r_k \end{aligned} \quad \text{(II.33)}$$

The correction factors r_0, r_1 and r_k are given for climate types in table II.2.

Table II.2. Correction factors for climate types [120,125,137,138]

Climate type	r_0	r_1	r_k
Tropical	0,95	0,98	1,02
Mid latitude summer	0,97	0,99	1,02
Subarctic summer	0,99	0,99	1,01
Mid latitude winter	1,03	1,01	1,00

II.4.2. Direct solar radiation incident on a collector

The daily direct solar radiation is the irradiance on the aperture summed over a full day from sunrise to sunset [125,132,133,139]:

$$H_{ba} = \int_{t_{sr}}^{t_{st}} I_{ba} \cdot dt \quad \text{(II.34)}$$

H_{ba} is the daily direct solar radiation, (J/m^2); and t_{sr} and t_{st} respectively the sunrise time and the sunset time expressed in hours.

By using the Trapeze method for second order, the equation (III.35) to calculate the daily beam aperture solar energy becomes:

$$Hba = h \sum_{i=1}^{S_0 - 1} Iba(t_{sr} + ih) \qquad \text{(II.35)}$$

With :

h : integration step is one hour, (3600 sec)

Iba(t_{sr}+*ih*): Direct normal irradiance in the step (t_{sr}+*ih*), (W/m^2)

II.5. Estimation Algorithm

A computer code in FORTRAN language is developed to predict direct normal irradiance and direct solar radiation. Using the insolation models and applying the appropriate sun angle calculations developed here, we can make hour-by-hour computations of the solar energy incident on the aperture of a collector. With appropriate summing, the daily direct solar radiation may also be calculated [140].

The diagram of algorithm is shown in figure II.8. to calculate the direct normal irradiance and daily direct solar radiation on a collector aperture. The input data required are the day, the location, and the orientation of the collector and whether the collector is fixed or tracks the sun about one or two axes. Since it doesn't change rapidly, the declination angle may be calculated only once a day. Hourly calculations are then made of the hour angle and the sun's altitude and azimuth. These values are used in the appropriate equation for the angle of incidence and the tracking angle.

Direct normal irradiance is calculated once per hour and stored in an array. The DNI is then summed over the day through application of linear averaging between hours to give the daily direct solar radiation.

Figure II.8. Computation diagram

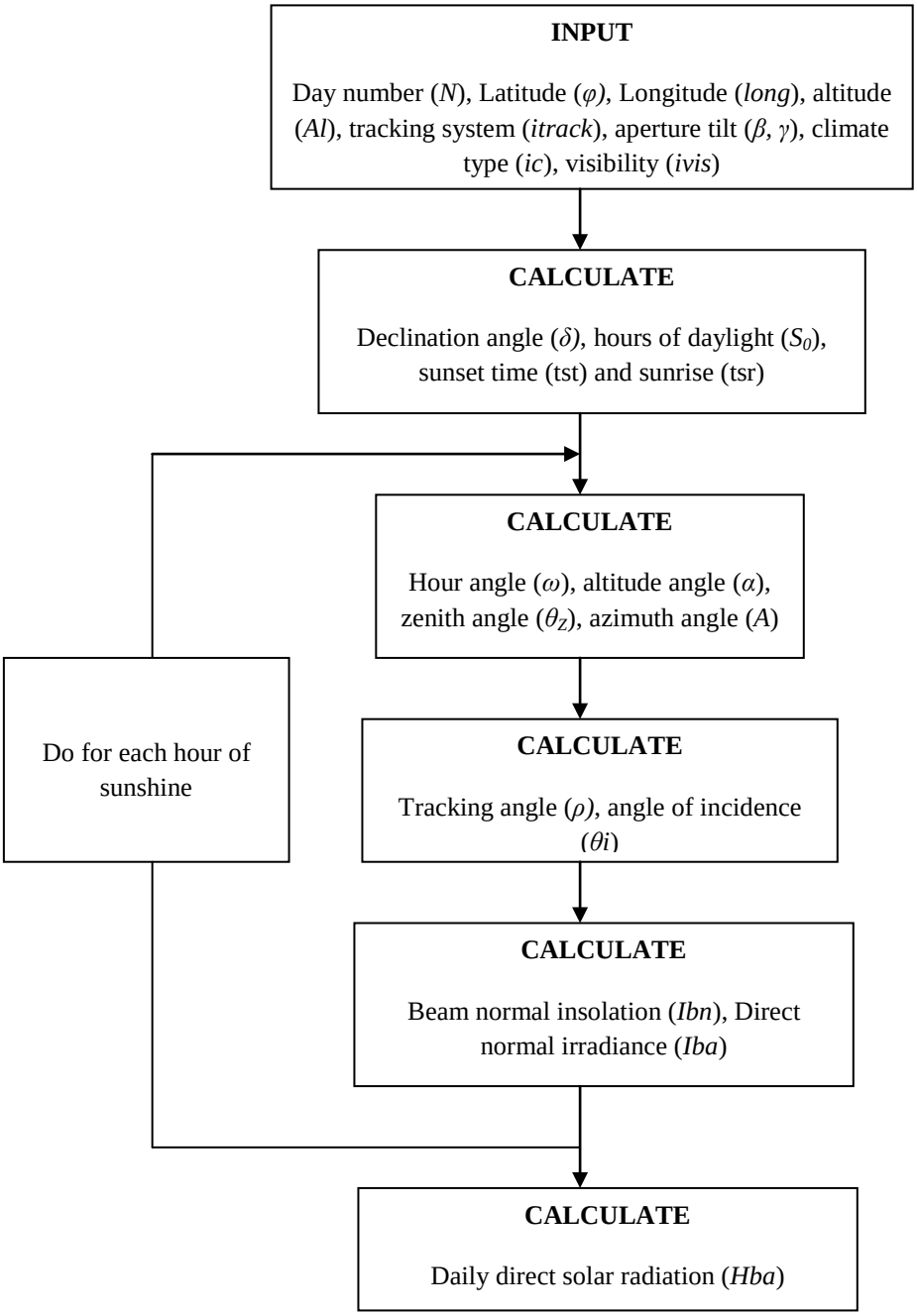

II.6. Results and discussion

Figure II.9 through figure II.12 show the results carried out for the location of Ghardaia (latitude +32,48°- longitude +3,66°- Altitude 500m). Figure II.9 and figure II.10 represent the direct normal irradiance and figures II.11 and II.12 represent the daily direct solar radiation on two typical clear days from summer and winter

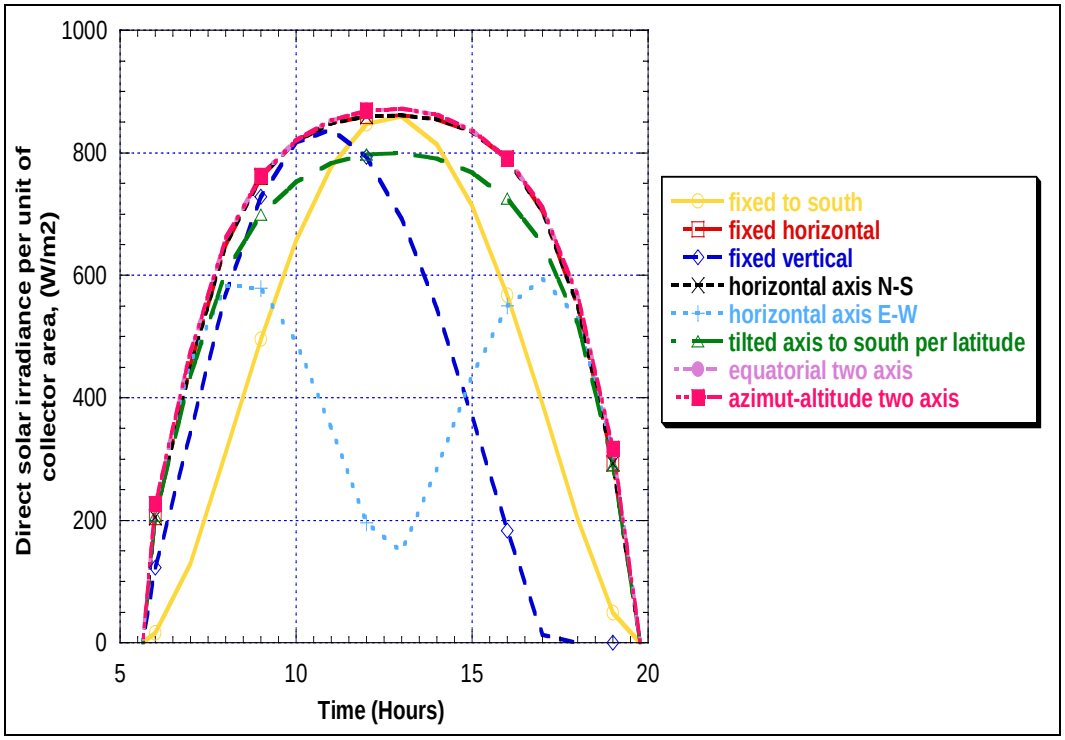

Figure II.9. Clear-day direct solar irradiance for different fixed and tracking system configurations for Ghardaia on June 21.

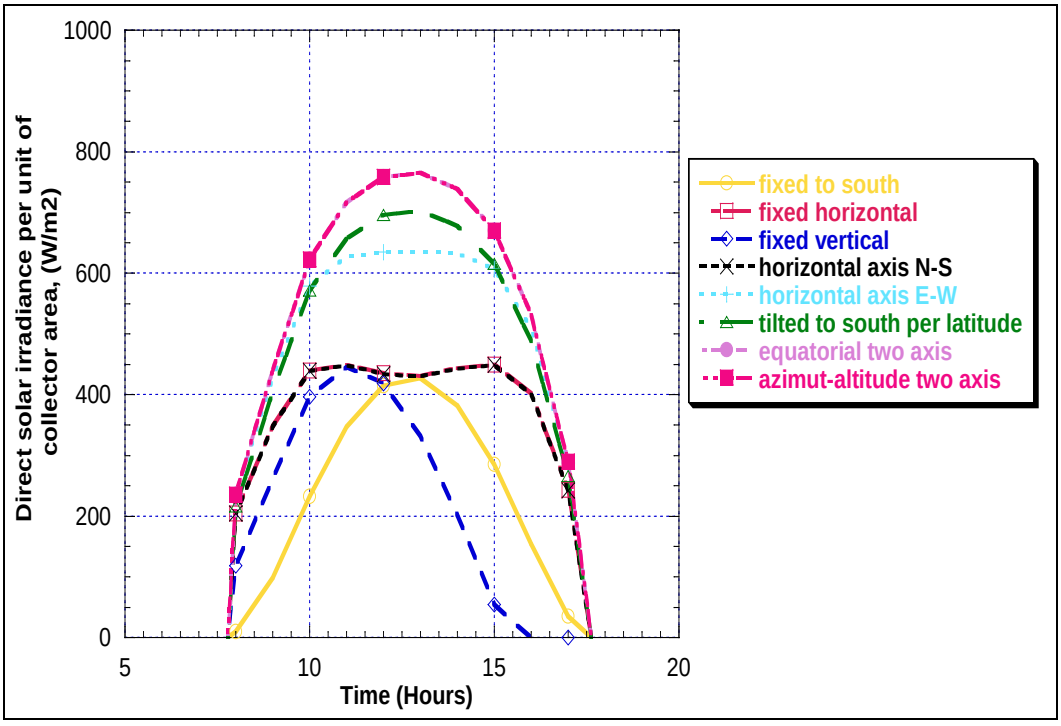

Figure II.10. Clear-day direct solar irradiance for different fixed and tracking system configurations for Ghardaia on December 21.

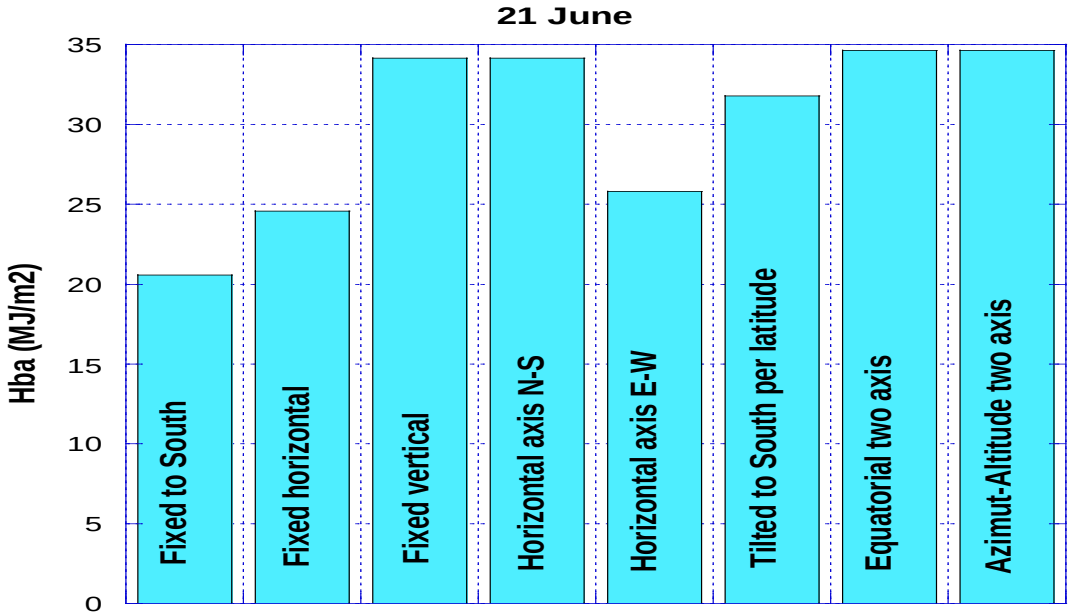

Figure II.11. Clear-day direct solar radiation for different fixed and tracking aperture configurations for Ghardaia on June 21

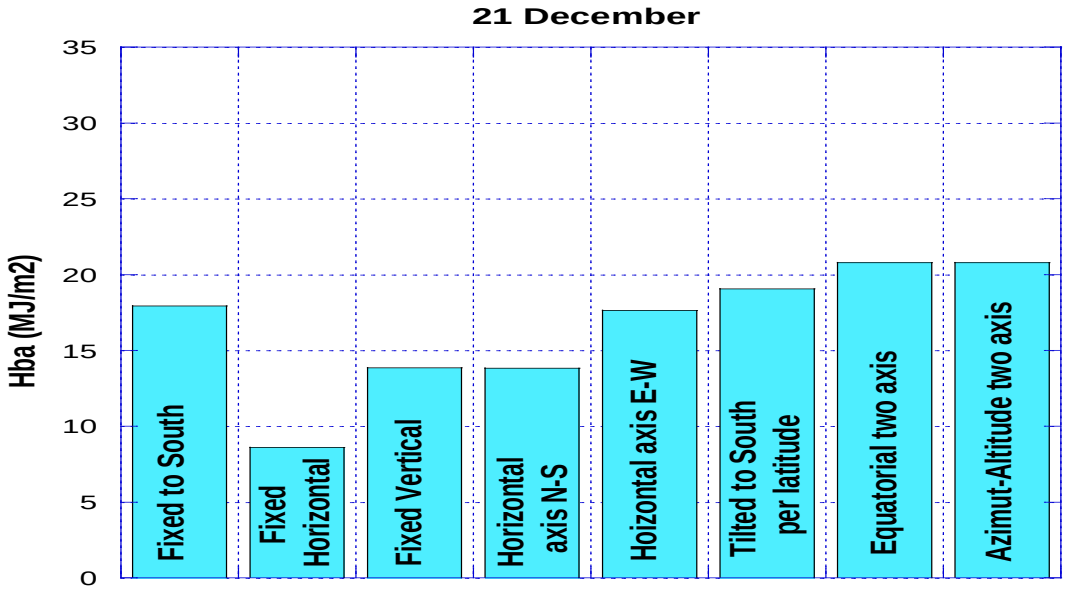

Figure II.12. Clear-day direct solar radiation for different fixed and tracking aperture configurations for Ghardaia on December 21

Figure II.9 and figure II.10 show that the maximum amount of the direct solar irradiance is collected when a collector aperture points directly towards the sun, therefore the angle of incidence is equal to zero. This occurs in the case of two-axis tracking aperture (equatorial and azimuth-altitude two axis). Figure II.9 and Figure II.11show that in the summer, if the single axis of tracking is oriented to the north/south (N/S) direction, the reduction in DNI from the two-axis tracking case is only about 1 percent. If the single

tracking axis is oriented in the east-west (E/W) direction, the amount of direct solar radiation entering the aperture of the E/W single-axis tracker is only 76 percent of the energy that could have been collected in two tracking system.

In the winter, as shown in Figure II.8, the reverse is true. The performance of the E/W oriented single axis tracked aperture approaches that of the two-axis tracked aperture even in the morning and afternoon. In fact, the E/W tracking aperture receives 84% of the maximum amount of energy, whereas the N/S-oriented single-axis tracking aperture receives only 64% of the maximum solar energy for that day, as can be seen in figure II.12. Taken over the entire year, the N/S-oriented single-axis-tracking aperture receives slightly more energy than does the E/W axis aperture. However, the variation of the daily irradiance over the year is much greater for the N/S axis orientation than for the E/W orientation.

For fixed aperture collector cases, the fixed horizontal aperture receives more direct normal irradiance over typical summer day than does latitude-tilted and south-facing apertures. In the winter, however, the horizontal fixed surface receives only 49 percent of the daily energy that a latitude- tilted surface does.

To select the most suitable solar tracking system over the year for the collector, we compared the monthly mean daily direct solar radiation with one and two axes tracking apertures in Ghardaia. The results are reported in figure II.13.

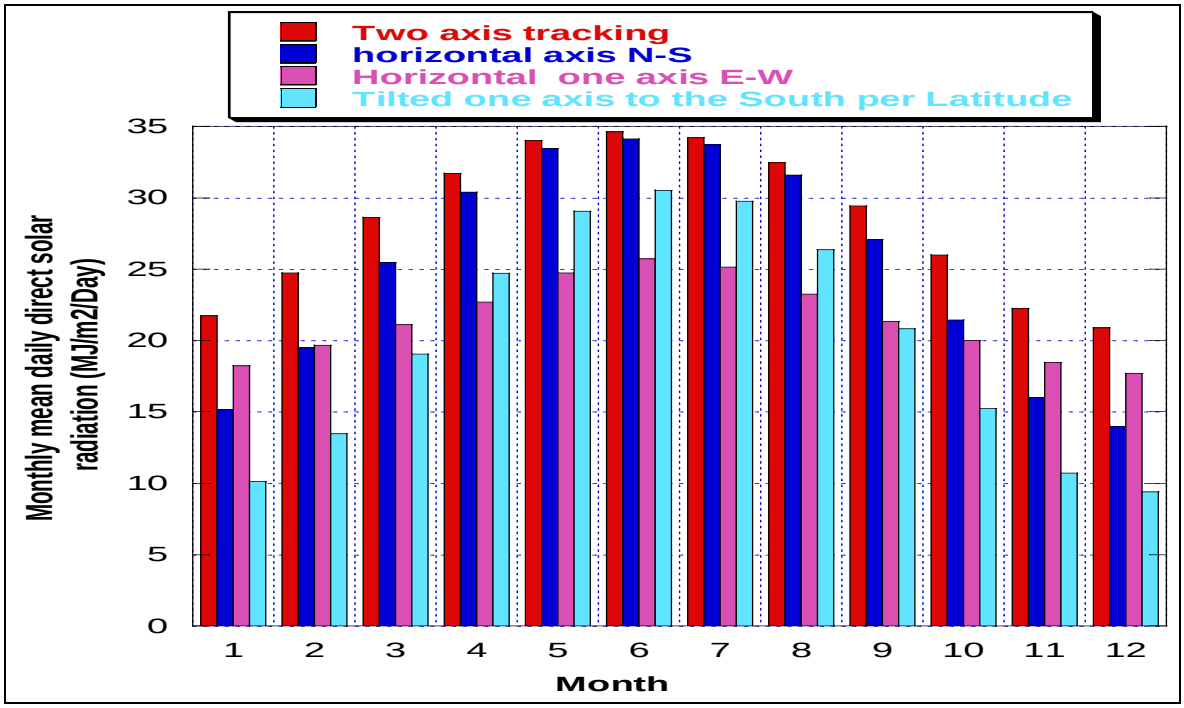

Figure II.13. Monthly mean daily direct solar radiation for one and two axis tracking system in Ghardaia.

The results in figure II.13 show clearly that the collector equipped with two-axis tracking system is most efficient than the collector equipped with one axis tracking system for the whole year. It can be seen also that the direct solar radiation provided by horizontal tracking axis North-South aperture is important in summer. In winter, the inverse is true; the direct solar radiation provided by horizontal tracking axis East-West is more important, while the tilted tracking axis aperture to the South per local latitude is the least efficient for all the year.

In order to compare the importance of direct solar radiation in different sites, we report in figure II.15 the monthly mean daily direct solar radiation for a two-axis tracking system at six typical locations in Algeria namely, Algiers, Annaba, Oran, Béchar, Ghardaia and Tamanrasset. As shown in figure II.14 these locations correspond to different climatic regions.

Figure II.14. Algerian map with the six selected locations, [141].

In Table II.3, the geographical positions and the type of climate for each location are reported.

Table II.3. Latitude angle, longitude angle, altitude from mean sea level, and climate type for different locations.

Climate type	Altitude (km)	Longitude (deg)	Latitude (deg)	Location
Mid latitude summer	0,025	3,15	36,43	Algiers
Mid latitude summer	0,040	7,8	36,8	Annaba
Mid latitude summer	0,099	-0,37	35,38	Oran
Tropical	0,806	-2,15	31,38	Bechar
Tropical	0,500	3,66	32,48	Ghardaia
Tropical	1,378	5,31	22,47	Tamanrasset

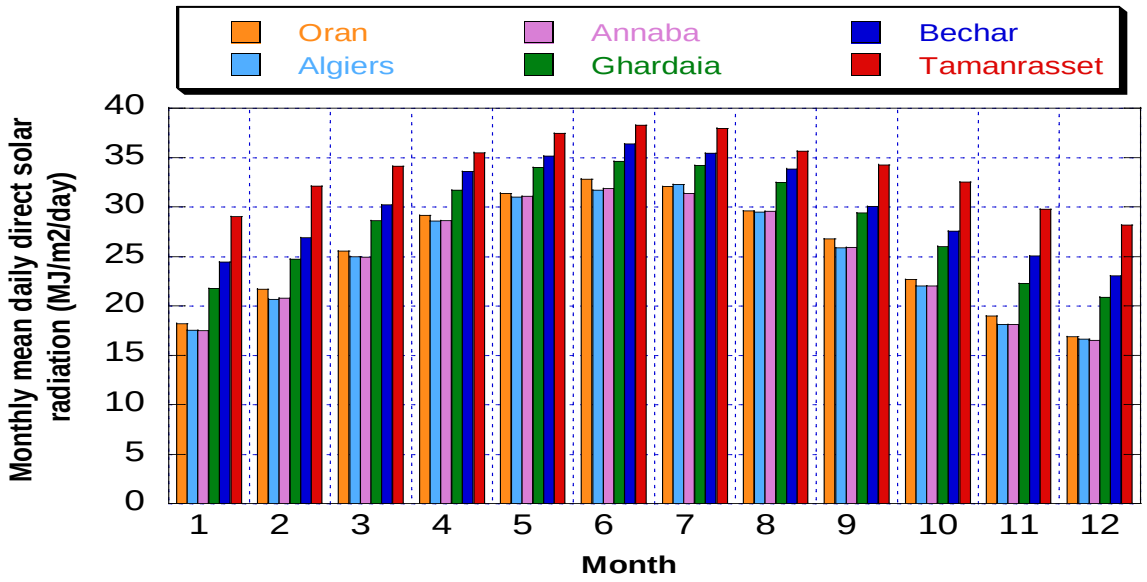

Figure II.15. Monthly mean daily direct solar radiation for a two-axis tracking system for different locations in Algeria.

Figure II.15 shows that the most important direct solar radiation potential is found in the Sahara for Ghardaia, Béchar and the best in Tamanrasset. The monthly mean daily direct solar radiation varies for Oran, Algiers and Annaba between 16 MJ/m^2/day and 32 MJ/m^2/day, for Bechar between 23 MJ/m^2/day and 37 MJ/m^2/day, Ghardaia between 20 MJ/m^2/day and 35 MJ/m^2/day and Tamanrasset between 28 MJ/m^2/day and 38 MJ/m^2/day. The peak of direct solar radiation occurs in July in the cases of Algiers with 32.25 MJ/m^2/day and June for Annaba, Oran, Bechar, Ghardaia and Tamanrasset with 31.85 MJ/m^2/day, 32.83 MJ/m^2/day, 36.37 MJ/m^2/day, 34.61 MJ/m^2/day and 38.24 MJ/m^2/day, respectively. In table

II.4, the annual direct normal solar radiation of two-axis tracking system was estimated and presesented for the six Algerian locations.

Table II.4. Annual direct normal solar radiation for two-axis tracking system for different locations in Algeria

Algerian Location	**Annual Direct Normal solar Irradiance (MWh/m^2/year)**
Oran	2.585
Algiers	2.518
Annaba	2.522
Ghardaia	2.88
Bechar	3.25
Tamanrasset	3.42

II.7. Conclusion

A model, based on the clear sky, has been used to estimate the direct solar radiation at different locations representative of different climatic conditions in Algeria. Direct Normal Irradiance (DNI) is used to estimate the potential for concentrating solar collectors. The model incorporates various geographical and meteorological factors. The values of hourly direct solar irradiance for Ghardaia have been estimated for different tilted and tracking systems. The results reveal that the two tracking axis system is the most efficient system for the CSP. The values of the monthly mean daily direct solar irradiation for the six selected locations have been also estimated. The results reveal also that the most important DNI potential is found in the Sahara for Ghardaia between 20 MJ/m^2/day and 35 MJ/m^2/day, Béchar between 23 MJ/m^2/day and 37 MJ/m^2/day and the best in Tamanrasset between 28 MJ/m^2/day and 38 MJ/m^2/day. Knowledge of the solar radiation enables us to derive information about the performance of solar energy systems with many applications in estimating the direct solar radiation for the cities studied and possibly elsewhere with similar climatic conditions. Results show that DNI is very important. Knowing that concentrating solar power systems are economic only for locations with DNI above 1800 kWh/m^2/year with an average daily DNI above 5 kWh/m^2/day, prove that Algerian solar radiation is more than sufficient for the solar thermal exploitation of solar energy. This is more particularly true in the south.

Chapter III: Parabolic Trough Collector: Energy Balance Model

III.1. Introduction

Algeria has several advantages for the extensive use of the solar energy [11]. In order to deliver high temperatures with good efficiency, a high performance solar collector is required. Systems with light structures and low cost technology with good efficiency could be obtained with solar parabolic trough collector (solar PTC) [142,143]. Solar PTC technology is the most proven and lowest cost large-scale solar power generation in the Sunbelt countries [76,87-89].

In this chapter, we present a heat transfer model of tracking Solar Parabolic Trough Collector. Numerical model to predict thermal performance of parabolic trough collector under Algerian conditions has been proposed. In this model, the climatic and topographical conditions specific to the area have been taken into account by exploiting the direct solar radiation. To develop this model, the receiver has been divided into several segments and the energy balance has been applied in each segment over a section of the solar receiver. The system of differential equations that govern the heat balances in each segment has been solved using the modified Euler method. Three comparative studies are considered in this part. The first one analyzes the temperature change, the HTF heat gain, the heat losses in the absorber and the glass envelope and the thermal efficiencies for typical winter and summer days. The second one investigates the use of different thermal oils as heat transfer fluid in the receiver and compares their temperature profile and their thermal energy cost. The last one presents a comparison of HTF monthly heat gain for different Algerian locations in order to study the influence of the climatic conditions and solar radiation on the performances of the PTC.

III.2. Energy balance model of the parabolic trough collector

PTCs are made by bending a sheet of reflective surface into a parabolic shape. Typically thermal fluid circulating through a metal black tube absorber is placed along the focal line of the receiver. The absorber is covered with a glass envelope, with vacuum in the space between the receiver and cover, to decrease convective heat losses. The glass envelope protects the absorber from degradation and reduces heat losses. It is made typically from Pyrex, which maintains good strength and transmittance under high temperatures [103,108,113]. The distance between the absorber tube and glass envelope is sufficient to prevent large deflections from the hot absorber tube that might cause breakages in the cover [106]. The absorber is typically made of stainless steel covered with a selective coating that

has a high absorptance of solar radiation, (about 95%) and low thermal emittance (10%, 673K) for thermal radiation loss [114,116,120,144].The following assumptions have been made in the mathematical model:

1) One dimensional flow.
2) Vacuum in the annular space; there is no conduction from the high temperature absorber tube to the low temperature glass envelope.
3) Constant diameters and concentrator surfaces.
4) Negligible conduction losses at the ends of each trough.

The heat transfer model is based on an energy balance between the fluid and the surroundings. As shown in Figure III.1, the solar energy is reflected by the mirrors to the collector absorber where it is converted into thermal heat. A large fraction of this thermal energy is transferred to the HTF by forced convection. The remaining energy is transferred back to the glass envelope by radiation and natural convection. This fraction passes through the glass envelope by conduction and along with the energy absorbed by the glass envelope is lost to the environment by convection and to the sky by radiation [103,109].

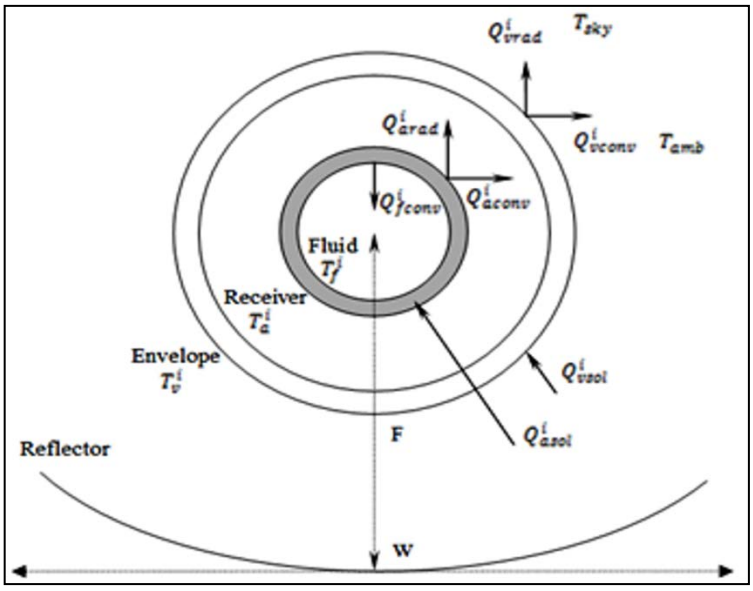

Figure III.1. Heat transfer plant for a solar PTC [145].

In order to obtain the ordinary differential equations that govern the heat transfer phenomena, the receiver and envelope were divided into several segments and the energy balance principle has been applied in each segment over a section of the solar receiver as shown in Figure III.2. The equations obtained for each component are showed below. It includes all equations and correlations necessary to predict the terms in the energy balances,

which depend on the collector type, HCE condition, nature of HTF, optical properties, and ambient conditions [104,109,120,146].

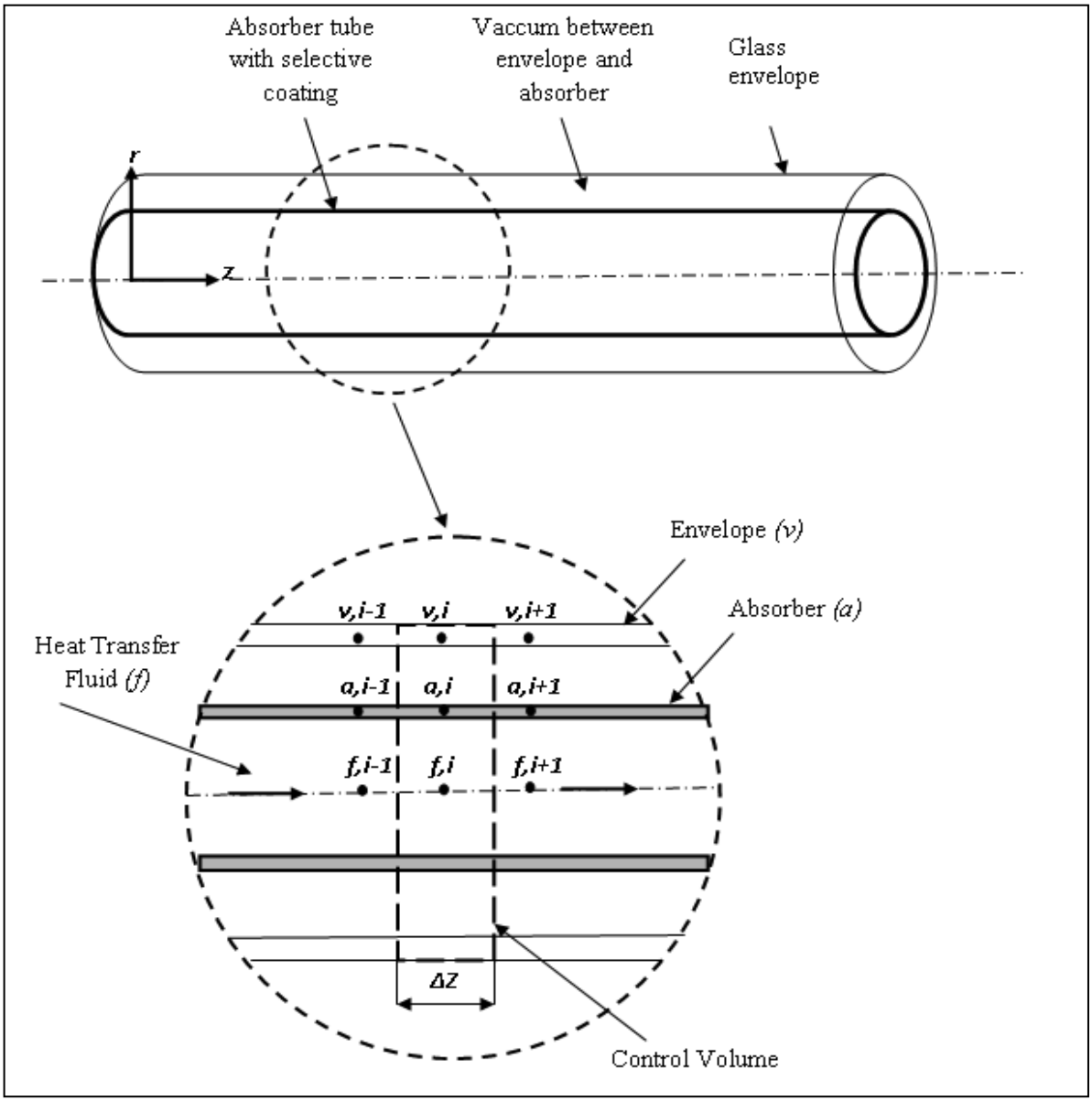

Figure III.2. Parts of a heat collection element (HCE).

III.2.1. Energy balance on the heat transfer fluid

We start with the HTF heat balance. This could be expressed by a temperature differential equation [104,120,146,147]. For a segment "*i*" of length Δz along the *z* position, the HTF partial equation is given by:

$$m_f^i \cdot C_f \cdot \frac{dT_f^i}{dt} = Q_z - Q_{(z+\Delta z)} + Q_{fconv}^i ; \qquad (i = 1, N) \tag{III.1}$$

From the above equation, the heat balance per unit of segment length is:

$$\rho_f \cdot A_f \cdot C_f \cdot \frac{dT_f^i}{dt} = F_f \cdot \rho_f \cdot C_f \cdot \left(T_f^{i-1} - T_f^i\right) / \Delta Z + h_f \cdot \pi \cdot D_{ai} \cdot \left(T_a^i - T_f^i\right) \quad \text{(III.2)}$$

With:

$$A_f = \pi \cdot \frac{D_{ai}}{4} \quad \text{(III.3)}$$

III.2.1.1. HTF convection heat transfer (h_f)

The HTF convection heat transfer coefficient h_f is given by:

$$h_f = Nu_f \cdot \frac{k_f}{D_{ai}} \quad \text{(III.4)}$$

The Nusselt number depends on the type of flow through the HCE. At typical operating conditions, the flow is well within the turbulent region. However, during off-solar hours, the flow may become transitional or laminar because of the viscosity of the HTF at lower temperatures. Therefore, the Nusselt number for each flow condition is:

III.2.1.1.1. Turbulent and transitional flow cases ($2300 \leq Re \leq 5.10^6$ and $0,5 \leq Pr \leq 2000$)

To estimate the convective heat transfer from absorber to the HTF for these cases, the following number correlation developed by Gnielinski (1976) [148, 149] is used.

$$Nu_f = \frac{(f/8)\cdot\left(Re_f - 1000\right)\cdot Pr_f}{1 + 12.7 \cdot \sqrt{f/8} \cdot \left(Pr_f^{2/3} - 1\right)} \quad \text{(III.5)}$$

With:

$$f = \left(0.79 \cdot \log_{10}\left(Re_f\right) - 1.64\right)^{-2} \quad \text{(III.6)}$$

$$Re_f = \frac{\rho_f \cdot v_f \cdot D_{ai}}{\mu_f} \quad \text{(III.7)}$$

$$Pr_f = \frac{C_f \cdot \mu_f}{k_f} \quad \text{(III.8)}$$

$$v_f = \frac{4 \cdot F_f}{\pi \cdot D_{ai}^2} \quad \text{(III.9)}$$

III.2.1.1.2. Laminar flow case ($Re < 2300$)

When the laminar option is chosen and the Reynolds number is lower than 2300, the Nusselt number will be constant. For pipe flow, the value will be 4.36 [148].

III.2.2. Energy balance on the receiver

By analogy with the equation of the HTF, the equation of the tube receiver on the segment "*i*" is given [104,120,150]:

$$m_a^i \cdot C_a \cdot \frac{dT_a^i}{dt} = Q_{asol} - Q_{fconv}^i - Q_{aconv}^i - Q_{arad}^i ; \quad (i = 1, N) \tag{III.10}$$

The heat balance per unit of segment length is then:

$$\rho_a \cdot A_a \cdot C_a \cdot \frac{dT_a^i}{dt} = \left[Q_{sol} \cdot \eta_a \cdot \alpha_a - h_f \cdot \pi \cdot D_{ai} \cdot \left(T_a^i - T_f^i\right) - h_a \cdot \pi \cdot D_{ae} \cdot \left(T_a^i - T_v^i\right) - \frac{\sigma \cdot \pi \cdot D_{ae} \cdot \left(T_a^{i4} - T_v^{i4}\right)}{\frac{1}{\varepsilon_a} + \frac{\left(1-\varepsilon_v\right) \cdot D_{ae}}{\varepsilon_v . D_{vi}}} \right] \tag{III.11}$$

With:

$$A_a = \frac{\pi}{4} \cdot \left(D_{ae}^2 - D_{ai}^2\right) \tag{III.12}$$

The direct normal incident solar irradiation received per unit length of receiver is:

$$Q_{sol} = I_{ba} \cdot \frac{A_c}{L} \tag{III.13}$$

With:

$$A_c = w \cdot L \tag{III.14}$$

The effective optical efficiency at the absorber is given by:

$$\eta_a = \eta_v \cdot \tau_v \tag{III.15}$$

The effective optical efficiency at the glass envelop is given by:

$$\eta_v = \varepsilon_1 \cdot \varepsilon_2 \cdot \varepsilon_3 \cdot \varepsilon_4 \cdot \varepsilon_5 \cdot \varepsilon_6 \cdot \rho_{cl} \cdot k \tag{III.16}$$

With:

$$k = \cos\theta_i + 0{,}000884 \cdot \theta_i - 0{,}00005369 \cdot \theta_i^2 \tag{III.17}$$

Where:

ε_1: HCE shadowing (bellows, shielding, supports)

ε_2: tracking error

ε_3: geometry error (mirror alignment)

ε_4: dirt on mirror

ε_5: dirt on HCE

ρ_{cl}: clean mirror reflectance

k: incident angle modifier.

θ_i: incident angle, (deg)

III.2.2.1. Convection heat transfer coefficient for the annulas gas (h_a)

Two heat transfer mechanisms are used to determine the convection heat transfer coefficient between the absorber and the glass envelop: the free-molecular convection and the natural convection.

III.2.2.1.1. Free-molecular convection ($P_a \leq 100$ mmHg)

When the HCE annulus is under vacuum, the convection heat transfer between the absorber and the glass envelope occurs by free-molecular convection [148]. Then, we have:

$$h_a = \frac{k_{std}}{\left(\frac{D_{ae}}{2 \cdot Ln(D_{vi}/D_{ae})} + b \cdot \lambda \cdot \left(\frac{D_{ae}}{D_{vi}} + 1\right)\right)} \quad \text{(III.18)}$$

With:

$$\lambda = \frac{2.331 \cdot 10^{-20} \cdot T_{moy1}}{P_a \cdot \delta^2} \quad \text{(III.19)}$$

$$b = \frac{(2-a) \cdot (9 \cdot \gamma - 5)}{2a \cdot (\gamma + 1)} \quad \text{(III.20)}$$

Where :

b: interaction coefficient;

λ : mean-free-path between collisions of a molecule, (cm);

δ : molecular diameter of annulus gas, (cm)

a : accommodation coefficient

γ : ratio of specific heats for the annulus

III.2.2.1.2. Natural convection ($P_a > 100$ mmHg)

When the HCE annulus loses vacuum (P_a>100mmHg), the convection heat transfer mechanism between the absorber and glass envelope occurs by natural convection. Incropera and De Witt (1990) correlation for natural convection in an annular space between horizontal cylinders is used for this case [148].

$$h_a = \frac{2 \cdot k_{eff}}{D_{ae} \cdot Ln(D_{vi}/D_{ae})} \quad \text{(III.21)}$$

With

$$\frac{k_{eff}}{k_a} = 0.386 \cdot \left(\frac{Pr_a}{0.861 + Pr_a} \right)^{1/4} \cdot Rac^{1/4} \quad \text{(III.22)}$$

$$Rac = \frac{g \cdot \beta \cdot (T_a - T_v) \cdot Lc^3}{\upsilon_a \cdot \alpha_a} \quad \text{(III.23)}$$

$$Lc = \frac{2_{.} \cdot \left[Ln(D_{vi}/D_{ae}) \right]^{4/3}}{\left[(D_{vi}/2)^{-3/5} + (D_{ae}/2)^{-3/5} \right]^{5/3}} \quad \text{(III.24)}$$

$$Pr_a = \frac{c_a \cdot \mu_a}{k_a} \quad \text{(III.25)}$$

$$\beta_a = \frac{1}{T_{moy1}} \quad \text{(III.26)}$$

Where:

k_{eff}: Effective thermal conductance of annulus gaz , (W/m.K);

k_a : thermal conductance of annulus gaz at Tmoy1, (W/m.K);

g : gravitational constant, (9,8 m^2/s);

β_a : volumetric thermal expansion coefficient (ideal gas), (K^{-1});

υ_a : kinematic viscosity of the annulus gaz, (m^2/s)

α_a : thermal diffusivity of the annulus gaz, (m^2/s)

c_a: HTF heat specific of the annulus gaz, (J/kg.K)

μ_a: Dynamic viscosity of the annulus gaz, (kg/m.s)

The correlation (III.22) is valid for range of $0,7 \leq Pr_a \leq 6000$ and $Rac \leq 10^7$. All physical properties (α_a, β_a, υ_a, k_a, c_a, μ_a) are evaluated at the average temperature Tmoy1.

III.2.3. Energy balance on the glass envelope

By analogy with the equation of the receiver and the HTF, the equation of the glass envelope on every segment "*i*" is given by [104,120,146, 148]:

$$m_v^i \cdot C_v \cdot \frac{dT_v^i}{dt} = \left[Q_{vsol}^i + Q_{arad}^i + Q_{aconv}^i - Q_{vrad}^i - Q_{vconv}^i \right]; \quad (i = 1, N) \quad \text{(III.27)}$$

The heat balance per unit of length is then:

$$\rho_v \cdot A_v \cdot C_v \cdot \frac{dT_v^i}{dt} = \left[\begin{array}{l} Q_{sol} \cdot \eta_v \cdot \alpha_v + h_a \cdot \pi \cdot D_{ae} \cdot \left(T_a^i - T_v^i\right) + \dfrac{\sigma \cdot \pi \cdot D_{ae} \cdot \left(T_a^{i4} - T_v^{i4}\right)}{(1/\varepsilon_a) + \left((1-\varepsilon_v) \cdot D_{ae}/\varepsilon_v \cdot D_{vi}\right)} - \\ h_v \cdot \pi \cdot D_{ve} \cdot \left(T_v^i - T_{amb}\right) - \sigma \cdot \pi \cdot D_{ve} \cdot \varepsilon_v \cdot \left(T_v{}^{i4} - T_{sky}{}^4\right) \end{array} \right] \quad \text{(III.28)}$$

With:

$$A_v = \frac{\pi}{4} \cdot \left(D_{ve}{}^2 - D_{vi}{}^2\right) \quad \text{(III.29)}$$

$$T_{sky} = 0.0552 \cdot T_{amb}^{1.5} \quad \text{(III.30)}$$

III.2.3.1. Convection heat transfer coefficient for air ambient (h_v)

The convection heat transfer coefficients form the glass envelope to the atmosphere is given by:

$$h_v = Nu_{air} \cdot \frac{k_{air}}{D_{ve}} \quad \text{(III.31)}$$

The Nusselt number depends on whether the convection heat transfer is natural or forced.

III.2.3.1.1. Wind case (forced convection)

If there is wind, the convection heat transfer will be forced convection. The correlation developed by Zhukauskas will be used to estimate the Nuselt number [148].

$$Nu_{air} = C \cdot Re_{air}^m \cdot Pr_{air}^n \cdot \left(\frac{Pr_{air}^{'}}{Pr_{air}^{''}}\right)^{1/4} \quad \text{(III.32)}$$

The correlation parameters are given in Table III.1:

Table III.1. Parameters of the correlation (III.32)

Re	***c***	***M***
1-40	0.75	0.4
40-1000	0.51	0.5
1000-200 000	0.26	0.6
200 000-1000 000	0.076	0.7

The exponential term is given by:

n=0.37 pour Pr≤10

n=0.36 pour Pr>10

The correlation given by equation (IV.32) is valid for the $0,7 \leq Pr \leq 500$ and $1 \leq Re \leq 10^6$.

III.2.3.1.2. No wind case (natural convection)

For this case, the correlation developed by Churchill et Chu (1990) will be used to estimate the Nusselt number [148, 151].

$$Nu_{air} = \left[0.6 + \frac{0.387 \cdot Ra^{1/6}}{\left[1 + (0.559/Pr)^{9/16} \right]^{8/27}} \right]^2 \quad \text{(III.33)}$$

With:

$$Ra = \frac{g \cdot \beta_{air} \cdot (T_v - T_{amb}) \cdot D_{ve}^{\ 3}}{\alpha_{air} \cdot \upsilon_{air}} \quad \text{(III.34)}$$

$$\beta_{air} = \frac{1}{T_{moy2}} \quad \text{(III.35)}$$

$$Pr_{air} = \frac{\upsilon_{air}}{\alpha_{air}} \quad \text{(III.36)}$$

Where

β_{air} : volumetric thermal expansion coefficient (ideal gas), (K^{-1})

α_{air} : thermal diffusivity for the air at Tmoy2, (m^2/s)

υ_{air} : kinematic viscosity for the air at Tmoy2, (m^2/s)

The correlation (III.33) is valid for the $10^5 \leq Ra \leq 10^{12}$.

III.2.4. Heat balance for the system

The global HTF heat gained per unit length of the receiver Q_{gain} (W/m) is given by:

$$Q_{gain} = \frac{F_f \cdot \rho_f \cdot C_f \cdot \left(T_f^{out} - T_f^{in} \right)}{L} \quad \text{(III.37)}$$

With:

T_f^{out} : The HTF temperature at the output of the receiver, (K)

T_f^{in} : The HTF temperature at the input of the receiver, (K)

The heat loss of the system per unit length of receiver, Q_{loss} (W/m), includes heat loss by convection and radiation from the absorber to the envelope and heat loss by convection and radiation from the envelope to the environment:

$$Q_{loss} = \frac{\sum_{1}^{N} (Q^{i}_{aconv} + Q^{i}_{arad} + Q^{i}_{vrad} + Q^{i}_{vconv}) \cdot \Delta Z}{L} \quad \text{(III.38)}$$

The model allows evaluation of the collector thermal efficiency. According to Eq. (III.39), the collector thermal efficiency is represented by the ratio between global heat gain and direct solar irradiance:

$$\eta_{col} = \frac{Q_{gain}}{Q_{sol}} \cdot 100 \quad \text{(III.39)}$$

The daily HTF global heat gained per unit of receiver length, $Q_{gainday}$ (W/m/Day), is given by:

$$Q_{gainday} = h \cdot \sum_{i=1}^{S_0 - 1} Q^{i}_{gain} \quad \text{(III.40)}$$

Where:

h: integration step is one hour, (3600 sec)

S_0: the hours of daylight.

III.3. Algorithm

To determine the thermal characterisations of the HCE system, the system of ordinary differential equations obtained above has been solved using the modified Euler method. To this end, a global algorithm, developed under FORTRAN language, is used.

- The physical properties including the density, the specific heat, the dynamic viscosity, and the thermal conductivity have been taken at the HTF saturation pressure for different temperatures.
- The chosen collector is of LS-2 type with vacuum in the annulus space between the absorber and the glass envelope. The LS-2 specifications are reported in the Appendix.2 in Table A.7. The operational experience of the LS-2 collector about 65% of the collectors installed in nine SEGS built in the Californian desert has indicated good thermal performance [99,152].

- We consider in this preliminary study a number of 100 Solar Collector Assembly (SCA) with 7.8 m in length divided on a loops of 20 SCAs to demonstrate the PTC performance under Algerian conditions. The proposed plant is presented in figure III.3.
- Ambient Conditions include direct normal solar irradiance, wind speed, ambient temperature from the selected location for clear days from different seasons of the year.

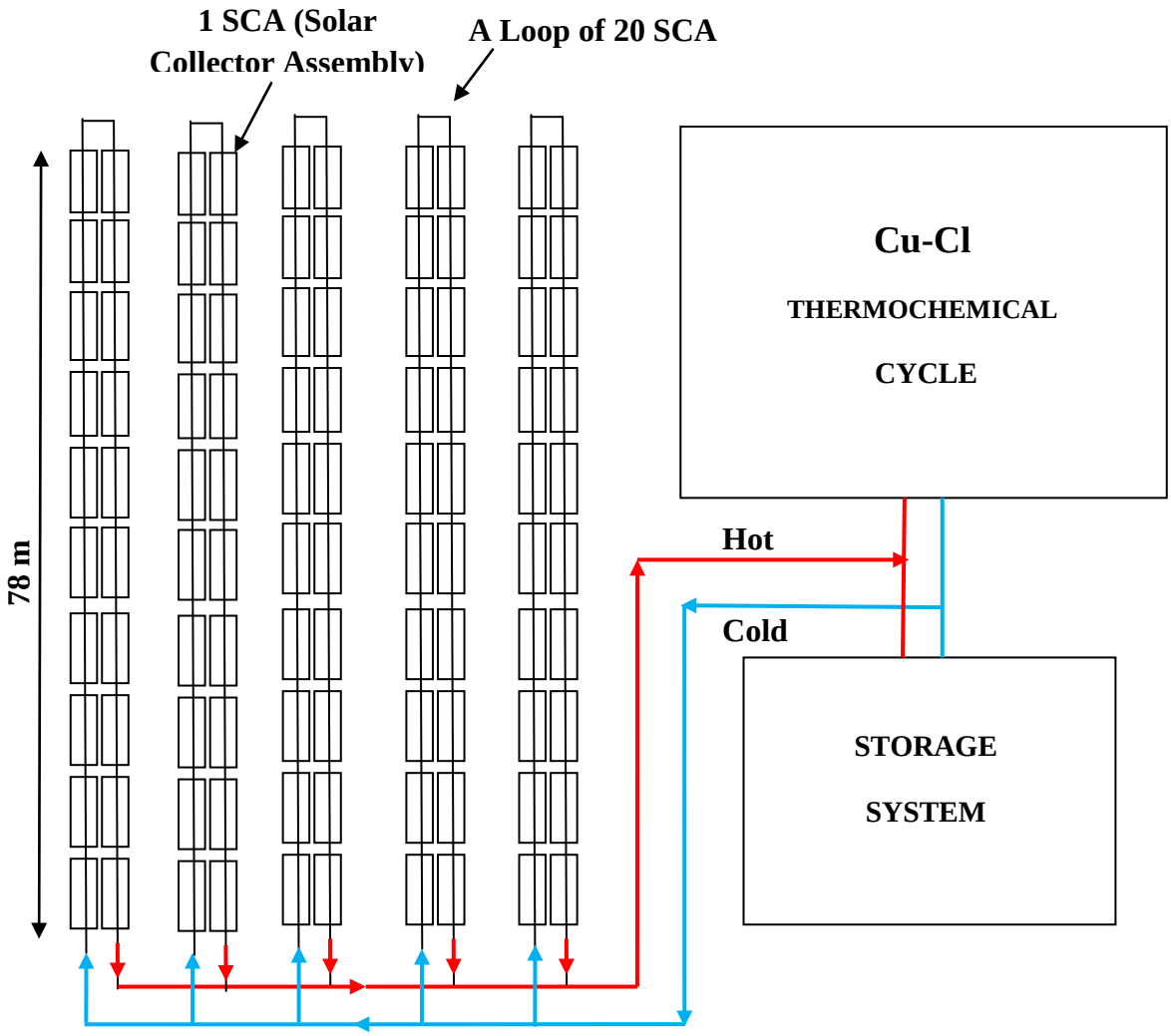

Figure III.3. Solar field layout for the proposed plant.

III.4. Results and discussion

The simulation results evaluate the thermal performance of PTC for different operating conditions. Different parameters are considered in this study, starting from temperature profile, heat gain, thermal efficiency, and heat loss with different tracking system, to the nature of the heat transfer fluid depending on geographic location of the plant.

III.4.1. Effect of the tracking system

In this part, Syltherm 800 HTF temperature profile have been estimated at the output of the receiver and compared with the temperature profiles of the absorber and the glass envelope. Two typical days of summer and winter are selected in the daylight period in clear sky to present this simulation. Three tracking system integrated with the PTC are studied namely; Two axis tracking system, one axis tracking system North-South and one axis tracking system East-West. Results are presented in Figure III.4.

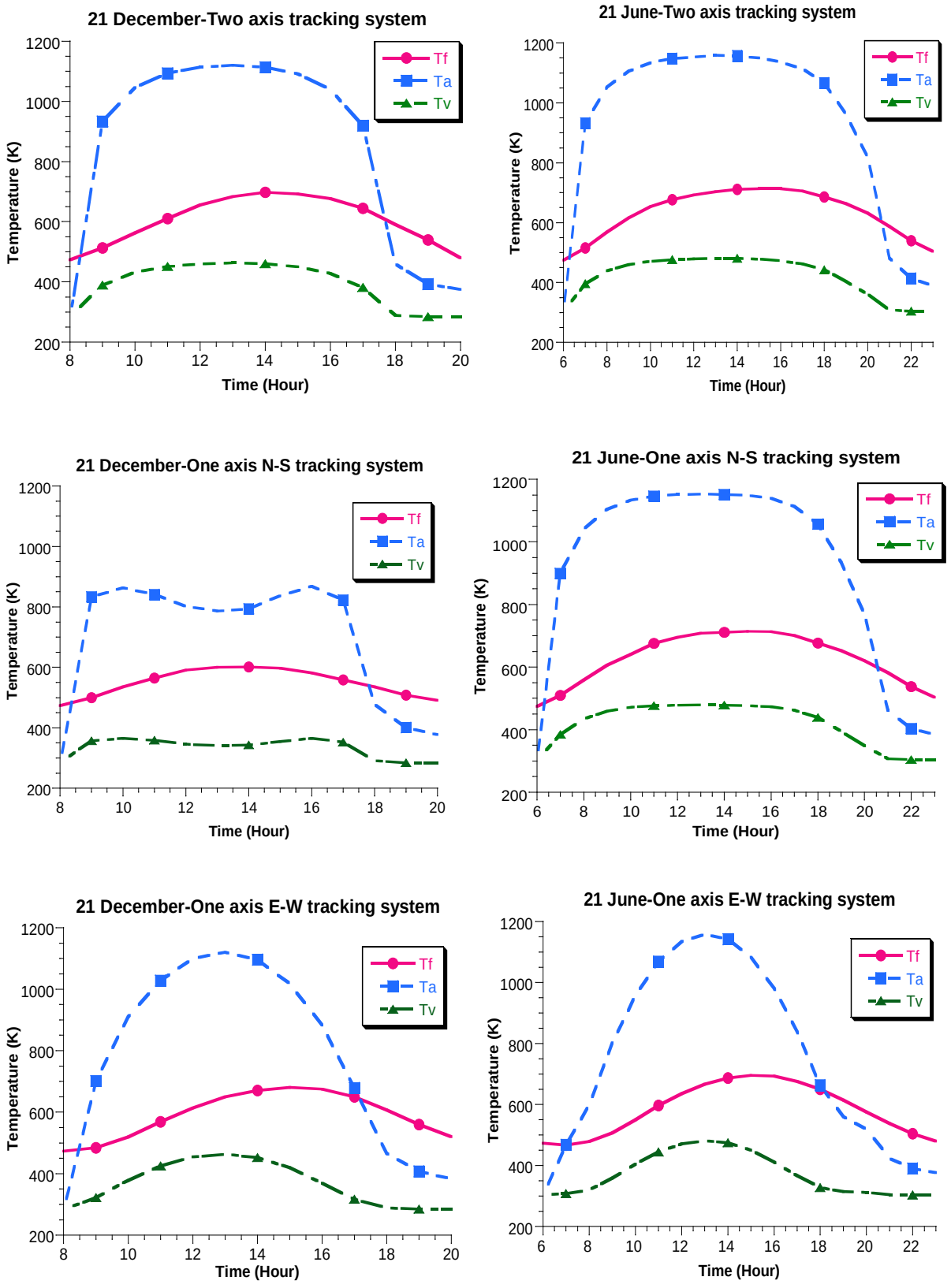

Figure III.4. Outlet Syltherm 800 temperature, absorber and glass envelope temperatures in day 21 December and 21 June for different tracking systems.

Figure III.4 presents the variation of the outlet temperatures of the Syltherm 800 HTF, of the absorber and the envelope as function of time for typical days of the year (summer and

winter) with different types of tracking system. According to the results, the maximum temperature of Syltherm 800 is reached in the case of PTC with two-axis tracking system. Figure III.4 shows that in the typical summer day, if the PTC is integrated with two axis tracking system or single axis oriented to the North/South, Syltherm 800 temperature exceeds 700K between 1 p.m. and 5 p.m. Furthermore, it reaches only 680 K around 3 p.m. with single axis oriented to the East/West tracking system. It can be seen also from figure III.4 that in the typical winter day, the HTF temperature exceeds 690K between 2 p.m. and 3 p.m. if the PTC is integrated with two axis, and exceeds 680 K around 3 p.m. with single axis E/W tracking system, whereas it reaches only 600 K with single axis N/S tracking system. These are due to the difference in the DNI and the sunshine duration. We note from Figure III.9 and Figure III.10 that the difference between the DNI on a N/S-oriented single-axis-tracking aperture and on a two-axis tracking aperture is only about 1 percent in summer. In the winter, the reverse is true, the E/W tracking aperture receives 80 percent of the maximum amount of DNI.

In order to study the thermal capacity of the PTC, Syltherm 800 heat gain and HCE heat loss per unit length of receiver in two typical days for different tracking systems are presented in Figure III.5. The collector thermal efficiency in these cases is also reported in Figure III.6.

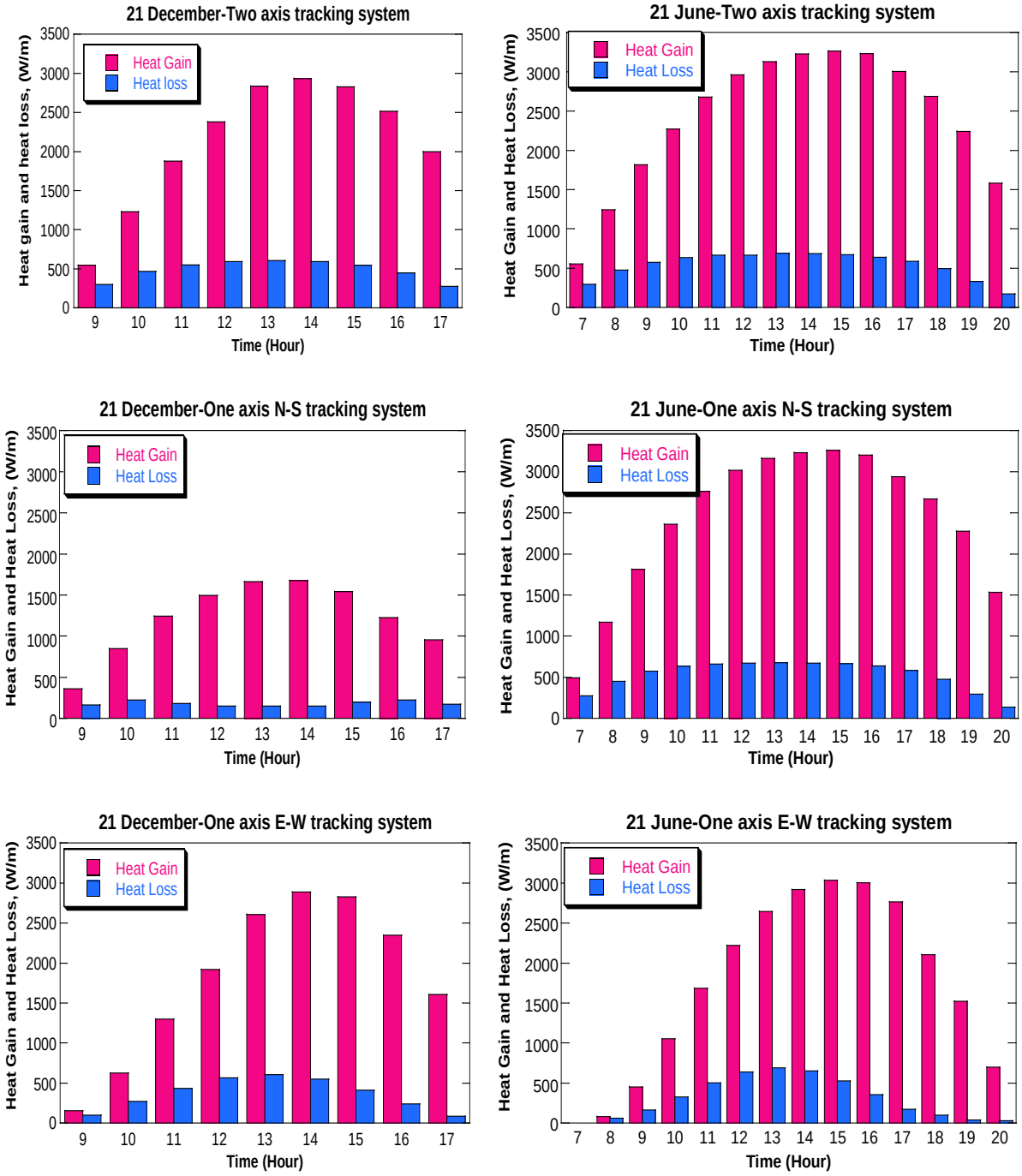

Figure III.5. Sylltherm 800 global heat gain and heat loss in 21 June and 21 December for different tracking system

We observe clearly from Figure III.4 and Figure III.5 that the heat gain follows perfectly the temperature profile of the thermal oil, whereas the heat loss follows the temperature profile of the absorber and the envelope. Figure III.5 and Figure III.6 prove that PTC equipped with two-axis tracking system is most efficient with global heat gain and thermal efficiency exceeds 3200 W/m and 75% in summer day, and reach 3000 W/m and 70% in winter day, respectively. These Figures prove also that heat gain provided by PTC equipped with horizontal axis N/S tracking system is important than horizontal axis E/W

tracking system in typical summer day with heat gain and thermal efficiency exceed 3000 W/m and 70%, respectively. In typical winter day, the inverse is true; the heat gain provided by PTC equipped with horizontal tracking axis E/W is more important with global heat gain and thermal efficiency exceed 2800 W/m and 65%, respectively.

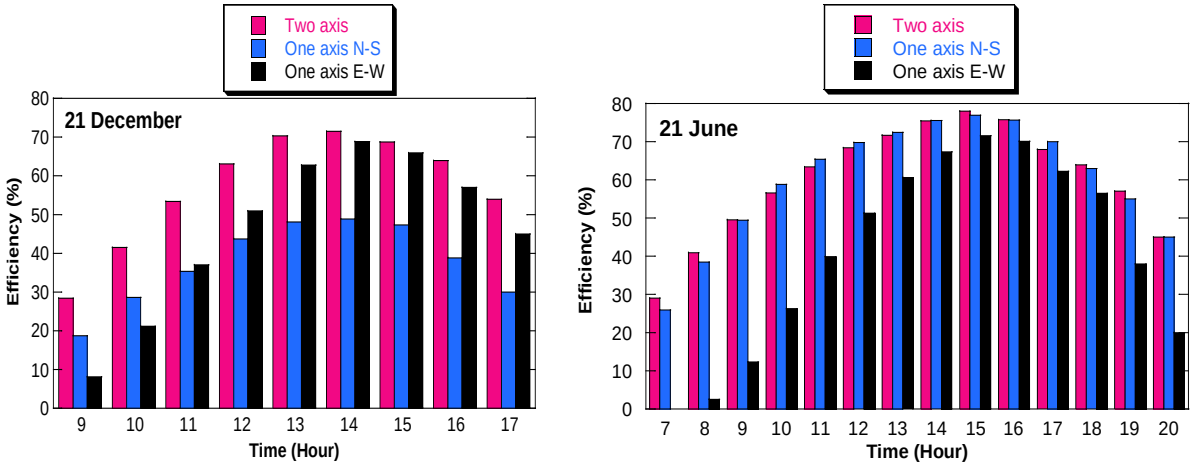

Figure III.6. Thermal efficiency in day 21 December and 21 June for different tracking system

III.4.2. Effect of the nature of HTF

In the second part of results, a comparison between the outlet temperatures profiles of different thermal oils used as heat transfer fluids is carried out. The HTF considered in this study are: Syltherm 800, Syltherm XLT, Marlotherm SH, Marlotherm X, Santotherm LT, Santotherm 59, and Therminol D12 [153].

The thermal oils considered in this study are not only highly stable but also designed for high temperature liquid phase operation with good heat transport and transfer properties. The fluids exhibit low potential for fouling and can often remain in service for many years. HTFs are also suitable for use in heating and cooling systems with good thermal stability in application range and non-corrosive to materials of construction.

This comparison is considered for the case of winter and summer in daylight period for clear sky with one axis tracking system oriented to the South-North direction. The results are reported in Figure III.7 and Figure III.8.

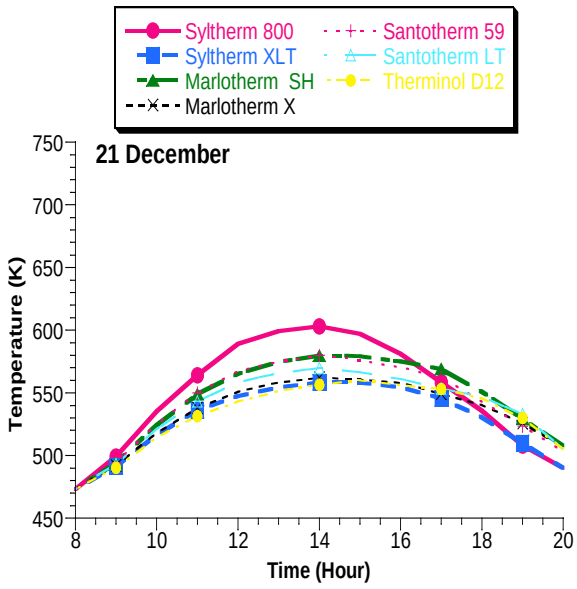

Figure III.7. HTFs temperature in 21 December

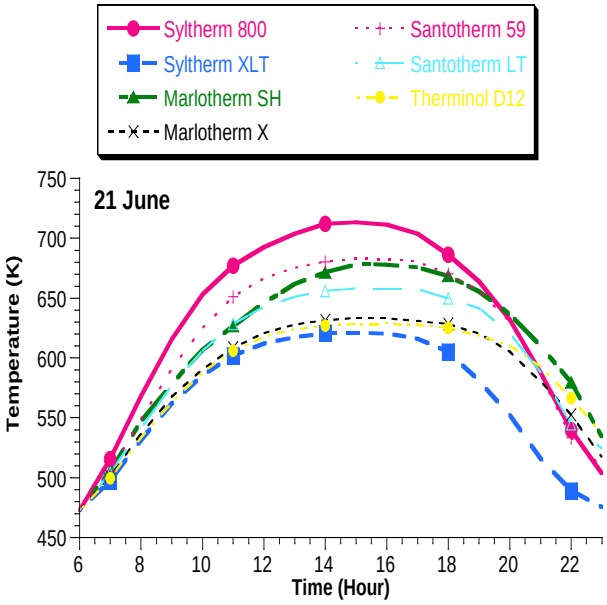

Figure III.8. HTFs temperature in 21 June

The curves in the above mentioned figures reveal that each type of fluid has a range of recommended operating temperatures. The highest peak of temperature is related to the Sylltherm 800 which exceeds 600 K in December and 700 K in June. The temperatures of the three thermal oils; Marlotherm SH, and Santotherm 59 exceed 680K in June and reach 580K in December. Whereas Therminol D12, Santotherm LT, Marlotherm X and Sylltherm XLT have showed the lowest temperature between 550K and 650K. We can explain these differences in HTFs temperatures by considering the evolution of HTFs physical properties (density, heat capacity conductivity and viscosity) reported in Figure III.9 trough Figure III.12. We noticed from these Figures that the four physical properties influence the temperature evolution of each fluid. Thus, the three fluids (Sylltherm 800, Marlotherm SH and santotherm 59) which have maximum range of temperature have the most important density, conductivity and viscosity and have lowest heat capacity.

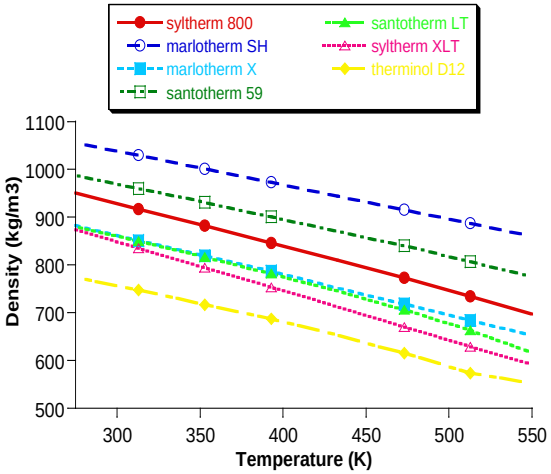

Figure III.9. HTFs density with temperature.

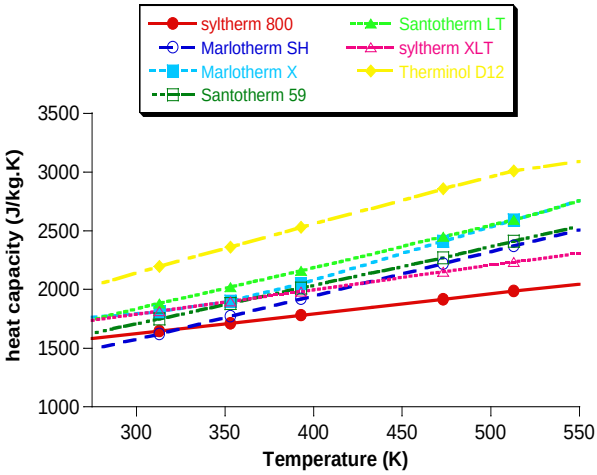

Figure III.10. HTFs heat capacity with temperature.

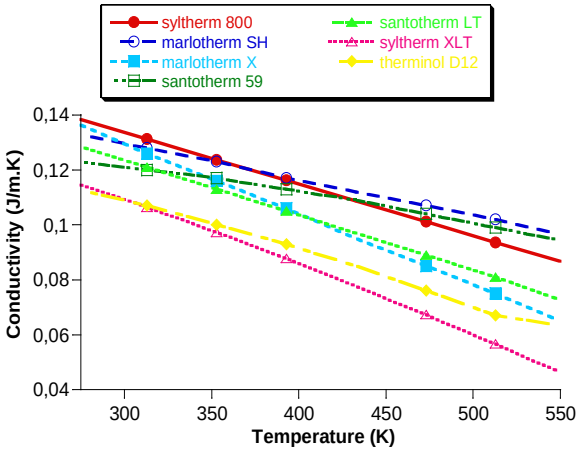

Figure III.11. HTFs thermal conductivity with temperature.

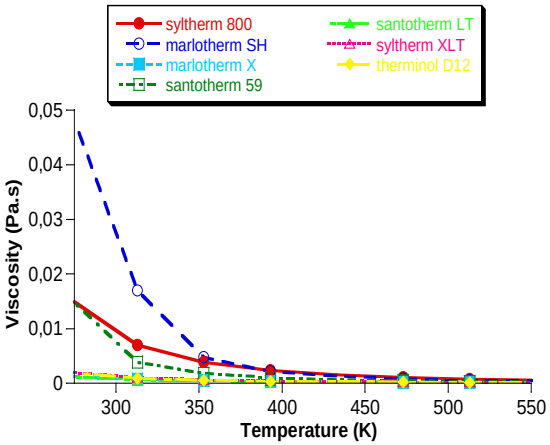

Figure III.12. HTFs viscosity with temperature.

III.4.3. Effect of the Algerian climatic regions

In this part, the monthly mean daily global heat gain of Syltherm 800 is determined for six Algerian locations in Figure III.13. The results are given for PTC system with one axis tracking system oriented to the North/South direction.

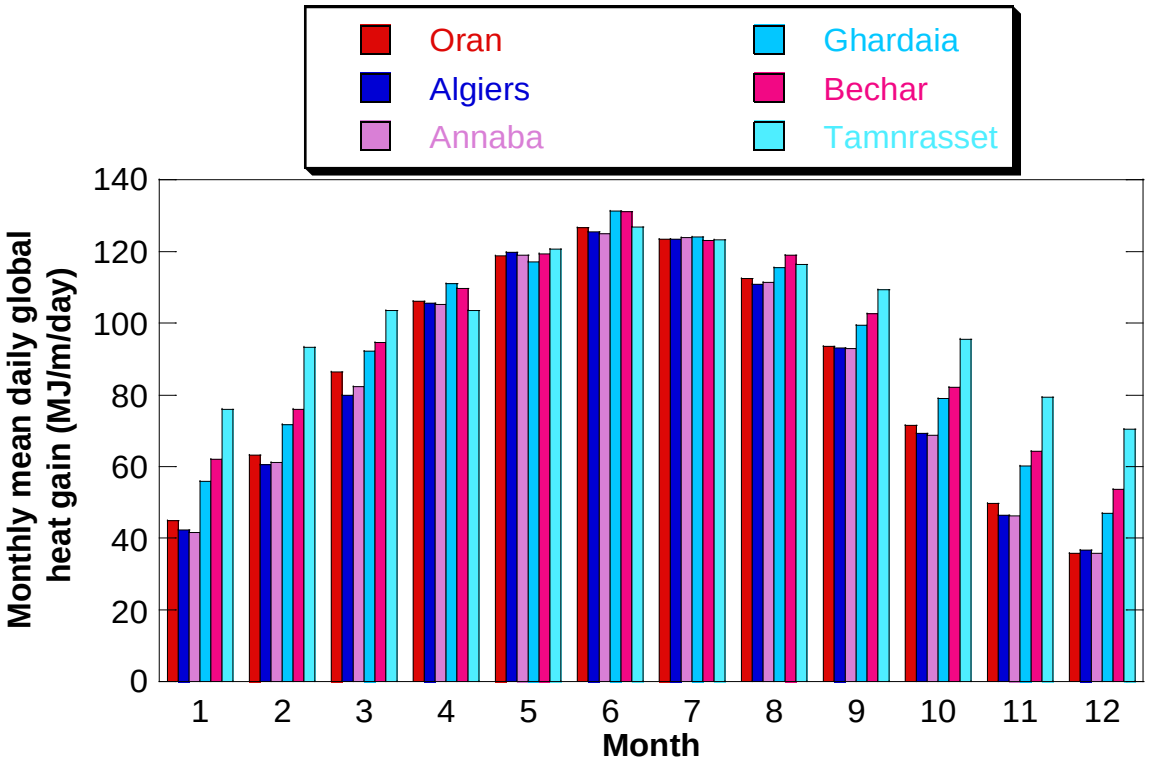

Figure III.13. Monthly mean daily global heat gain of syltherm 800 for different locations in Algeria.

Figure III.13 reveals that the monthly mean daily heat gain is influenced by the climatic conditions of each site like the DNI, the ambient temperature and the wind speed. It is noticed that the summer season (high DNI) has the most important monthly mean daily heat gain in the six selected sites. In addition, we note that the monthly mean daily heat gain in summer is about 120 to 130 MJ/m/day for all the studied regions. This is due to the warm climate of the entire Algerian territory in this period. In winter, a difference can be seen from the North to the South with an average of 35 to 60 MJ/m/day in the north (Oran, Algiers and Annaba), an average of 50 to 70 MJ/m/day in Bechar and Ghardaia and more than 70 MJ/m/day in Tamanrasset. In table III.2, the annual heat gain by one axis N/S tracking system of PTC was estimated and presented for the six Algerian locations.

Table III.2. Annual Heat Gain by one axis N/S tracking system of PTC for different locations in Algeria

Algerian Location	Annual Heat Gain by PTC System (MWh/m/year)
Oran	8.73
Algiers	8.56
Annaba	8,56
Ghardaia	9,33
Bechar	9,61
Tamanrasset	10,28

III.5. Conclusion

Against increasing energy demand and growing environmental problems in Algeria due to the use of fossil fuels, parabolic trough solar thermal power plants technologies offer interesting opportunities for the country. Algeria has favorable climatic conditions for the construction of parabolic trough solar thermal power plants. Numerical model has been presented in this chapter by simulation of the HTF temperature change, HTF heat gain, thermal efficiency, and PTC heat loss during the period of daylight for typical days with different tracking systems. We conclude that the two tracking system and one axis tracking system North/South represent the best heat collection, while the thermal efficiency of the N/S tracking system decreases in the winter season. However, due to the complexity of the two tracking system implementation and its high cost, the one axis tracking system is more adequate for the application in the Algerian conditions.

The HTFs thermal oils performances have been estimated in the Algerian climatic conditions. Each type of fluid has a range of recommended operating temperatures. The Syltherm 800 can reach a temperature between 600K and 700K; while the temperature of Marlotherm SH, and Santotherm 59 varies between 580K and 680K. Concerning Therminol D12, Santotherm LT, Marlotherm X and Syltherm XLT, the temperatures do not exceed 650K. A comparison has also been carried out to evaluate the influence of the location on the PTC heat gain. The estimation of the monthly mean heat gain using Syltherm 800 in the six locations selected from the Algerian territory shows the influence of the solar radiation on HCE performance. The best monthly heat gain was observed in increasing direct solar

radiation locations which is noticed in the South of the country. The results reveal also that the annual heat gain by one axis N/S tracking PTC system is found in the Sahara for Ghardaia about 9.33 MWh/m/year, Béchar about 9.61 MWh/m/year and the best in Tamanrasset with about 10.28 MWh/m/year.

Chapter IV: Thermodynamic Analysis of Cu-Cl Thermochemical Cycle for Hydrogen Production

IV.1. Introduction

Thermochemical cycles are alternative and potentially more efficient methods to produce hydrogen from water splitting [71,154]. Theses cycles are processes that primarily make use of heat and a series of intermediate chemical reactions to break down water into hydrogen and oxygen [154]. The thermodynamic evaluation of the thermochemical water decomposition processes is analyzed and illustrated by applying informative methodologies like energy and exergy analysis, which can assist in improving efficiencies and identifying limiting efficiencies [57,63,74]. Recent developments, particularly using solar energy sources, suggest that thermochemical hydrogen production could become commercial, and help meet the anticipated future demand for hydrogen as an energy vector. Consequently, research is likely to continue to improve thermochemical water decomposition processes.

In this chapter, we propose and study the Cu–Cl cycle integrated with solar parabolic trough collectors system. The objective is to develop a model to analyze the Cu–Cl cycle using solar PTC as heat source under Algerian conditions. To describe the different steps of the Cu–Cl cycle for hydrogen production, we perform a thermodynamic analysis accounting for relevant chemical reactions and including the determination of energy and exergy efficiencies. A parametric study is conducted to investigate the effect of heat gain from the PTC on the hydrogen production rate. Furthermore, the rate production of hydrogen by the Cu–Cl cycle is analyzed and compared for performance improvement of the system for different climatic regions in Algeria.

IV.2. System description

The Cu–Cl cycle in this system is developed in the Clean Energy Research Laboratory (CERL) at the UOIT [57]. It is a hybrid process using heat essentially and some electricity to split water to produce hydrogen. The setup is based on the four-step Cu–Cl cycle given by Orhan et al. [57], in Fig. IV.1. The Cu–Cl cycle is divided into four steps, namely: (a) the hydrolysis, (b) the oxygen production, (c) the drying and (d) the hydrogen production [57,72,74,155]. In the hydrolysis, the high temperature steam at approximately 400°C is brought in contact with solid $CuCl_2$ in order to achieve aqueous HCl and solid Cu_2OCl_2 as the products. The reaction occurring in the hydrolysis section is written as [57,72,74,155]:

$$H_2\,0\,(g) + 2CuCl_2\,(s) + Q_I \xrightarrow{400°C} CuOCuCl_2\,(s) + 2HCl\,(g) \quad \text{(IV.1)}$$

The Cu_2OCl_2 produced in the hydrolysis section is then passed through the oxygen production step. In this step, approximately a temperature of 500°C is required to break Cu_2OCl_2 into O_2 and CuCl. The produced oxygen is then passed through a heat exchanger where its temperature is lowered to the point where it can be used. The produced CuCl, passes through the heat exchanger to reach a mixer where it is mixed with HCl and water. The reaction occurring in this step becomes [57,72,74,155]:

$$CuOCuCl_2\,(s) + Q_{II} \xrightarrow{500°C} 2CuCl\,(l) + \tfrac{1}{2}O_2\,(g) \quad \text{(IV.2)}$$

In the drying process, water is removed from the aqueous $CuCl_2$. The dried $CuCl_2$ in solid form is then passed through the heat exchanger to enter the hydrolysis section. The water separated from the aqueous $CuCl_2$ is passed through the pump and heat exchanger in order to meet the electrolyzer temperature and lower its temperature to that of the mixture [57,72,74,155]:

$$CuCl_2\,(aq) \xrightarrow{80°C} CuCl_2\,(s) + H_2O\,(g) \quad \text{(IV.3)}$$

The fourth step in a four step Cu–Cl cycle is the hydrogen production step. In the hydrogen production step, aqueous CuCl and HCl from the mixture enter the electrolyzer. In the electrolyzer electrical energy is provided to dissociate CuCl and HCl into aqueous $CuCl_2$ and H2. The hydrogen produced is sent to the storage tank where as aqueous $CuCl_2$ produced is passed through the heat exchanger network where its temperature is increased in order to separate water from the solution. The reaction taking place in this step is [57,72,74,155]:

$$2HCl\,(aq) + 2CuCl\,(aq) \xrightarrow{25°C} 2CuCl_2\,(aq) + H_2\,(g) \quad \text{(IV.4)}$$

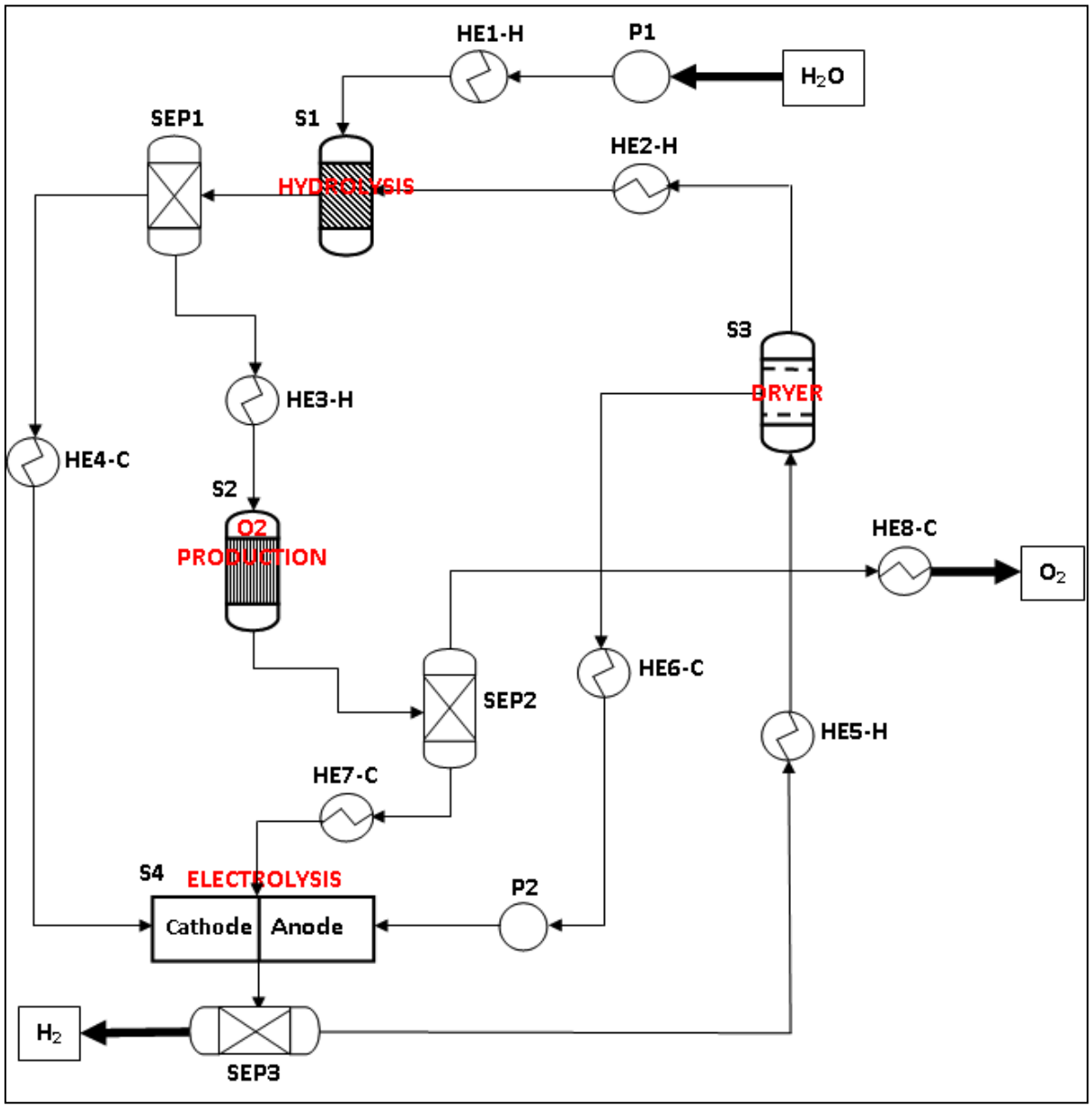

Figure IV.1. Thermochemical Cu-Cl Cycle [57,70].

IV.3. Energy and Exergy study of the Cu-Cl cycle

A thermochemical cycle performs a series of intermediate reactions to achieve the overall splitting of water into hydrogen and oxygen. It typically forms a closed cycle that uses water as the only input substance, while hydrogen and oxygen are the only two products. The Cu–Cl cycle splits water into hydrogen and oxygen through intermediate copper and chlorine compounds. Decomposing water into hydrogen and oxygen implies that sufficient energy must be provided to break the chemical bond of hydrogen and oxygen atoms. From a thermodynamic perspective, this energy is expressed in terms of enthalpy. However, a series of intermediate processes are required to split water. As a consequence, the energy required to

split water will also be a function of the processes, not solely the thermodynamic state alone. Therefore, to evaluate the total energy required by the copper–chlorine cycle, the thermal efficiency, optimization and complexity of the thermal network become paramount. The energy required by the Cu–Cl cycle includes heat, mechanical energy and electricity. In this study, a thermodynamic analysis will be performed to determine the heat released or absorbed by each step of the Cu–Cl cycle [39]. We consider one mole of hydrogen produced per cycle, so all quantities are provided per mole of hydrogen produced. Also, we assume that [31,59,60,63]:

- The reference environment temperature (T0) and pressure (P0) are 298.15K and 1atm, respectively.
- The chemical reaction reactants and products are at the reaction temperature and a pressure of 1atm.
- The process occurs at steady state and steady-flow with negligible potential and kinetic energy changes.
- The heat exchanger effectiveness is assumed to be 100%, based on the study conducted by Dincer and Rosen [156].

IV.3.1. Study of Hydrolysis step (HCl production), TI=400°C

$$H_2 0\,(g) + 2CuCl_2\,(s) + Q_I \xrightarrow{400°C} CuOCuCl_2\,(s) + 2HCl\,(g)$$

IV.3.1.1. Mass balance

Mass is conserved in chemical reactions, as the masses of products and reactants are equal, so a general steady-state mass rate balance can be expressed as follows [31,59,61,63]:

$$\dot{m}in = \dot{m}\text{out} \qquad \text{(IV.5)}$$

With:

$\dot{m}$: mass rate (kg/s)

The mass balance for the HCl production reaction is:

$$n_{H2O} \cdot M_{H2O} + n_{CuOCuCl2} \cdot M_{CuOCuCl2} = n_{HCl} \cdot M_{HCl} + n_{CuOCuCl2} \cdot M_{CuOCuCl2} \qquad \text{(IV.6)}$$

With:

n: mole number (mol/mol H2)

M: molecular mass (kg/mol)

IV.3.1.2. Heat balance

The heat transfer for a chemical process involving no work interaction W is determined from the energy balance applied to the system with W=0 [31,60,61,63]:

$$\Delta \dot{E} = \dot{E}in - \dot{E}out \quad \text{(IV.7)}$$

With:

$\dot{E}$: Heat rate (KJ/s)

For a steady-state reaction process, the energy balance for the HCl production reaction is reduces to [58,60,66,69,157]:

$$Q_I = \Delta H_I(T_I) = \Delta H_I^{\circ}(T_0) + n_{CuOCuCl2} \cdot (h - h_0)_{CuOCuCl2} + n_{HCl} \cdot (h - h_0)_{HCl} - n_{H2O} \cdot (h - h_0)_{H2O} - n_{CuCl2} \cdot (h - h_0)_{CuCl2} \quad \text{(IV.8)}$$

With:

Q_I: the heat flow into the hydrolysis step (negative for exothermic reactions), kJ/mole H_2.

$\Delta H_I\ (T_I)$: enthalpy change of hydrolysis step at T_I, kJ/mole H_2;

$\Delta H_I^{\circ}(T_0)$: enthalpy change of hydrolysis step at standard conditions, kJ/mole H_2;

$(h\text{-}h_0)_i$: molar enthalpy change of the substance i, kJ/mol;

$(s\text{-}s_0)_i$: molar entropy change of the substance i, kJ/mol.K.

IV.3.1.3. Exergy balance

The exergy balance for a chemical reactions involving no work interaction W can be written as [31,59,60,63,75]:

$$\Delta Ex_{sysI} = (\sum Ex_{in} - \sum Ex_{out}) - Ex_{destruction} \quad \text{(IV.9)}$$

For a steady-state process, $\Delta Ex_{sysI} = 0$:

$$Ex_{desI} = \sum Ex_{in} - \sum Ex_{out} \quad \text{(IV.10)}$$

The exergy balance for the HCl production reaction is reduces to:

$$Ex_{desI} = n_{CuCl2} \cdot ex(CuCl2) + n_{H2O} \cdot ex(H20) - n_{CuOCuCl2} \cdot ex(CuOCuCl2) - n_{HCl} \cdot ex(HCl) + \left(1 - \frac{T0}{TI}\right) \cdot Q_I \quad \text{(IV.11)}$$

Where Ex_{desI} (kJ/mole H_2), is the destruction exergy in the hydrolysis step. The molar exergy ex, (kJ/mol) associated with a flow at a specified state is the sum of two contributions: thermomechanical and chemical [31,59,60,63,154]. Thus, the specific exergy of a flow can be expressed as:

$$ex_i = \left[(h - h_0) - T_0 \cdot (s - s_0) + \frac{v^2}{2} + g \cdot z + ex^{ch}\right]_i \quad \text{(IV.12)}$$

For the chemical reactions in the Cu–Cl cycle, it is reasonable to assume the specific kinetic exergy and specific potential exergy of the flows are equal to zero:

$$\frac{v^2}{2} = g \cdot z = 0 \quad \text{(IV.13)}$$

Then, the exergy balance becomes:

$$Ex_{desI} = n_{CuCl2} \cdot [(h - h_0) - T0 \cdot (s - s_0) + ex^{ch}]_{CuCl2} + n_{H2O} \cdot [(h - h_0) - T0 \cdot (s - s_0) + ex^{ch}]_{H2O} - n_{CuOCuCl2} \cdot [(h - h_0) - T0 \cdot (s - s_0) + ex^{ch}]_{CuOCuCl2} - n_{HCl} \cdot [(h - h_0) - T0 \cdot (s - s_0) + ex^{ch}]_{HCl} + \left(1 - \frac{T0}{TI}\right) \cdot QI \quad \text{(IV.14)}$$

IV.3.2. Study of O_2 production step (TII=500°C)

$$CuOCuCl_2\,(s) + Q_{II} \xrightarrow{500°C} 2CuCl\,(l) + \frac{1}{2} O_2\,(g)$$

IV.3.2.1. Mass balance

Similar to Eq (IV.6), the steady-state mass rate balance for the O_2 production step can be expressed as follows [31,59,61,63]:

$$n_{CuOCuCl2} \cdot M_{CuOCuCl2} = n_{O2} \cdot M_{O2} + n_{CuCl} \cdot M_{CuCl} \quad \text{(IV.15)}$$

IV.3.2.2 Heat balance

Similar to Eq (IV.10), the steady-state heat rate balance for the O_2 production step involving no work interaction can be expressed as follows [58,60,66,69,157]:

$$QII = \Delta Hr(T_{II}) = \Delta Hr(T_0) + n_{CuCl}\cdot (h - h_0)_{CuCl} + n_{O2}\cdot (h - h_0)_{O2} - n_{CuOCuCl2}\cdot (h' - h'_0)_{CuOCuCl2} \quad \text{(IV.16)}$$

With:

Q_{II}: the heat flow into O_2 production step (negative for exothermic reactions), kJ/mole H_2.

$\Delta H_{II}\ (T_{II})$: enthalpy change of O_2 production step at T_{II}, kJ/mole H_2;

$\Delta H^{\circ}_{II}(T_0)$: enthalpy change of O_2 production step at standard conditions, kJ/mole H_2;

IV.3.2.3. Exergy balance

Similar to Eq (IV.11), the steady-state exergy rate balance for the O_2 production step with no work interaction can be reduced to [31,59,60,63]:

$$Ex_{desII} = n_{CuCl2}\cdot ex'(CuOCuCl2) - n_{O2}\cdot ex(O_2) - n_{CuCl}\cdot ex(CuCl) + \left(1 - \frac{T0}{TII}\right)\cdot Q_{II} \quad \text{(IV.17)}$$

Where Ex_{desII} (kJ/mole H_2), is the destruction exergy in the O_2 production step. The specific exergy of a flow can be expressed as [31,59,60,63,154]:

$$Ex_i = \left[(h - h_0) - T_0\cdot (s - s_0) + \frac{v^2}{2} + g\cdot z + ex^{ch}\right]_i \quad \text{(IV.18)}$$

For the chemical reactions in the Cu–Cl cycle, it is reasonable to assume the specific kinetic exergy and specific potential exergy of the flows are equal to zero. Then, the exergy balance for the O_2 production step becomes:

$$Ex_{desII} = n_{CuOCuCl2}\cdot [(h - h_0) - T0\cdot (s - s_0) + ex^{ch}]_{CuOCuCl2} - n_{O2}\cdot [(h - h_0) - T0\cdot (s - s_0) + ex^{ch}]_{O2} - n_{CuCl}\cdot [(h - h_0) - T0\cdot (s - s_0) + ex^{ch}]_{CuCl} + \left(1 - \frac{T0}{TI}\right)\cdot Q_{II} \quad \text{(IV.19)}$$

IV.3.3. Parameters of the equations steps

After writing mass, energy and exergy balances for the chemical reactions, enthalpy change of reaction in standard conditions, enthalpy and entropy change of each compound are evaluated here. The enthalpy change of reactions at standard conditions $\Delta H_r^\circ(T_0)$ is given by Hess Equation:

$$\Delta H_r^\circ(T_0) = \sum n_i \cdot \Delta H_f^\circ(i)_{product} - \sum n_i \cdot \Delta H_f^\circ(i)_{reactant} \quad \text{(IV.20)}$$

With:

$\Delta H_f^\circ(i)$: standard enthalpy of formation of compound (i), kJ/mole.

In order to determine the heating values, enthalpy and entropy data are needed for the working substances. The calculation procedures below will use these typical heating values. The following analysis provides a summary of key calculations in the overall heat requirements of the Cu–Cl cycle. To calculate the enthalpy change of a substance that is cooled or heated over a particular temperature range without phase change, an isobaric process could be assumed and the enthalpy change can be calculated as [65,69,157,158]:

$$(h - h_0)_i = \int_{Ti}^{Tf} Cp_i \cdot dT \quad \text{(IV.21)}$$

$$(s - s_0)_i = \int_{Ti}^{Tf} Cp_i \cdot \frac{dT}{T} \quad \text{(IV.22)}$$

Where Cp_i (J/mol.K) is the specific heat of the substance based on a molar quantity and the subscripts on Ti and Tf are the initial and final temperatures, respectively.

The equations above cannot be directly applied to substances with phase change. The enthalpy change caused by the phase must be added to the value calculated to obtain the total enthalpy and entropy change for those substances.

IV.3.3.1. Parameters of the step 1 equations

The enthalpy change of the hydrolysis step reaction in standard conditions is given by:

$$\Delta H_I^\circ(T_0) = \Delta H_f^\circ(CuOCuCl_2)_s + 2\Delta H_f^\circ(HCl)_g - \Delta H_f^\circ(H_2O)_g - 2\Delta H_f^\circ(CuCl_2)_s \quad \text{(IV.23)}$$

For $CuOCuCl_2$(s):

The enthalpy and entropy change required for $CuOCuCl_2$(s) production in the hydrolysis step consists of the enthalpy and entropy required for increasing the temperature from T0 to TI is calculated as follows:

$$(h - h_0)_{CuOCuCl2} = \int_{T0}^{TI} Cp_{CuOCuCl2}(s) \cdot dT \quad \text{(IV.24)}$$

$$(s - s_0)_{CuOCuCl2} = \int_{T0}^{TI} Cp_{CuOCuCl2}(s) \cdot \frac{dT}{T} \quad \text{(IV.25)}$$

Where Cp is found from the following correlation [67]:

$$Cp_{CuOCuCl2}(s) = 99.23243 + 21.62162 \cdot t \quad \text{(IV.26)}$$

With t is 1/1000 of the specified temperature (in K) of a compound, i.e., t=T(K)/1000.

For the $CuCl_2$(s):

The enthalpy and entropy change required for $CuCl_2$(s) production in the hydrolysis step consists of the enthalpy and entropy required for increasing the temperature from T0 to TI is calculated as follows:

$$(h - h_0)_{CuCl2} = \int_{T0}^{TI} Cp_{CuCl2}(s) \cdot dT \quad \text{(IV.27)}$$

$$(s - s_0)_{CuCl2} = \int_{T0}^{TI} Cp_{CuCl2}(s) \cdot \frac{dT}{T} \quad \text{(IV.28)}$$

Where Cp for $CuCl_2$(s) are calculated using the following correlations [68]:

$$Cp_{CuCl2(s)} = 70.21882 + 23.36132 \cdot t - 14.86876 \cdot t^2 + 4.053899 \cdot t^3 - 0.366203/t^2 \quad \text{(IV.29)}$$

With: t=T(K)/1000

For H2O(g):

The enthalpy and entropy change required for steam production in the hydrolysis step consists of the enthalpy and entropy required for increasing the temperature of water from T0 to Tv, vaporizing water at Tv, and increasing the temperature of steam from Tv to TI.

$$(h - h_0)_{H20} = \int_{T0}^{Tv} Cp_{H20}\,(l)\cdot dT + Lv(H2O) + \int_{Tv}^{TI} Cp_{H20}\,(g)\cdot dT \qquad \text{(IV.30)}$$

$$(s - s_0)_{H2O} = \int_{T0}^{Tv} Cp_{H20}\,(l)\cdot \frac{dT}{T} + \frac{Lv(H20)}{Tv} + \int_{Tv}^{TI} Cp_{H20}\,(g)\cdot \frac{dT}{T} \qquad \text{(IV.31)}$$

With

Tv=373K, the water evaporation temperature at the standard pressure (1atm).

Lv(H_2O), the vaporization enthalpy of water at Tv, kJ/mole.

The specific heat for liquid and water vapor is calculated by using Eqs. (IV.32) and (IV.33) respectively [68]:

$$Cp_{H2O(l)} = 203.606 + 1523.29\cdot t - 3196.413\cdot t^2 + 2474.544\cdot t^3 + 3.855326/t^2 \qquad \text{(IV.32)}$$

$$Cp_{H2O(g)} = 30.092 + 6.832514\cdot t - 6.793435\cdot t^2 - 2.53448\cdot t^3 + 0.082139/t^2 \qquad \text{(IV.33)}$$

With: t=T(K)/1000

For HCl(g):

The enthalpy and entropy change required for HCl(g) production in the hydrolysis step consists of the enthalpy and entropy required for increasing the temperature from T0 to TI is calculated as follows:

$$(h - h_0)_{HCl} = \int_{T0}^{TI} Cp_{HCl}\,(g)\cdot dT \qquad \text{(IV.34)}$$

$$(s - s_0)_{HCl} = \int_{T0}^{TI} Cp_{HCl}\,(g)\cdot \frac{dT}{T} \qquad \text{(IV.35)}$$

Where Cp for HCl(g) is calculated using the following correlations [68]:

$$Cp_{HCl(g)} = 32.12392 - 13.45805\cdot t + 19.86852\cdot t^2 - 6.853936\cdot t^3 - 0.049672/t^2 \qquad \text{(IV.36)}$$

With: t=T(K)/1000

IV.3.3.2. Parameters of step 2 equations

Similar to Eq. (IV.23), the enthalpy change of O_2 production reaction at standard conditions is given by:

$$\Delta H_{II}^{\circ}(T_0) = 2\Delta H_f^{\circ}(CuCl)_l + \tfrac{1}{2}\Delta H_f^{\circ}(O_2)_g - \Delta H_f^{\circ}(CuOCuCl_2)_s \quad \text{(IV.37)}$$

For CuOCuCl2(s):

Similar to Eq. (IV.23) and Eq. (IV.24), the enthalpy and entropy change required for $CuOCuCl_2$(s) production in the O2 production step for increasing the temperature from T0 to TII is calculated as follows:

$$(h' - h'_0)_{CuOCuCl2} = \int_{T0}^{TII} Cp_{CuOCuCl2}(s)\cdot dT \quad \text{(IV.38)}$$

$$(s' - s'_0)_{CuOCuCl2} = \int_{T0}^{TII} Cp_{CuOCuCl2}(s)\cdot \frac{dT}{T} \quad \text{(IV.39)}$$

For CuCl(l):

The enthalpy and entropy change required for CuCl(l) production in the O_2 prodction step consists of the enthalpy and entropy required for increasing the temperature of CuCl(s) from T0 to Tf, fusion CuCl at Tf, and increasing the temperature of CuCl(l) from Tf to TII:

$$(h - h_0)_{CuCl} = \int_{T0}^{Tf} Cp_{CuCl}(s)\cdot dT + Lf(CuCl) + \int_{Tf}^{TII} Cp_{CuCl}(l)\cdot dT \quad \text{(IV.40)}$$

$$(s - s_0)_{CuCl} = \int_{T0}^{Tf} Cp_{CuCl}(s)\cdot \frac{dT}{T} + \frac{Lf(CuCl)}{Tf} + \int_{Tf}^{TII} Cp_{CuCl}(l)\cdot \frac{dT}{T} \quad \text{(IV.41)}$$

With:

Tf=703K, representing the CuCl temperature of fusion at standard pressure (1 atm).

Lf(CuCl), is the enthalpy of fusion or latent heat of fusion of CuCl at Tf, kJ/mol.

Where Cp for molten and solid CuCl is calculated using the following correlations [68]:

$$Cp_{CuCl(s)} = 75.271 - 26.83212\cdot t + 25.69156\cdot t^2$$

$$-7.357982\cdot t^3 - 1.847747/t^2 \quad \text{(IV.42)}$$

$$Cp_{CuCl(l)} = 66.944 - 3.699628.10^{-10}\cdot t + 2.166748.10^{-10}\cdot t^2$$

$$-3.90046.10^{-11}\cdot t^3 - 9.813196.10^{-12}/t^2 \quad \text{(IV.43)}$$

With: t=T(K)/1000

For O2(g):

The enthalpy and entropy change required for O_2(g) production in the O_2 production step for increasing the temperature from T0 to TII is calculated as follows:

$$(h - h_0)_{O2} = \int_{T0}^{TO2} Cp_{O2}\,(1)\cdot dT + \int_{TO2}^{TII} Cp_{O2}\,(2)\cdot dT \quad \text{(IV.44)}$$

$$(s - s_0)_{O2} = \int_{T0}^{TO2} Cp_{O2}\,(1)\cdot \frac{dT}{T} + \int_{TO2}^{TII} Cp_{CuCl}\,(2)\cdot \frac{dT}{T} \quad \text{(IV.45)}$$

Using Eq. (IV.46), which is valid for the temperature range 100-700 K, and Eq. (IV.47), which is valid for the temperature range 700-2000 K. We can express Cp as follows [68]:

$$Cp_{O2(1)}[100K - 700K] = 31.32234 - 20.2353\cdot t + 57.86644\cdot t^2 -$$

$$36.50624\cdot t^3 - 0.007374/t^2 \quad \text{(IV.46)}$$

$$Cp_{O2(2)}[700K - 2000K] = 30.03235 + 8.772972\cdot t - 3.988133\cdot t^2$$

$$+0.788313\cdot t^3 - 0.741599/t^2 \quad \text{(IV.47)}$$

With: t=T(K)/1000

V.3.4. Study of heat exchangers

In order to produce hydrogen from the process, heat exchangers are required to take the different compounds, used for each reaction of the cycle, to the desired temperatures. For the four steps Cu-Cl cycle, heat exchangers are needed; four exchangers for heating the compounds and four exchangers for cooling the compounds as follow:

Heating exchangers

$$HE1: H2O(l)at\ T0 \rightarrow H2O(g)at\ TI$$
$$HE2: CuCl2(s)at\ TIII \rightarrow CuCl2(s)at\ TI \quad \text{(IV.48)}$$
$$HE3: CuOCuCl2(s)at\ TI \rightarrow CuOuCl2(s)at\ TII$$

$$HE5: CuCl2(aq) at\ TIV \rightarrow CuCl2(aq) at\ TIII$$

Cooling exchangers

$$\begin{aligned} &HE4: HCl(g) at\ TI \rightarrow HCl(g) at\ TIV \\ &HE6: H2O(l) at\ TIII \rightarrow H2O(l) at\ TIV \\ &HE7: CuCl(l) at\ TII \rightarrow CuCl(l) at\ TIV \\ &HE8: O2(g) at\ TII \rightarrow O2(g) at\ T0 \end{aligned} \quad \text{(IV.49)}$$

The following analysis provides calculation of heat requirements of heat exchangers. To calculate the heat or the enthalpy change of a substance that is cooled or heated in a heat exchanger over a particular temperature range without phase change, an isobaric process could be assumed and the enthalpy change can be calculated as follow [39,62,68,157,158]:

$$Q_{HEi} = n_i \left[\int_{Ti}^{Tf} Cp_i \cdot dT\right] \quad \text{(IV.50)}$$

Where Q_{HEi} (kJ/mol H_2) is the heat in each exchanger, where Cp_i (J/mol.K) is the specific heat of the substance based on a molar quantity, n_i the molar quantity of the substance and the subscripts on Ti and Tf are the initial and final temperatures, respectively.

The equation (IV.50) cannot be directly applied to substances with phase change. The enthalpy change caused by the phase must be added to the value calculated to obtain the total enthalpy and entropy change for those substances.

The thermal exergy Ex_{HEic}(kJ/mol H_2) in each heat exchanger is defined from the heat in each exchanger as [70,72,74,75]:

$$Ex_{HEi} = \left(1 - \frac{T0}{Ti}\right) \cdot Q_{HEi} \quad \text{(IV.51)}$$

Where Q_{HEi} is posistive for heating exchangers and negative for cooling exchangers.

IV.3.4.1. Heat exchanger HE1

The heat in the Heat exchanger HE1 is the heat required for steam production to the hydrolysis step, which consists of the heat required for increasing the temperature of water from water input temperature to the cycle (T0) to vaporizing water temperature (Tv), also the heat required for vaporizing water at (Tv), and heat required for increasing steam temperature to hydrolysis temperature step (TI). It is given by:

$$Q_{HE1} = n_{H20}\left[\int_{T0}^{Tv} Cp_{H2O}(g)\cdot dT + Lv(H2O) + \int_{Tv}^{TI} Cp_{H2O}(l)\cdot dT\right] \quad \text{(IV.52)}$$

The exergy in the Heat exchanger HE1is given by:

$$Ex_{HE1} = \left(1 - \frac{T0}{TI}\right)\cdot Q_{HE1} \quad \text{(IV.53)}$$

IV.3.4.2. Heat exchanger HE2

The heat in the Heat exchanger HE2 is the heat required for increasing the temperature of $CuCl_{2(s)}$ from dryer temperature (TIII) to hydrolysis temperature step (TI):

$$Q_{HE2} = n_{CuCl2}\left[\int_{TIII}^{TI} Cp_{CuCl2}(s)\cdot dT\right] \quad \text{(IV.54)}$$

The exergy in the Heat exchanger HE2 is given by:

$$Ex_{HE2} = \left(1 - \frac{T0}{TI}\right)\cdot Q_{HE2} \quad \text{(IV.55)}$$

IV.3. 4. 3. Heat exchanger HE3

The heat in the Heat exchanger HE3 is the heat required for increasing the temperature of $CuOCuCl_{2(s)}$ from hydrolysis temperature step (TI) to the temperature of oxygen production step (TII):

$$Q_{HE3} = n_{CuOCuCl2}\left[\int_{TI}^{TII} Cp_{CuOCuCl2}(s)\cdot dT\right] \quad \text{(IV.56)}$$

The exergy in the Heat exchanger HE2 is given by:

$$Ex_{HE3} = \left(1 - \frac{T0}{TII}\right)\cdot Q_{HE3} \quad \text{(IV.57)}$$

IV.3.4.4. Heat exchanger HE4

The heat in the Heat exchanger HE4 is the heat required for cooling HCl(g) hydrolysis temperature step (TI) to electrolysis temperature step (TIV):

$$Q_{HE4} = n_{HCl}\left[\int_{TI}^{TIV} Cp_{HCl}(g)\cdot dT\right] \quad \text{(IV.58)}$$

The exergy in the Heat exchanger HE4 is given by:

$$Ex_{HE4} = \left(1 - \frac{T0}{TIV}\right) \cdot Q_{HE4} \quad \text{(IV.59)}$$

IV.3.4.5. Heat exchanger HE5

The heat in the Heat exchanger HE5 is the heat required for increasing the temperature of $CuCl_{2(aq)}$ from electrolysis temperature step (TIV) to dryer temperature step (TIII):

$$Q_{HE5} = n_{H2O}\left[\int_{TIV}^{TIII} Cp_{H2O}(l) \cdot dT\right] + n_{CuCl2}\left[\int_{TIV}^{TIII} Cp_{CuCl2}(s) \cdot dT\right] \quad \text{(IV.60)}$$

The exergy in the Heat exchanger HE5 is given by:

$$Ex_{HE5} = \left(1 - \frac{T0}{TIII}\right) \cdot Q_{HE5} \quad \text{(IV.61)}$$

IV.3.4.6. Heat exchanger HE6

The heat in the Heat exchanger HE6 is the heat required for decreasing the temperature of water from dryer temperature step (TIII) to electrolysis temperature step (TIV):

$$Q_{HE6} = n_{H2O}\left[\int_{TIII}^{TIV} Cp_{H2O}(l) \cdot dT\right] \quad \text{(IV.62)}$$

The exergy in the Heat exchanger HE6 is given by:

$$Ex_{HE6} = \left(1 - \frac{T0}{TIV}\right) \cdot Q_{HE6} \quad \text{(IV.63)}$$

IV.3.4.6. Heat exchanger HE7

The heat in the Heat exchanger HE7 is the heat required for decreasing the temperature of $CuCl_{(l)}$ from O_2 production temperature step (TII) to solidification temperature (Ts=Tf), heat required for solidification at Tf, and heat required for decreasing CuCl(s) temperature to electrolysis temperature step (TIV):

$$Q_{HE7} = n_{CuCl}\left[\int_{TII}^{Tf} Cp_{CuCl}(l) \cdot dT - Lf(CuCl) + \int_{Tf}^{TIV} Cp_{CuCl}(s) \cdot dT\right] \quad \text{(IV.64)}$$

The exergy in the Heat exchanger HE7 is given by:

$$Ex_{HE7} = \left(1 - \frac{T0}{TIV}\right) \cdot Q_{HE7} \quad \text{(IV.65)}$$

IV.3.4.8. Heat exchanger HE8

The heat in the Heat exchanger HE8 is the heat required for decreasing the temperature of oxygen gaz from O_2 production temperature step (TII) to exit cycle temperature (Tex):

$$Q_{HE8} = n_{O2}\left[\int_{TII}^{TO2} Cp_{O2}\,(2)\cdot dT + \int_{TO2}^{T0} Cp_{O2}\,(1)\cdot dT\right] \quad \text{(IV.66)}$$

The exergy in the Heat exchanger HE8 is given by:

$$Ex_{HE8} = \left(1 - \frac{T0}{T0}\right)\cdot Q_{HE8} \quad \text{(IV.67)}$$

IV.3.4. Energy and Exergy efficiency

IV.3.4.1 Energy efficiency

There has been much debate as to whether the higher heating value (HHV) or lower heating value (LHV) of hydrogen should be used in efficiency calculations. The HHV of 286 kJ/mol is the absolute value of standard enthalpy of the formation of liquid water at 298.15K. The LHV of 241.83 kJ/mol is the absolute value of standard enthalpy of the formation of water vapor at 298.15K and 1atm [64,71,157,159,160]. The energy efficiency of the process is defined as energy out divided by energy in. Based on the HHV for hydrogen, the efficiency of this process is given by:

$$\eta_{energy} = \frac{HHV(H2)}{Qin+Welec} \quad \text{(IV.68)}$$

Where:

Welec: is the electrical work required for the elecrolyzer and the dryer steps.

Qin: is the total heat requirement for the endothermic processes to produce a unit amount of product hydrogen, kJ/mole H_2.

IV.3.4.2. Exergy efficiency

An exergy efficiency can be formulated for the reacting system. At steady state, the rate at which exergy enters the reacting system equals to the rate at which exergy exits plus the rate at which exergy is destroyed within the system. We assume the reactor is well

insulated, so there is no heat transfer and thus no accompanying exergy transfer. An exergy efficiency can be written as [62,63]:

$$\eta_{exergy} = \frac{Ex_{H2}}{Ex_{in}+Ex_{elec}} \quad \text{(IV.69)}$$

Where Ex_{in}, (kJ/mole H_2), is the exergy input to the process that enters with the reactants plus heat, and $Ex_{H2,}$ (kJ/mole H_2), is the exergy content of hydrogen, as well as $Ex_{elec,}$ (kJ/mole H_2), is the exergy associated with electricity work. The exergy content of hydrogen is given as [70]:

$$Ex(H2) = (ex^{ch}(H2) + ex^{ph}(H2)) \quad \text{(IV.70)}$$

Where:

$$ex^{ph}(H2) = \Delta H^{\circ}\ (H2) - T0\cdot \Delta S^{\circ}\ (H2) \quad \text{(IV.71)}$$

The equation (IV.70) becomes:

$$Ex(H2) = \left(ex^{ch}(H2) + \Delta H\ \ (H2) - T0\cdot \Delta S\ \ (H2)\right) \quad \text{(IV.72)}$$

With [156,158]:

$$\Delta H\ \ (H2) = HHV = 286\frac{kJ}{mole}$$

$$\Delta S\ \ (H2) = 44.33\frac{J}{mole\cdot K}$$

The standard enthalpy of formation and standard chemical exergies at 298.15K and 1atm of all compounds involved in the the Cu–Cl cycle are given in Table (IV.1) [60,63]:

Table.IV.1.: Standard enthalpy of formation and standard chemical exergy for chemical compounds [60,63]

Compound	**ΔH°f (kJ/mole)**	**ex^{ch} (kJ/mole)**
$CuCl_2(s)$	-205.83	82.47
$CuOCuCl_2(s)$	-384.65	21.08
HCl(g)	-92.312	84.531
$H_2O(g)$	-241.82	9.437
CuCl(l)	-136.82	75
$O_2(g)$	0	3.97
$H_2(g)$	0	235.15

IV.4. Results and discussions

Using the thermodynamic methods detailed in the previous sections and specifying the operating conditions from experimental data in literature, the Cu–Cl cycle has been simulated successfully. The model calculates the heat of reactions at the specified conditions. The results are presented per mol of hydrogen in this study. The heat, exergy, work requirements and other values for the processes at various transfer points are shown in Table (IV.2). Based on results given in this table, the energy efficiency of the cycle and the corresponding exergy efficiency are evaluated.

From Table (IV.2), the total heat requirement for the endothermic processes is 619.3 kJ/mol and heat recovery from the exothermic processes is 113.42 kJ per mol of hydrogen. For electrolysis and dryer steps, the electrical energy requirement is given by Orhan et al. [57], as 88.2 kJ/mol H_2. The predicted energy efficiency of the system without heat recovery is found to be 40.42% as compared to 40.04% reported by Orhan et al. (2012), [57], and 52% reported by Ratlamwala et al. (2012), [70]. The energy efficiency of the system with heat recovery is found to be 48.14% . This behavior is observed due to the fact that in without heat recovery system all the heat rejected by the system is dumped into the atmosphere whereas in heat recovery system all of the waste heat is recycled backed and is utilized to enhance the efficiency:

- Without the recovered heat within the cycle again:

$$\eta_{energy} = \frac{286}{619.3+88.2} = 40.42\ \%$$

- Using the recovered heat within the cycle again, for endothermic processes:

$$\eta_{energy} = \frac{286}{619.3-113.42+88.2} = 48.14\ \%$$

The total exergy requirement for the processes is 464.761 kJ/mol from the Table (IV.2). The predicted exergy efficiency of the system is found to be 92.25% as compared to 82.91% reported by Ratlamwala et al. (2012), [70]:

$$\eta_{exergy} = \frac{507.94}{464.761+88.2} = 92.25\%$$

Table.IV.2.: Energy balances of the Cu-Cl cylcle

Step	**Process**	**Q_{in} (kJ/mole H2)**	**Q_{out} (kJ/mole H2)**	**Ex_{in} (kJ/mole H2)**	**Ex_{out} (kJ/mole H2)**	**Welec (kJ/mole H2)**
Hydrolysis (HCl production)	$H_20\ g + 2CuCl_2\ s + Q_I \xrightarrow{400°C} CuOCuCl_2 s + 2HClg$	242.84		221.62	212.57	
Oxygen Production	$CuOCuCl_2 + Q_{II} \xrightarrow{500°C} 2CuCl_l + \frac{1}{2}O_2 g$	233.87		174.69	12.94	
Dryer	$CuCl_2\ aq \xrightarrow{80°C} CuCl_2 s + H_20\ g$					33,2 [57]
Electrolysis (Hydrogen prodcution)	$2HClaq + 2CuCl\ aq \xrightarrow{25°C} 2CuCl_2 aq + H_2 g$					55 [57]
Heat Exchanger $HE1$	$H2O(l) at\ Tin \rightarrow H2O(g) at\ TI$	45.75		25.49		
Heat Exchanger $HE2$	$CuCl2(s) at\ TIII \rightarrow CuCl2(s) at\ TI$	50.409		28.08		
Heat Exchanger $HE3$	$CuOCuCl2(s) at\ TI \rightarrow CuOuCl2(s) at\ TII$	11.49		7.06		
Heat Exchanger $HE4$	$HCl(g) at\ TI \rightarrow HCl(g) at\ TIV$		-22.39		00	
Heat Exchanger $HE5$	$CuCl2(aq) at\ TIV \rightarrow CuCl2(aq) at\ TIII$	34.94		5.444		
Heat Exchanger $HE6$	$H2O(l) at\ TIII \rightarrow H2O(l) at\ TIV$		-26.54		00	
Heat Exchanger $HE7$	$CuCl(l) at\ TII \rightarrow CuCl(l) at\ TIV$		-57		00	
Heat Exchanger $HE8$	$O2(g) at\ TII \rightarrow O2(g) at\ Tex$		-7.48		00	
Total	**Cu-Cl Cycle**	**619.3**	**-113.42**	**464.761**	**225.51**	**88,2**

IV.4.1. Hydrogen production rate

Using the results of the Cu–Cl cycle simulation. The heat, exergy, work requirements and other values for the processes at various transfer points are shown in Table (IV.2). Based on results given in this table, the capacity of the cycle combined with a PTC in the Algerian conditions is evaluated. Since Algeria has favorable climatic conditions for the construction of parabolic trough solar thermal power plants as presented in the previous chapter. The monthly mean heat gain using parabolic trough power plant has been estimated for six locations selected from the Algerian territory. The hydrogen production rate is calculated from:

$$R(H_2) = \frac{Qgain}{Qin} \cdot \frac{M(H2)}{\rho(H2)} \qquad \text{(IV.73)}$$

Where $R(H_2)$, in liters (H_2)/s, is the hydrogen production rate, Q_{gain} (Watts), is the solar heat gained from the PTCs solar field using the Syltherm 800 as heat transfer fluid. ρ(H2) is the density of hydrogen expressed on kg/liter.

The daily hydrogen production rate is calculated from the Cu-Cl cycle combined with a solar parabolic trough power plant, as follows:

$$R_{day}(H_2) = h \cdot \left[\sum_{i=1}^{S_0 - 1} \mathrm{R}(\mathrm{H}_2)^{\,i} \right] \cdot M(H_2) \qquad \text{(IV.74)}$$

Where $R_{day}(H_2)$, in Tons(H_2)/day, is the daily hydrogen production rate, h (one hour or 3600 sec), is the integration step. S_0, is the hours of daylight.

IV.4.2. Effect of heat gain from PTC

In an integrated solar system, studying the effect of fluctuation in heat gain from this system is very important as heat gain is not constant throughout the day. Syltherm 800 thermal oil is selected as heat transfer fluid in the PTC power plant equipped with one axis tracking system oriented North/South, because Syltherm 800 represents the best thermal capacity over all the year for the studied locations. The rate of hydrogen production by the combined Cu-Cl cycle and the global heat gain from PTC in the daylight period of two typical days of winter and summer are presented in Figure IV.2 through Figure IV.3.

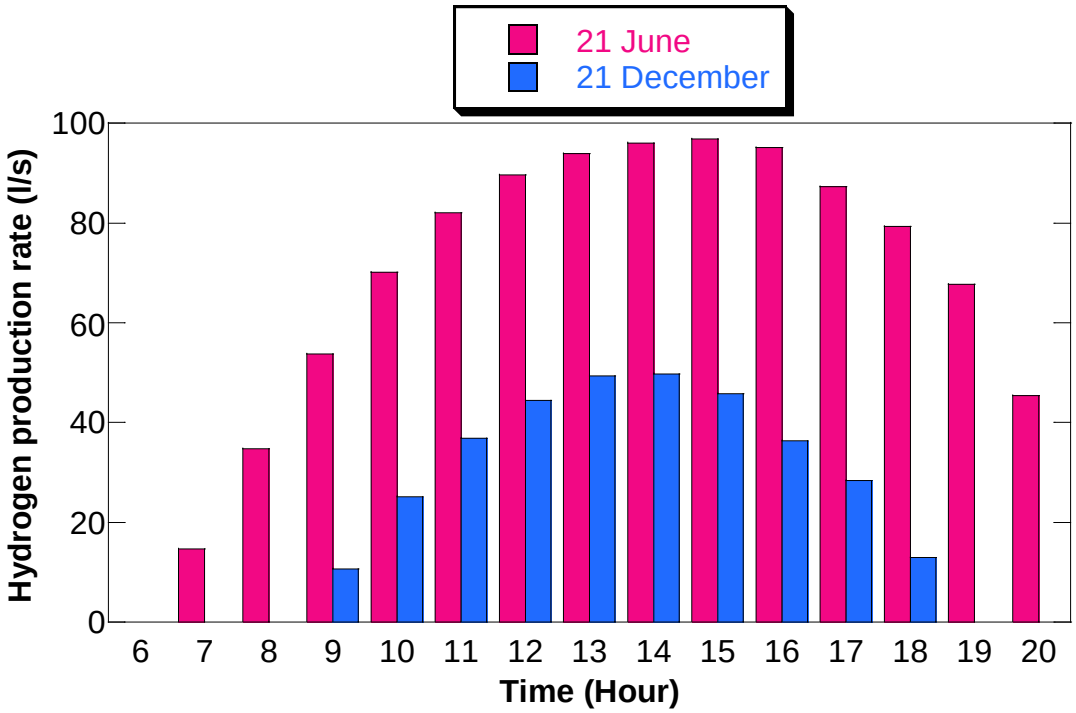

Figure IV.2. Hydrogen Production Rate in Ghardaia, (l/s)

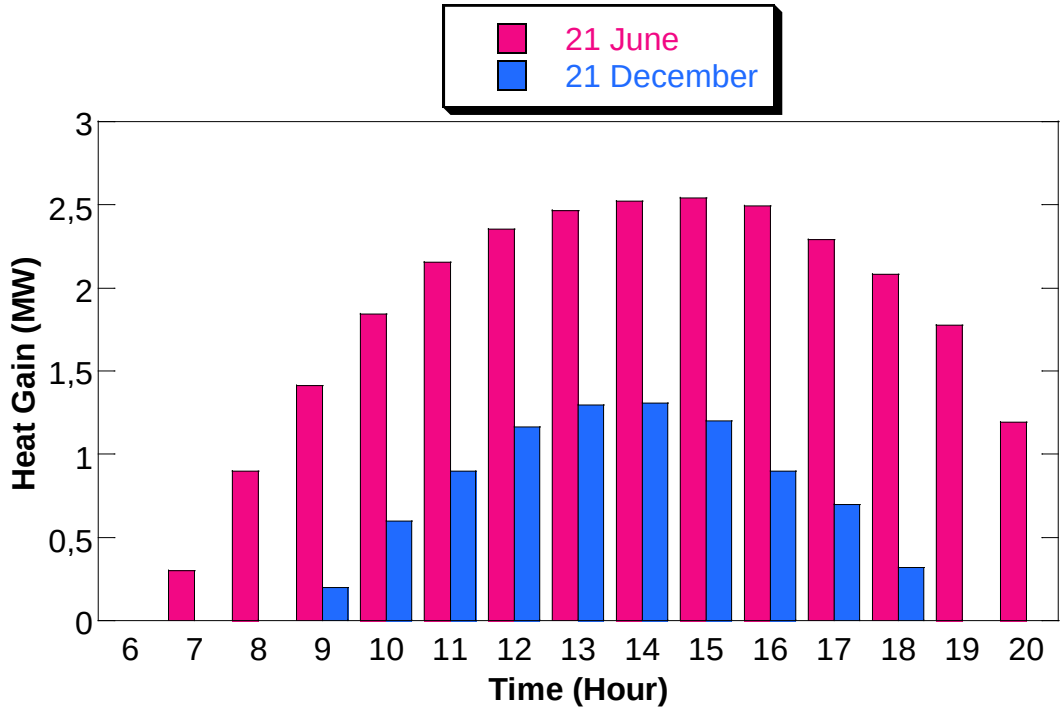

Figure IV.3. Global heat gain form PTC system in Ghardaia, (MW)

It is observed from figure IV.2 that, for typical summer day, the rate of hydrogen produced by the system increases from 15 l/s in the morning to 96.8 l/s around 3 p.m., then starts to decrease to the end of the daylight period. In the typical winter day, same remarks was observed, the rate of hydrogen produced by the system increases to 50 l/s around 2 p.m.,

then starts to decrease to the end of the daylight period. It is noticed form figure IV.3 that the profile of the hydrogen production rate corresponds to that of the heat gain from the solar field. Such behavior is observed because the increases of the global heat gain is proportional to the increase of fluid temperature used in the absorber of the parabolic trough collector. Syltherm 800 absorbs heat from the solar receiver due to its capabilities of catering large temperature ranges. With the increase in the rate of heat transfer by the syltherm 800 coming from the solar receiver, the amount of heat supplied to the Cu–Cl cycle increases. The ability of the Cu–Cl cycle of being mainly heat dependent helps in recovering the excess heat and therefore, producing higher amount of hydrogen.

IV.4.3. Effect of the Algerian climatic regions

Six typical locations in Algeria namely, Algiers, Annaba, Oran, Béchar, Ghardaia and Tamanrasset are selected for this study. These locations are presented in chapter II. We present in Figure IV.4 the monthly hydrogen production for the six Algerian locations.

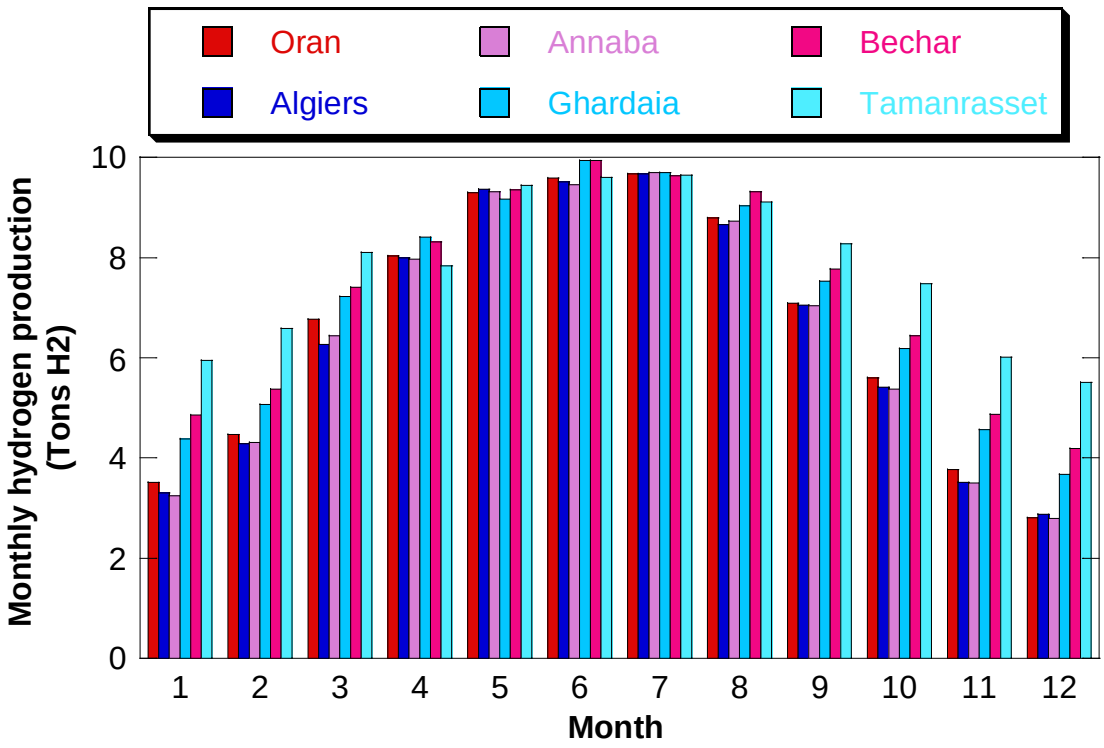

Figure IV.4. Monthly production of Hydrogen, (Ton H_2).

Figure IV.4 reveals that the heat collected from the PTC affects the hydrogen production rate from the Cu-Cl cycle. On the other hand, since the monthly heat gain is influenced by the climatic conditions of each site, the hydrogen production is also influenced

by the location. We observe from Figure IV.4 that the hydrogen production is most important in the South of Algeria for Ghardaia, Bechar and Tamanrasset overall the year which is due to the important heat gain from PTC due to the increasing direct solar radiation in the south of the country. In addition, the maximum hydrogen production is observed in the summer season which occurs in June with about 10 Ton H_2. In winter, a difference can be seen from the North to the South with an average of 2.8 to 5 Ton H_2 in the north (Oran, Algiers and Annaba), an average of 4 to 7 Ton H_2 in Bechar and Ghardaia and more than 5.5 Ton H_2 in Tamanrasset. In table V.3, the annual hydrogen production was estimated and presented for the six Algerian locations.

Table IV.3. Annual hydrogen production for different locations in Algeria

Algerian Location	**Annual Hydrogen Production (Ton H_2/year)**
Oran	79,40
Algiers	77.90
Annaba	77.86
Ghardaia	84.87
Bechar	87.44
Tamanrasset	93.55

IV.5. Conclusion

The present study deals with comparative energy and exergy analyses of Cu–Cl cycle for hydrogen production combined with solar parabolic trough collector and testing the performance in the Algerian conditions. A thermodynamic analysis has been developed for relevant chemical reactions and including the determination of energy and exergy efficiencies of Cu-Cl cycle. The overall energy and exergy efficiencies of the Cu-Cl cycle are obtained as 40.42% and 92.25%, respectively, based upon the reference conditions. A parametric study is conducted to investigate the effects of several operating parameters such as heat gain from the solar PTC on the rate of hydrogen produced. A comparative assessment is carried out to study the effect of different Algerian locations and climates on hydrogen production rate from Cu–Cl. These analyses have revealed that the rate of hydrogen production by the Cu–Cl cycle is proportional to the heat gain from the solar PTC. In addition, the maximum annually

hydrogen production is obtained for the Southern Algerian regions, for Ghardaia, Bechar and Tamanrasset with 84.87 Ton H_2, 87.44 Ton H_2 and 93.55 Ton H_2, respectively. For the Northern Algerian regions, the best hydrogen production is observed for the Western site with 79.4 Ton H_2 for Oran. In this regard, it is better to use solar energy through hybrid or thermochemical cycles for sustainable hydrogen production which appears to be an eco-friendly and sustainable option for the countries having abundant solar energy resources as Algeria. The main energy input needed by such systems is high temperature heat. However, some electricity is still needed to transport materials, operate pumps, compressors, electrochemical reaction, and so forth. In all cases, the electricity represents a small fraction of the total energy input inventory.

Conclusions and Recommendations

1. Conclusions

This thesis has presented an effective method for modelling the collector field and energy conversion plant of a parabolic trough collectors. The study consists of a solar model for the direct solar radiation, a dynamic model for the collector field and a steady-state model for Cu-Cl thermochemical cycle. The solar model, the collector field model and the Cu-Cl cycle for hydrogen production model were combined to an entire plant model that was evaluated under Algerian conditions.

First, for the solar field, a model, based on the clear sky, has been used to estimate the direct solar radiation at different locations representative of different climatic conditions in Algeria. Direct Normal Irradiance was used to estimate the potential for concentrating solar collectors. The model incorporates various geographical and meteorological factors and various fixed and tracking systems. The results reveals that the two tracking axis system is the most efficient system for the concentrating solar plant. The solar model was also interpolated over the entire year as a function of the sun's azimuth and elevation angles for the six selected locations. The results reveals that the important DNI potential is found in the Sahara for Ghardaia with 2.88 MWh/m^2/year, Béchar with 3.25 MWh/m^2/year and the best in Tamanrasset with 3.42 MJ/m^2/year.

Second, for the collector field, a thermal model was developed to predict thermal performance of parabolic trough collectors under Algerian conditions. We conclude that the two tracking system and one axis tracking system North/South represent the best heat collection. However, due to the complexity of the two tracking system implementation and its high cost, the one axis tracking system is more adequate for the application in the Algerian conditions. Different thermal oils were employed as heat transfer fluid in the receiver to compare their temperature profile. Results shown that each type of fluid has a range of recommended operating temperatures. The Syltherm 800 can reach a temperature between 600K and 700K; while the temperature of Marlotherm SH and Santotherm 59 varies between 580K and 680K. Concerning Therminol D12, Santotherm LT, Marlotherm X and Syltherm XLT, the temperatures do not exceed 650K. In order to study the influence of the climatic conditions and solar radiation on the performances of the PTC, a comparison of monthly heat gain was evaluated for different Algerian locations. The best monthly heat gain was observed in increasing direct solar radiation locations which is noticed in the South of the country. The

annual heat gain by one axis N/S tracking PTC system is found in the Sahara for Ghardaia about 9.33 MWh/m/year, Béchar about 9.61 MWh/m/year and the best in Tamanrasset with about 10.28 MWh/m/year. The energy recovered from the parabolic trough solar field was used to supply the required energy for the thermochemical hydrogen production.

Third, hydrogen was discussed as a possible solution to storage of excess energy from solar energy source. The four steps cycle configuration of the copper-chlorine cycle was simulated to determine the performance of the cycle. A thermodynamic model was developed for relevant chemical reactions of Cu–Cl cycle for hydrogen production combined with solar parabolic trough collectors and testing its performance under Algerian conditions. The overall energy and exergy efficiencies of the Cu-Cl cycle were obtained as 40.42% and 92.25%, respectively, based upon the reference conditions. A parametric study was conducted to investigate the effects of several operating parameters such as heat gain from the solar PTC on the rate of hydrogen produced. A comparative assessment was carried out to study the effect of different Algerian locations and climates on hydrogen production rate from Cu–Cl. The maximum annually hydrogen production is obtained for the Southern Algerian region, for Ghardaia, Bechar and Tamanrasset with 84.87 Ton H_2, 87.44 Ton H_2 and 93.55 Ton H_2, respectively. For the Northern Algerian region, the best hydrogen production is observed for the Western site with 79.4 Ton H_2 for Oran.

2. Recommendations

The conclusions gathered from this thesis should encourage further research into the use of inexpensive but robust technology in solar collector fields. The economic benefit from employing these collectors could make solar thermal parabolic trough technology more competitive combined with thermochemical cycles of hydrogen production. With the design of several new solar thermal facilities underway in different areas of the World, the innovative collector field designs explored in this study could prove to be advantageous to these future plants in the Southern Algeria.

A complementary and recommended study is to provide the electricity needed to transport materials, operate pumps, compressors, electrochemical reaction and dryer steps using a solar power plant integrated to the solar thermal PTC. This combination is able to provide both heat and power to the hydrogen production thermochemical cycle which makes the installation led completely by solar thermal energy.

A preliminary study of a number of 100 collectors with 7.8 m in length to demonstrate the thermal model performance. A larger scale study is recommended to quantify the performance of this technology to a broader scale under Algerian conditions.

To more accurately and precisely evaluate the economics behind the parabolic trough and Cu-Cl themochemical technologies, it is recommended that an in depth cost analysis be conducted. Such an analysis should include manufacturing and installation costs, as well as forecasted maintenance costs.

REFERENCES

[1] UNITED NATIONS, A Global new green deal for Climate, Energy and Development, New York, 2009

[2] B. J. Thomas, L. Burnham, H. Kelly, A.K.N. Reddy, R. H. Williams, Renewable Energy: Sources for Fuels and Electricity, *edited by Washington, DC: Island Press*, 1993.

[3] C. W. Forsberg, Future hydrogen markets for large scale hydrogen production systems, *International Journal of Hydrogen*, Vol. 32, pp. 431-439, 2007.

[4] M. Balat, Potential importance of hydrogen as a future solution to environmental and transportation problems, *International Journal of Hydrogen*, Vol. 33, pp. 4013-4029, 2008.

[5] Y. Haseli, 'Analysis of Hydrodynamic Transport Phenomena in a Fluidized Bed for Thermochemical Hydrogen Production', *Master thesis*, *University of Ontario Institute of Technology*, *Canada*, 2008.

[6] International Energy Agency, *Key World Energy Statistics*, 2010.

[7] A. Khaled (Elhaj Yasin), 'Technical and Economic Performance of Parabolic Trough in Jordan', *Master thesis, University of Kassel, Germany*, 2012

[8] A. F. Ghoniem, "Needs, resources and climate change: Clean and efficient conversion technologies", *Progress in Energy and Combustion Science*, Vol. 37, pp. 15-51, 2011.

[9] P. Ekins, Hydrogen energy: economic and social challenges, *Earthscan, London, UK*, 2010.

[10] K. Schultz, K. Year, Thermochemical production of hydrogen from Solar and Nuclear energy In: *Stanford Climate change and Energy project, San Diego*. 1-44, 2003.

[11] T. E. Boukelia, M.S. Mecibah, Parabolic trough solar thermal power plant: Potential, and projects development in Algeria, *Renewable and Sustainable Energy Reviews*, Vol. 21, pp. 288–297, 2013

[12] T. E. Boukelia, M. S. Mecibah, Solid waste as renewable source of energy: current and future possibility in Algeria, *International Journal of Energy and Environmental Engineering*, (3:17), 2012.

[13] B. Bouchekima, D. Bechki, H. Bouguettaia, S. Boughali, T. M. Mohamed, The underground brackish waters in South Algeria: potential and viable resources. *Available from: http://www.World water congress 2008.Org/resource/authors/abs827_article.pdf*, [accessed in 2012].

[14] F. Tabkhi, 'Optimisation de Réseaux de Transport de Gaz', *Doctor thesis, Institut National Polytechnique de Toulouse, France*, 2007.

[15] Sonelgaz. Available from: *http://www.sonelgaz.dz*, [accessed in 2013].

[16] Sonatrach-Group. Available from: *http://www.sonatrach.com*, [accessed in 2013].

[17] G. Cohen, M. Skowronski, R. Cable, F. Morse, CH. Jaehne, D. Kearney et al., Solar thermal parabolic trough electric power plants for electric utilities in California PIER final project report. *California Energy Commission, Available on-line at: http://www.energy.ca.gov/2005publications/CEC-500-2005-175/CEC-500-2005-175.pdf*, [accessed in 2013].

[18] H. M. Steinhagen, F. Trieb, Concentrating solar power—a review of the Technology. *available From: http://www.dlr.de/Portaldata/41/Resources/dokumente/institut/system/publications/Concentrating_Solar_Power_Part_1.pdf*, [accessed in 2013].

[19] S. Ghandehariun, 'Thermal management of the copper-chlorine cycle for hydrogen production: Analytical and experimental investigation of heat recovery from molten salt', *Doctor thesis, University of Ontario Institute of Technology, Canada*, 2012.

[20] P. P. Edwards, V. I. Kuznetsov, W. I. F. David, N. P. Brandon, Hydrogen and fuel cells: Towards a sustainable energy future, *Energy Policy*, Vol. 36, pp. 4356-4362, 2008.

[21] E. Martinot, C. Dienst, L. Weiliang, C. Qimin, Reneable energy futures: Targets, scenarios, and pathways, *Annual Review of Environment and Resources*, Vol. 32, pp. 205-239, 2007.

[22] N. Lior, Energy resources and use: The present situation and possible paths to the future, *Energy*, Vol. 33, pp. 842-857, 2008.

[23] A. Verbruggen, Renewable and nuclear power: A common future?, *Energy Policy*, Vol. 36, pp. 4036-4047, 2008.

[24] A. Midilli, M. Ay, M. A. Rosen, On hydrogen and hydrogen energy strategies I: current status and needs, *Renewable and sustainable energy reviews*, Vol. 9, pp. 255-271, 2005.

[25] C. Winter, Hydrogen energy - Abundant, efficient, clean: A debate over the-energy-system-of-change, *International Journal of Hydrogen Energy*, Vol. 34, pp. 1-59, 2009.

[26] J. Nowotny, T. N. Veziroglu, Impact of hydrogen on the environment, *International Journal of Hydrogen Energy*, Vol. 36, pp. 3218-3224, 2011.

[27] P. Marioarty, D. Honnery, Hydrogen's role in an uncertain energy future, *International Journal of Hydrogen Energy*, Vol. 34, pp. 31-39, 2009.

[28] I. Dincer, M. A. Rosen, Sustainability aspects of hydrogen and fuel cell systems, *Energy for Sustanable Development*, Vol. 15, pp. 137-146, 2011.

[29] F. Barbir, PEM electrolysis for production of hydrogen from renewable energy sources, *Solar Energy*, Vol. 78, pp. 661-669, 2005.

[30] N.N. Ponomarev-Stepnoi, Nuclear-hydrogen power, *Atomic Energy*, Vol. 96, pp. 375–385, 2004.

[31] M. F. Orhan, I. Dincer, M. A. Rosen, Thermodynamic analysis of the copper production step in a copper–chlorine cycle for hydrogen production, *Thermochimica Acta*, Vol. 480, pp. 22–29, 2008.

[32] T. Alleau, A state-of-the-art of hydrogen and fuel cell technologies: diffusion perspectives and barriers, *The Economic Dynamics of Fuel Cell Technologies*, pp. 23-42, 2003.

[33] C. W. Forsberg, Hydrogen, nuclear energy, and the advanced nuclear reactor, *International Journal of Hydrogen Energy*, Vol. 28, pp. 1073-1081, 2003.

[34] J. M. Ogden, Prospects for building a hydrogen energy infrastructure, *Annual Review of Energy and Environment*, Vol. 24, pp. 227–279, 1999.

[35] L. S. Mapamba, 'Simulation of the copper-chlorine thermochemical cycle', *Master thesis, Noordwes-Universiteit Potchefstroomkampus, South Africa*, 2011.

[36] J. E. Funk, Thermochemical hydrogen production: past and present, *International Journal of Hydrogen Energy*, Vol. 26:3, pp. 185-190, 2001.

[37] Y. Haseli, I. Dincer, G.F. Naterer, Hydrodynamic gas–solid model of cupric chloride particles reacting with superheated steam for thermochemical hydrogen production, *Chemical Engineering Science*, Vol. 63, pp. 4596-4604, 2008.

[38] S. Saito, Nuclear energy and hydrogen production. The Japanese situation, *Policy Debate on the Potential Contribution of Nuclear Energy to Production of Hydrogen, OECD/NEA*, 15 October 2004.

[39] G.F. Naterer, K. Gabriel, Z.L. Wang, V.N. Daggupati, R. Gravelsins, Thermochemical hydrogen production with a copper–chlorine cycle. I: oxygen release from copper oxychloride decomposition, *International journal of hydrogen energy*, Vol. 33, pp. 5439–5450, 2008.

[40] B. Yildiz , M. S. Kazimi, Efficiency of hydrogen production systems using alternative nuclear energy technologies. *International Journal of Hydrogen Energy*, Vol. 31, pp. 77–92, 2006.

[41] FCHEA, Renewable Hydrogen Production Using Electrolysis, *Fuel Cell & Hydrogen Energy Association, Washington, DC 20036 (202) 261-1331*, 2013.(available at http://www.fchea.org/index.php?id=49).

[42] Johanna Ivy, Summary of Electrolytic Hydrogen Production, *Milestone Completion Report, National Renewable Energy Laboratory, NREL/MP-560-36734*, September 2004. (available at http://www.nrel.gov/publications/).

[43] I. Dincer, M. T. Balta, Potential thermochemical and hybrid cycles for nuclear-based hydrogen production, *International Journal of Energy Research*, Vol. 35, pp. 123-137, 2011.

[44] L. C. Brown, J. F. Funk, S. K. Showalter, Initial screening of thermochemical water splitting cycles for high efficiency generation of hydrogen fuels using nuclear power,

Lexington, Kentucky. General Atomics, 2000.

[45] C. H. Gooding, Analysis of alternative flowsheets for the hybrid chlorine cycle, *International Journal of Hydrogen Energy*, Vol. 34, pp. 4168-4178, 2009.

[46] M. B. Gorensek, W. A. Summers, Hybrid sulfur flowsheets using PEM electrolysis and a bayonet decomposition reactor, *International Journal of Hydrogen Energy*, Vol. 34, pp. 4097-4114, 2009.

[47] V. Law, J. C. Prindle, A. Lupulescu, W. Shensky, Aspen modelling of the three reaction version of the copper- chlorine thermochemical cycle for Hydrogen production from water, *New Orleans. Tulane University*, 2008.

[48] Z. L. Wang, G. F. Naterer, K. S. Gabriel, R. Gravelsins, V. N. Daggupati, Comparison of different copper-chlorine cycles for hydrogen production, *International Journal of Hydrogen Energy*, Vol. 34, pp. 3267-3276, 2009.

[49] Z. L. Wang, G. F. Naterer, K. S. Gabriel, R. Gravelsins, V. N. Daggupati, Comparison of sulfur–iodine and copper–chlorine thermochemical hydrogen production cycles, *International Journal of Hydrogen Energy*, Vol. 30, pp. 1-11, 2009.

[50] M. Serban, M. Lewis, J. Basco, Kinetic study of the hydrogen and oxygen production reactions in the copper-chloride thermochemical cycle, *AIChE Spring National Meeting, New Orleans, LA*, April 25–29, 2004.

[51] G. F. Naterer, S. Suppiah , M. Lewis, K. S. Gabriel, I. Dincer, M. A. Rosen, M. Fowler, G. Rizvi, E. B. Easton, B. M. Ikeda, M. H. Kaye, L. Lu, I. Pioro, P. Spekkens, P. Tremaine, J. Mostaghimi, J. Avsec, J. Jiang, Recent Canadian advances in nuclear-based hydrogen production and the thermochemical Cu-Cl cycle, *International Journal of Hydrogen Energy*, Vol. 34, pp. 2901–2917, 2009.

[52] M. A. Lewis, M. S. Ferrandon, D. F. Tatterson, P. Mathias, Evaluation of alternative thermochemical cycles-part III. Further development of the Cu-Cl cycle, *International Journal of Hydrogen Energy*, Vol. 34, pp. 4136–4145, 2009a.

[53] M. A. Lewis, J. G. Masin, The evaluation of alternative thermochemical cycles-part II. The down selection process, *International Journal of Hydrogen Energy*, Vol. 34, pp. 4125–4135, 2009b.

[54] V. N. Daggupati, G. F. Naterer, I. Dincer, Convective heat transfer and solid conversion of reacting particles in a copper (II) chloride fluidized bed, *Chemical Engineering Science*, Vol. 66, pp. 460–468, 2011.

[55] M. A. Lewis, M. Serban, J. K. Basco, Hydrogen production at <550°C using a low temperature thermochemical cycle, *ANS/ENS Exposition, New Orleans*, November 2003.

[56] V. N. Daggupati, G. F. Naterer, K. S. Gabriel, Diffusion of gaseous products through a particle surface layer in a fluidized bed reactor, *International Journal of Heat and Mass Transfer*, Vol. 53, pp. 2449-2458, 2010.

[57] M. F. Orhan, I. Dinçer, M. A. Rosen, Efficiency comparison of various design schemes for copper–chlorine (Cu-Cl) hydrogen production processes using Aspen Plus software, *Energy Conversion and Management*, Vol. 63, pp. 70-86, 2012.

[58] M. F. Orhan, I. Dincer, M. A. Rosen, Efficiency analysis of a hybrid copper–chlorine (Cu–Cl) cycle for nuclear-based hydrogen production, *Chemical Engineering Journal*, Vol. 155, pp. 132–137, 2009.

[59] M. F. Orhan, I. Dincer, M. A. Rosen, The oxygen production step of a copper–chlorine thermochemical water decomposition cycle for hydrogen production: Energy and exergy analyses, *Chemical Engineering Science*, Vol. 64, pp. 860-869, 2009.

[60] M. F. Orhan, I. Dincer, M. A. Rosen, Energy and exergy analyses of the fluidized bed of a copper–chlorine cycle for nuclear-based hydrogen production via thermochemical water decomposition, *chemical engineering research and design*, Vol. 87, pp. 684–694, 2009.

[61] M. F. Orhan, I. Dincer, G. F. Naterer, M. A. Rosen, Coupling of copper-chloride hybrid thermochemical water splitting cycle with a desalination plant for hydrogen production from nuclear energy, *International Journal of Hydrogen Energy*, Vol. 35, pp. 1560-1574, 2010.

[62] M. F. Orhan, I. Dincer, M. A. Rosen, Exergoeconomic analysis of a thermochemical copper–chlorine cycle for hydrogen production using specific exergy cost (SPECO) method, *Thermochimica Acta*, Vol. 497, pp. 60–66, 2010.

[63] M. T. Balta, I. Dincer, A. Hepbasli, Energy and exergy analyses of a new four-step

copper-chlorine cycle for geothermal-based hydrogen production, *Energy*, Vol. 35, pp. 3263-3272, 2010.

[64] G.F. Naterer, S. Suppiah , L. Stolberg , M. Lewis, Z. Wang, V. Daggupati, K. Gabriel, I. Dincer, M.A. Rosen, P. Spekkens, S.N. Lvov, M. Fowler, P. Tremaine, J. Mostaghimi, E.B. Easton, L. Trevani, G. Rizvi, B.M. Ikeda, M.H. Kaye, L. Lu, I. Pioro, W.R. Smith, E. Secnik, J. Jiang, J. Avsec, Canada's program on nuclear hydrogen production and the thermochemical Cu-Cl cycle, *International journal of hydrogen energy*, Vol. 35, pp. 10905-10926, 2010.

[65] G.D. Marin, Z. Wang, G.F. Naterer, K. Gabriel, Byproducts and reaction pathways for integration of the Cu-Cl cycle of hydrogen production, *International journal of hydrogen energy*, Vol. 36, pp. 13414-13424, 2011.

[66] M. F. Orhan, I. Dincer, M. A. Rosen, Design of systems for hydrogen production based on the Cu-Cl thermochemical water decomposition cycle: Configurations and performance, *International Journal of Hydrogen Energy*, Vol. 36, pp. 11309-11320, 2011.

[67] Rong Xu, Theodore F. Wiesner, Dynamic model of a solar thermochemical water-splitting reactor with integrated energy collection and storage, *International Journal of Hydrogen Energy*, Vol. 37, pp. 2210-2223, 2012.

[68] S. Ghandehariun, M. A. Rosen, G. F. Naterer, Z. Wang, Pinch analysis for recycling thermal energy in the Cu-Cl cycle, *International Journal of Hydrogen Energy* , Vol. 37, pp. 16535-16541, 2012.

[69] K. Pope, Z.L. Wang, G.F. Naterer, E. Secnik, Interfacial thermodynamics and X-ray diffraction of hydrolysis products in multiphase reacting flow of the Cu-Cl cycle, *International Journal of Hydrogen Energy* , Vol. 37, pp. 15011-15019, 2012.

[70] T.A.H. Ratlamwala, I. Dincer, Energy and exergy analyses of a Cu–Cl cycle based integrated system for hydrogen production, *Chemical Engineering Science*, Vol. 84, pp. 564–573, 2012.

[71] C. Zamfirescu, G.F. Naterer, I. Dincer, Photo-electro-chemical chlorination of cuprous chloride with hydrochloric acid for hydrogen production, *International Journal of Hydrogen Energy* , Vol. 37, pp. 9529-9536, 2012.

[72] T.A.H. Ratlamwala, I. Dincer, Performance assessment of solar-based integrated Cu–Cl systems for hydrogen production, *Solar Energy*, Vol. 95, pp. 345–356, 2013.

[73] M. Ozturk, I. Dincer, Thermodynamic analysis of a solar-based multi-generation system with hydrogen production, *Applied Thermal Engineering*, Vol. 51, pp.1235-1244, 2013.

[74] I. Dincer, T.A.H. Ratlamwala, Development of novel renewable energy based hydrogen production systems: A comparative study, *Energy Conversion and Management*, Vol. 72, pp. 77–87, 2013.

[75] Yildiz Kalinci, A. Hepbasli, I. Dincer, Performance assessment of hydrogen production from a solar-assisted biomass gasification system, *International Journal of Hydrogen Energy*, Vol. 38, pp. 6120-6129, 2013.

[76] L. Stoddard, J. Abiecunas J., R. O'Connell, Economic, Energy, and Environmental Benefits of Concentrating Solar Power in California, *National Renewable Energy Laboratory, Subcontract Report NREL/SR-550-39291*, April 2006

[77] G. Augsburger, 'Thermo-economic optimisation of large solar tower power plants', *Doctor thesis, École Polytechnique Fédérales de Lausanne, Switzerland*, 2013.

[78] O. Behar, A. Khellaf , K. Mohammedia, A review of studies on central receiver solar thermal power plants, *Renewable and Sustainable Energy Reviews*, Vol. 23, pp.12–39, 2013.

[79] G. Elsaket, ' Simulating the integrated solar combined cycle for power plants application in Libya', *Master thesis, Cranfield University, UK*, 2007.

[80] European Commission, European Research on Concentrated Solar Thermal Energy, *Brussels*, 2004. *available at: http://ec.europa.eu/research/energy/pdf/cst_en.pdf.*

[81] H. Alrobaei, Integrated Gas Turbine - Solar Power Plant, (2006a), *available at: http://www.energycentral.com/centers/knowledge/whitepapers/report.cfm?rid=102295*

[82] P. Schwarzbozl, R. Buck, C. Sugarmen, A. Ring, C. Marcos, P. Altwegg, and J. Enrile, Solar gas turbine systems: Design, cost and perspectives, *Solar Energy*, Vol. 80:10, pp. 1231-1240, (2006/10).

[83] J. Rheinlander, F. Lippke, Electricity and potable water from a solar tower power

plant, *Renewable Energy,* Vol. 14, No. 1-4, pp. 23-28, (1998/0).

[84] F. Trieb, Concentrating Solar Power Now, *DLR, Berlin,* Germany, 2006.

[85] DLR, Concentrating Solar Power Now, *D-11055, The Federal Ministry for the Environment, Nature Conservation and Nuclear Safety (BMU), Berlin*, Germany, 2002.

[86] V. Quaschning, Solar Thermal Power Plants, *Renewable Energy World,* Vol. 6, pp. 109-113, 2003.

[87] H. Price, E. Lupfert, D. Kearney, E. Zarza, G. Cohen, GeeR, et al., Advances in parabolic trough solar power technology, *Journal of Solar Energy Engineering, Transactions of the ASME,* Vol. 124, pp. 109–25, 2002.

[88] A. Ferna´ndez-Garcı´a, E. Zarza, L. Valenzuela, M. Pe´ rez, Parabolic-trough solar collectors and their applications, *Renewable and Sustainable Energy Reviews* , Vol. 14, pp. 1695–721, 2010.

[89] R. Kistner, H. W. Price, Financing solar thermal power plants, *Prepared for the Proceedings of the ASME Renewable and Advanced Energy Systems for the 21st Century Conference, Maui, Hawaii* , April 11-14, 1999.

[90] E. Jacobson, N. Ketjoy, S. Nathakaranakule. and W. Rakwichian, Solar parabolic trough simulation and application for a hybrid power plant in Thailand, *Science Asia*, Vol. 32:2, pp. 187-199, 2006.

[91] M. Günther, M. Joemann, S. Csambor, Parabolic Trough Technology, *Chapter 5, Advanced CSP Teaching Materials, enerMENA, DLR, Berlin,* Germany, *available at: http://www.dlr.de/sf/en/desktopdefault.aspx/tabid-7066/, (accessed 2013).*

[92] Flagso GmbH, *Brief Technical Description of the SKAL-ET Collector, available at: http://www.flagsol.com* (accessed 2007).

[93] U. Herrmann, B. Kelly, and H. Price, Two-tank molten salt storage for parabolic trough solar power plants, *Energy,* Vol. 29, No. 5-6, pp. 883-893, (2004/0).

[94] R. Hosseini, M. Soltani, and G. Valizadeh, Technical and economic assessment of the integrated solar combined cycle power plants in Iran, *Renewable Energy,* Vol. 30: 10, pp. 1541-1555, (2005/8).

[95] Greenpeace International, Solar Thermal Power 2020 -Exploiting the Heat from the Sun to Combat Climate Change, *ISBN:90-73361-82-6, Greenpeace and the European Solar Thermal Industry Association,* 2003.

[96] Siemens, The unrivaled benchmark in solar receiver efficiency, The Siemens UVAC 2010 is designed for outstanding thermal output. *available at: http://www.energy.siemens.com/co/en/power-generation/renewables/solar-power/concentrated-solar-power/receiver.htm,* (accessed 2011).

[97] J. Clark J, An analysis of the technical and economic performance of a parabolic trough concentrator for solar industrial process heat application, *Int J Heat Mass Trans*, Vol. 25:9, pp. 1427–38, 1982.

[98] W. Heidemann , K. Spindler, E. Hahne , Steady-state and transient temperature field in the absorber tube of a direct steam generating solar collector, *Int J Heat Mass Trans*, Vol. 35:3, pp.649–57, 1992.

[99] V. E. Dudley, J. G. Kolb, A. R. Mahoney, T. R. Mancini, C. W. Matthews, Sloan and D. Kearney, Test results: SEGS LS-2 solar collector, *Report of Sandia National Laboratories (SANDIA-94-1884),* 1994.

[100] A. Thomas, S. Thomas, Design data for the computation of thermal loss in the receiver of a parabolic trough concentrator, *Energy Convers Manage,* Vol. 35:7, pp. 555–68, 1994.

[101] S. Kalogirou, S. Lloyd, J. Ward , Modelling, optimisation and performance evaluation of a parabolic trough solar collector steam generation system, *Solar Energy*, Vol. 60:1, pp. 49-59, 1997.

[102] S. Odeh, G. Morrison, M. Behnia, Modelling of parabolic trough direct steam generation solar collectors, *Solar energy,* Vol. 62:6, pp. 395–406, 1998.

[103] R. Forristall, Heat transfer analysis and modeling of a parabolic trough solar receiver implemented in engineering equation solver, *National Renewable Energy Laboratory* (NREL), 2003.

[104] O. Garcı´a-Valladares , N. Velazquez, Numerical simulation of parabolic trough solar collector: improvement using counter flow concentric circular heat exchangers, *Int J Heat Mass Trans,* Vol. 52, N. 3–4, pp. 597–609, 2009.

[105] R. K. Kumar, K. S. Reddy, Thermal analysis of solar parabolic trough with porous disc receiver, *Applied Energy,* Vol. 86:9, pp. 1804-1812, 2009.

[106] Z. Cheng, Y. He, J. Xiao, Y. Tao, R. Xu, Three-dimensional numerical study of heat transfer characteristics in the receiver tube of parabolic trough solar collector, *Int Commun Heat Mass Trans,* Vol. 37:7, pp. 782–7, 2010.

[107] G. Gong, X. Huang, J. Wang, M. Hao, An optimized model and test of the China's first high temperature parabolic trough solar receiver, *Solar Energy,* Vol. 80:12, pp. 2230-2245, 2010.

[108] Y. He, J. Xiao, Z. Cheng, Y. A. Tao, A MCRT and FVM coupled simulation method for energy conversion process in parabolic trough solar collector, *Renew Energy,* Vol. 36, pp. 976–85, 2011.

[109] R. Vasquez Padilla, G. Demirkaya, D. Y. Goswami, E. Stefanakos, M. M. Rahman, Heat transfer analysis of parabolic trough solar receiver, *Applied Energy,* Vol. 88, pp. 5097-5110, 2011.

[110] Z. D. Cheng, Y. L. He, F. Q. Cui, R. J. Xu, Y. B. Tao, Numerical simulation of a parabolic trough solar collector with nonuniform solar flux conditions by coupling FVM and MCRT method, *Solar Energy,* Vol. 86:6, pp. 1770-1784, 2012.

[111] M. ZekiYılmazoglu, A. Durmaz, D. Baker , Solar repowering of Soma-A thermal power plant, *Energy Conversion and Management*, Vol. 64, pp. 232-237, 2012.

[112] A. Kalogirou Soteris, A detailed thermal model of a parabolic trough collector receiver, *Energy,* Vol. 48:1, pp. 298-306, 2012.

[113] P. Wang, D. Y. Liu, C. Xu, Numerical study of heat transfer enhancement in the receiver tube of direct steam generation with parabolic trough by inserting metal foams, *Applied Energy,* Vol. 102, pp. 449-460, 2013.

[114] Dongqiang Lei, Qiang Li, Zhifeng Wang, Jian Li, Jianbin Li, An experimental study of thermal characterization of parabolic trough receivers, *Energy Conversion and Management*, Vol. 69, pp. 107-115, 2013.

[115] Badescu V.; Dumitrescu A., New models to compute solar global hourly irradiation from point cloudiness, *Energy Conversion and Management*, Vol. 67, pp. 75–91,

2013.

[116] R.K. McGovern, W.J. Smith, Optimal concentration and temperatures of solar thermal power plants, *Energy Conversion and Management*, Vol. 60, pp. 226–232, 2012.

[117] T. Markvart, Solar electricity, *2nd ed. New York: John Wiley and Sons Inc*., 1996.

[118] A. Hossein Mousazadeh, A. Alireza Keyhani, B. Arzhang Javadi, A. Hossein Mobli, C. Karen Abrinia, B. Ahmad Sharifi, A review of principle and sun-tracking methods for maximizing solar systems output, *Renewable and Sustainable Energy Reviews*, Vol. 13, pp. 1800–1818, 2009.

[119] Robert W. Bialobrzeski, Optimization of a SEGS solar field for cost effective power output, *Master thesis of Science in Mechanical Engineering, Georgia Institute of Technology*, 2007.

[120] J. A. Duffie, W. A. Beckman, Solar engineering Transmittance of thermal processes, *2nd ed. Madison: John Wiley &Sons, Inc*., 1991.

[121] M. Iqbal, An introduction to solar radiation, *Canada: Academic Press. ISBN 0-12-373752-4*, 1983.

[122] Mehmet Yorukoglu, Ali Naci Celik, A critical review on the estimation of daily global solar radiation from sunshine duration, *Energy Conversion and Management*, Vol. 47, pp. 2441–2450, 2006.

[123] Sobel, D., Longitude - The True Story of a Lone Genius Who Solved the Greatest Scientific Problem of His Time, *Fourth Estate Ltd., London*, 1995.

[124] G. Notton , P. Poggi, C. Cristofari, Predicting hourly solar irradiations on inclined surfaces based on the horizontal measurements: Performances of the association of well-known mathematical models, *Energy Conversion and Management*, Vol. 47, pp. 816–1829, 2006.

[125] H. C. Hottel, A simple model for estimating the transmittance of direct solar radiation through clear atmospheres, *Solar Energy*, Vol. 18, USA, pp. 129-134, 1976.

[126] Germain Augsburger, Thermo-economic optimisation of large solar tower power plants, Doctor thesis of Science, *Ecole Polytechnique Fédérale de Lausanne, Suisse*, 2013.

[127] J. Radosavljević, A. Đorđević, Defining of the intensity of solar radiation on horizontal and oblique surfaces on earth, *Working and Living Environmental Protection*, Vol. 2:1, pp. 77 - 86, 2001.

[128] K. Scharmer and J. Greif, The European Solar radiation ATLAS, Vol. 1: *Fundamentals and maps, Les Presses de l'École des Mines, Paris*, 2000.

[129] L. O. Lamm, A New Analytic Expression for the Equation of Time, *Solar Energy*, Vol. 26:5, 465, 1981.

[130] M. Alata, M. A. Al-Nimr , Y. Qaroush, Developing a multipurpose sun tracking system using fuzzy control, *Energy Conversion and Management*, Vol. 46, pp. 1229–1245, 2005.

[131] PI. Cooper, The absorption of solar radiation in solar stills, *Solar Energy*, Vol. 12:3, pp. 313–31, 1969.

[132] J. C. Zimmerman, Sun pointing programs and their accuracy, *Sandia National Laboratories Report SAND81-0761*, September 1981.

[133] J. K. Linn, J. C. Zimmerman, A Method for calculating shadows cast by two-axis tracking solar collectors, *Report SAND79-0190, Sandia National Laboratories, Albuquerque NM*, November 1979.

[134] K. K. Chong, C. W. Wong, General formula for on-axis sun-tracking system and its application in improving tracking accuracy of solar collector, *Solar Energy*, Vol. 83, pp. 298–305, 2009.

[135] C. George Bakos, Design and construction of a two-axis Sun tracking system for parabolic trough collector (PTC) efficiency improvement, *Renewable Energy*, Vol. 31, pp. 2411–2421, 2006.

[136] H. R. Ghosh, N. C. Bhowmik, M. Hussain, Determining seasonal optimum tilt angles, solar radiations on variously oriented, single and double axis tracking surfaces at Dhaka, *Renewable Energy*, Vol. 35:6, pp.1292–1297, 2010.

[137] İnci TÜRK TOĞRUL, Estimation of solar radiation from angstroms coefficients by using geographical and meteorological data in Bishkek, Kyrgyzstan, Isı Bilimi ve Tekniği Dergisi, *J. of Thermal Science and Technology*, Vol. 29:2, pp. 99-108, 2009.

[138] Maria Eugênia Vieira da Silva, Alex Sandro de Araújo, and Marcelo Ricardo Queiroz Medeiros, Adjustment of the Clear Sky Coefficients for the Transmission of Solar Radiation under the Ambient Conditions in Fortaleza, *RIO 02 - World Climate & Energy Event*. January 6-11, 2002.

[139] Nalin K. Gautam and N. D. Kaushika, A Model for the Estimation of Global Solar Radiation Using Fuzzy Random Variables**,** *Centre for Energy Studies, Indian Institute of Technology, Delhi, India* 2002.

[140] M. Ouagued, A. Khellaf, L. Loukarfi, Estimation of the temperature, heat gain and heat loss by solar parabolic trough collector under Algerian climatic using different thermal oil, *Energy Conversion and Management*, Vol.75, pp. 191–201, 2013.

[141] National Geographic Society, W*ashinton D. C., available at: http://media.maps101.com/SUB/ng_maps/ngxx_algeria.gif*, (accessible 2013).

[142] S. A. Kalogirou, Solar thermal collectors and applications, *Prog. Energy Combust. Sci.*, Vol. 30:3, pp. 231–295, 2004.

[143] H. Price, Guidelines for Reporting Parabolic Trough Solar Electric System Performance, *NREL/CP-550-22729. Golden, CO: National Renewable Energy Laboratory,* 1997.

[144] DQ. Lei, ZF. Wang, J. Li, The calculation and analysis of glass-to-metal sealing stress in solar absorber tube, *Renew Energy*, Vol.35:2, pp. 405–11, 2010.

[145] M. Ouagued, A. Khellaf, Simulation of the Temperature and Heat Gain by Solar Parabolic Trough Collector in Algeria, *World Academy of Science, Engineering and Technology*, Vol. 67, pp. 802-808, 2012.

[146] N. ESKIN,Transient performance analysis of cylindrical parabolic concentrating collectors and comparison with experimental results, *Energy Conversion and Management*, Vol. 40, pp. 175-191, 1999.

[147] Sefa, I., Demirtas, M., Olak, I., Application of one-axis sun tracking system, *Energy Conversion and Management*, Vol. 50, pp. 2709–2718, 2009.

[148] F. Incropera, D. DeWitt, Fundamentals of Heat and Mass Transfer, *sixth Edition*, 1990.

[149] V. Gnielinski, New Equations for Heat and Mass Transfer in Turbulent Pipe and Channel Flow, *International Chemical Engineering*, Vol. 16:2, pp. 359–363, 1976.

[150] R. Siegel, J. Howell, Thermal Radiation Heat Transfer, *Fourth Edition. New York, NY: Taylor & Francis*, 2002.

[151] S.W. Churchill and H.H.S. Chu, Correlating equations for laminar and turbulent free convection from a horizontal cylinder, *Int. J. Heat Mass Transfer*, Vol. 18:9, pp.1049–1053, 1975.

[152] S. Quoilin, Concentrator Solar Power Plants, (en Français), *Faculty of Applied Sciences, University of Liège*, 2007.

[153] http://www.celsius-process.com/outils.php, 2013.

[154] M.J. Moran, H.N. Shapiro, Fundamentals of Engineering Thermodynamics, *sixth ed. Wiley, USA*, 2007.

[155] G.F. Naterer, S. Suppiah, L. Stolberg, M. Lewis, Z. Wang, I. Dincer, M.A. Rosen, K. Gabriel, E. Secnik, E.B. Easton, I. Pioro, S. Lvov, J. Jiang, J. Mostaghimi, B.M. Ikeda, G. Rizvi, L. Lu, A. Odukoya, P. Spekkens, M. Fowler, J. Avsec, Progress of international hydrogen production network for the thermochemical CueCl cycle, *International journal o f hydrogen energy*, Vol.38, pp.740-759, 2013.

[156] I. Dincer, MA. Rosen, Exergy: energy, *environment and sustainable development, London: Elsevier, UK*, 2007

[157] Andreas Heintz, Solar energy combined with chemical reactive systems for the production and storage of sustainable energy. A review of thermodynamic principles, *J. Chem. Thermodynamics*, Vol. 46, pp. 99-108, 2012.

[158] Rong Xu, Theodore F. Wiesner, Dynamic model of a solar thermochemical water-splitting reactor with integrated energy collection and storage, *International journal of hydrogen energy*, Vol. 37, pp. 2210-2223, 2012.

[159] Michele A. Lewis, Joseph G. Masin, Patrick A. O'Hare, Evaluation of alternative thermochemical cycles, Part I: The methodology, *International journal of hydrogen energy*, Vol. 34, pp. 4115–4124, 2009.

[160] Rachael Elder, Ray Allen, Nuclear heat for hydrogen production: Coupling a very

high/high temperature reactor to a hydrogen production plant, Progress in Nuclear Energy, Vol. 51, pp. 500–525, 2009.

Appendices

Appendix.1. Climatological data of the Algerian studied sites

Table A.1. Monthly mean temperature and wind speed at Oran

Month	Monthly average temperature (K)	Monthly average wind speed, 10m above the ground (m/s)
January	283.35	4
February	284.15	4
March	286.45	4
April	288.55	5
May	291.45	5
June	294.95	5
July	297.65	5
August	298.25	4
September	296.05	4
October	291.55	4
November	287.35	3
December	284.25	3

Table A.2. Monthly mean temperature and wind speed at Algiers

Month	Monthly average temperature (K)	Monthly average wind speed, 10m above the ground (m/s)
January	285.35	3
February	285.95	3
March	287.35	5
April	289.55	5
May	292.4	3
June	295.05	5
July	297.85	3
August	298.65	3
September	297.05	3
October	293.45	3
November	289.25	3
December	286.15	3

Table A.3. Monthly mean temperature and wind speed at Annaba

Month	Monthly average temperature (K)	Monthly average wind speed, 10m above the ground (m/s)
January	284.15	4
February	284.65	4
March	285.65	4
April	287.75	4
May	290.95	5
June	294.35	4
July	297.75	4
August	298.05	3
September	295.95	4
October	292.75	4
November	288.55	4
December	285.35	4

Table A.4. Monthly mean temperature and wind speed at Ghardaia

Month	Monthly average temperature (K)	Monthly average wind speed, 10m above the ground (m/s)
January	283.65	3
February	285.95	3
March	288.95	3
April	293.25	4
May	297.85	4
June	303.45	4
July	306.55	3
August	305.85	3
September	301.05	3
October	295.55	3
November	288.15	3
December	284.25	3

Table A.5. Monthly mean temperature and wind speed at Bechar

Month	Monthly average temperature (K)	Monthly average wind speed, 10m above the ground (m/s)
January	282.85	4
February	285.75	4
March	289.16	5
April	292.85	6
May	297.55	6
June	302.75	6
July	306.65	5
August	306.15	5
September	301.15	5
October	294.35	4
November	288.05	4
December	283.15	3

Table A.6. Monthly mean temperature and wind speed at Tamanrasset

Month	Monthly average temperature (K)	Monthly average wind speed, 10m above the ground (m/s)
January	286.05	4
February	288.55	4
March	292.45	5
April	295.55	4
May	299.65	4
June	302.35	4
July	301.45	5
August	301.55	5
September	299.95	4
October	295.75	3
November	290.85	3
December	286.95	3

Appendix.2. Solar PTC specification used in the model validation

Table A.7. Solar PTC specification used in the model validation [99,152]

Receiver length	7.80 m
Collector width	5 m
Focal distance	1.84
Receiver internal diameter	0.066 m
Receiver external diameter	0.07 m
Receiver thermal conductivity	54 w/m.K
Glass cover internal diameter	0.115 m
Glass cover internal diameter	0.109 m
Concentration ratio	22.42
Receiver absorptance	0.906
Receiver emittance	0.14
Glass cover transmittance	0.95
Heat transfer fluid flow rate	3.10^{-4} m^3/s
Annulus pressure	0.01 mmHg
Density of the absorber selective coating	$8.02 \cdot 10^3$ kg/m^3
Absorber specific heat	500 J/kg.K
Density of Pyrex glass envelope	$2.23 \cdot 10^3 kg/m^3$
Glass envelope specific heat	1090 J/kg.K
HCE Shadowing	0.974
Tracking Error	0.994
Geometry Error (mirror alignment)	0.98
Reflected surface reflectivity	0.93
Clean Mirror Reflectance	0.935
Glass envelope emittance	0.86
Glass envelope absorptance	0.02
HTF initial temperature	473K

Appendix.3. Enthalpy and entropy changes of substances in Cu-Cl cycle

A.3.1. HCl Production step

For $CuOCuCl_2$(s):

$$(h-h_0)_{CuOCuCl2} = 99.23243\cdot (TI-T0) + \frac{21.62162}{2000}\cdot (TI^2-T0^2)$$

$$(s-s_0)_{CuOCuCl2} = 99.23243\cdot Ln(TI/T0) + \frac{21.62162}{1000}\cdot \left(TI \quad -T0 \quad\right)$$

For the $CuCl_2$(s):

$$\begin{aligned}(h-h_0)_{CuCl2} = {} & 70.21882\cdot (TI-T0) + 23.36132\cdot \frac{10^{-3}}{2}\cdot (TI^2-T0^2)\\ & - 14.86876\cdot \frac{10^{-6}}{3}\cdot (TI^3-T0^3) \quad + 4.053899\cdot \frac{10^{-9}}{4}\cdot (TI^4-T0^4)\\ & - 0.366203\cdot 10^6\cdot \left(\frac{1}{TI}-\frac{1}{T0}\right)\end{aligned}$$

$$\begin{aligned}(s-s)_{CuCl2} = {} & 70.21882\cdot ln(TI/T0) + 23.36132\cdot 10^{-3}\cdot \left(TI \quad -T0 \quad\right)\\ & - 14.86876\cdot \frac{10^{-6}}{2}\cdot (TI^2-T0^2) \quad + 4.053899\cdot \frac{10^{-9}}{3}\cdot (TI^3-T0^3)\\ & - 0.366203\cdot \frac{10^6}{2}\cdot \left(\frac{1}{TI^2}-\frac{1}{T0^2}\right)\end{aligned}$$

For H2O(g):

$$\begin{aligned}(h-h_0)_{H2O} = {} & 203.606\cdot (Tv-T0) + 1523.29\cdot \frac{10^{-3}}{2}\cdot (Tv^2-T0^2)\\ & - 3196.413\cdot \frac{10^{-6}}{3}\cdot (Tv^3-T0^3) \quad + 2474.544\cdot \frac{10^{-9}}{4}\cdot (Tv^4-T0^4)\\ & - 3.855326.10^6\cdot \left(\frac{1}{Tv}-\frac{1}{T0}\right) + Lv(H20) + 30.092\cdot (TI-Tv)\\ & + 6.832514\cdot \frac{10^{-3}}{2}\cdot (TI^2-Tv^2) - 6.793435\cdot \frac{10^{-6}}{3}\cdot (TI^3-Tv^3)\\ & - 2.53448\cdot \frac{10^{-9}}{4}\cdot (TI^4-Tv^4) - 0.082139\cdot 10^6\cdot \left(\frac{1}{TI}-\frac{1}{Tv}\right)\end{aligned}$$

$$\begin{aligned}(s-s_0)_{H2O} = {} & 203.606\cdot Ln(Tv/T0) + 1523.29\cdot 10^{-3}\cdot \left(Tv \quad -T0 \quad\right)\\ & - 3196.413\cdot \frac{10^{-6}}{2}\cdot (Tv^2-T0^2) \quad + 2474.544\cdot \frac{10^{-9}}{3}\cdot (Tv^3-T0^3)\\ & - 3.855326\cdot \frac{10^6}{2}\cdot \left(\frac{1}{Tv^2}-\frac{1}{T0^2}\right) + \frac{Lv(H20)}{Tv} + 30.092\cdot Ln(TI/Tv)\\ & + 6.832514\cdot 10^{-3}\cdot \left(TI \quad -Tv \quad\right) - 6.793435\cdot \frac{10^{-6}}{2}\cdot (TI^2-Tv^2)\\ & - 2.53448\cdot \frac{10^{-9}}{3}\cdot (TI^3-Tv^3) - 0.082139\cdot \frac{10^6}{2}\cdot \left(\frac{1}{TI^2}-\frac{1}{Tv^2}\right)\end{aligned}$$

For HCl(g):

$$(h - h_0)_{HCl} = 32.12392 \cdot (TI - T0) - 13.45805 \cdot \frac{10^{-3}}{2} \cdot (TI^2 - T0^2) + 19.86852 \cdot \frac{10^{-6}}{3} \cdot (TI^3 - T0^3) \quad - 6.853936 \cdot \frac{10^{-9}}{4} \cdot (TI^4 - T0^4) + 0.049672 \cdot 10^6 \cdot \left(\frac{1}{TI} - \frac{1}{T0}\right)$$

$$(s - s_0)_{HCl} = 32.12392 \cdot ln(TI/T0) - 13.45805 \cdot 10^{-3} \cdot (TI \quad - T0 \quad) + 19.86852 \cdot \frac{10^{-6}}{2} \cdot (TI^2 - T0^2) \quad - 6.853936 \cdot \frac{10^{-9}}{3} \cdot (TI^3 - T0^3) + 0.049672 \cdot \frac{10^6}{2} \cdot \left(\frac{1}{TI^2} - \frac{1}{T0^2}\right)$$

A.3.2. O2 production step of Cu-Cl Cycle

For CuOCuCl2(s):

$$(h-h_0)_{CuOCuCl2} = 99.23243\cdot (TII - T0) + \frac{21.62162}{2000}\cdot (TII^2 - T0^2)$$

$$(s-s_0)_{CuOCuCl2} = 99.23243\cdot Ln(TII/T0) + \frac{21.62162}{1000}\cdot \left(TII \quad - T0 \quad\right)$$

For CuCl(l):

$$\begin{aligned}(h-h_0)_{CuCl} = {} & 75.271\cdot (Tf - T0) - 26.83212\cdot \frac{10^{-3}}{2}\cdot (Tf^2 - T0^2) \\ & + 25.69156\cdot \frac{10^{-6}}{3}\cdot (Tf^3 - T0^3) \quad - 7.357982\cdot \frac{10^{-9}}{4}\cdot (Tf^4 - T0^4) \\ & + 1.847747\cdot 10^6\cdot \left(\frac{1}{Tf} - \frac{1}{T0}\right) + Lf(CuCl) + 66.944\cdot (TII - Tf) \\ & - 3.699628\cdot \frac{10^{-13}}{2}\cdot (TII^2 - Tf^2) + 2.166748\cdot \frac{10^{-16}}{3}\cdot (TII^3 - Tf^3) \\ & - 3.90046\cdot \frac{10^{-20}}{4}\cdot (TII^4 - Tf^4) + 9.813196\cdot 10^{-6}\cdot \left(\frac{1}{TII} - \frac{1}{Tf}\right)\end{aligned}$$

$$\begin{aligned}(s-s_0)_{CuCl} = {} & 75.271\cdot Ln(Tf/T0) - 26.83212\cdot 10^{-3}\left(Tf \quad - T0 \quad\right) \\ & + 25.69156\cdot \frac{10^{-6}}{2}\cdot (Tf^2 - T0^2) \quad - 7.357982\cdot \frac{10^{-9}}{3}\cdot (Tf^3 - T0^3) \\ & + 1.847747\cdot \frac{10^6}{2}\cdot \left(\frac{1}{Tf^2} - \frac{1}{T0^2}\right) + \frac{Lf(CuCl)}{Tf} + 66.944\cdot Ln(TII/Tf) \\ & - 3.699628\cdot 10^{-13}\left(TII \quad - Tf \quad\right) + 2.166748\cdot \frac{10^{-16}}{2}\cdot (TII^2 - Tf^2) \\ & - 3.90046\cdot \frac{10^{-20}}{3}\cdot (TII^3 - Tf^3) + 9.813196\cdot \frac{10^{-6}}{2}\cdot \left(\frac{1}{TII^2} - \frac{1}{Tf^2}\right)\end{aligned}$$

For O2(g):

$$\begin{aligned}(h-h_0)_{O2} = {} & 31.32234\cdot (TO2 - T0) - 20.2353\cdot \frac{10^{-3}}{2}\cdot (TO2^2 - T0^2) \\ & + 57.86644\cdot \frac{10^{-6}}{3}\cdot (TO2^3 - T0^3) \quad - 36.50624\cdot \frac{10^{-9}}{4}\cdot (TO2^4 - T0^4) \\ & + 0.007374\cdot 10^6\cdot \left(\frac{1}{TO2} - \frac{1}{T0}\right) + 30.03235\cdot (TII - TO2) \\ & + 8.772972\cdot \frac{10^{-3}}{2}\cdot (TII^2 - TO2^2) - 3.988133\cdot \frac{10^{-6}}{3}\cdot (TII^3 - TO2^3) \\ & + 0.788313\cdot \frac{10^{-9}}{4}\cdot (TII^4 - TO2^4) + 0.741599\cdot 10^6\cdot \left(\frac{1}{TII} - \frac{1}{TO2}\right)\end{aligned}$$

$$
\begin{aligned}
(s - s_0)_{CuCl} = {} & 31.32234 \cdot Ln\left(\frac{TO2}{T0}\right) - 20.2353 \cdot 10^{-3} \cdot \left(TO2 \quad - T0 \quad\right) \\
& + 57.86644 \cdot \frac{10^{-6}}{2} \cdot (TO2^2 - T0^2) \quad - 36.50624 \cdot \frac{10^{-9}}{3} \cdot (TO2^3 - T0^3) \\
& + 0.007374 \cdot \frac{10^{6}}{2} \cdot \left(\frac{1}{TO2^2} - \frac{1}{T0^2}\right) + 30.03235 \cdot Ln\left(\frac{TII}{TO2}\right) \\
& + 8.772972 \cdot 10^{-3} \cdot \left(TII \quad - TO2 \quad\right) - 3.988133 \cdot \frac{10^{-6}}{2} \cdot (TII^2 - TO2^2) \\
& + 0.788313 \cdot \frac{10^{-9}}{3} \cdot (TII^3 - TO2^3) + 0.741599 \cdot \frac{10^{6}}{2} \cdot \left(\frac{1}{TII^2} - \frac{1}{TO2^2}\right)
\end{aligned}
$$

Appendix.4. Energy and exergy balances of heat exchangers in Cu-Cl cycle

A.4.1. Heat exchanger HE1

$$Q_{HE1} = n_{H20}\Big[203.606\cdot (Tv - T0) + 1523.29\cdot \frac{10^{-3}}{2}\cdot (Tv^2 - T0^2) - 3196.413\cdot \frac{10^{-6}}{3}\cdot (Tv^3 - T0^3) \quad + 2474.544\cdot \frac{10^{-9}}{4}\cdot (Tv^4 - T0^4) - 3.855326\cdot 10^6\cdot \left(\frac{1}{Tv} - \frac{1}{T0}\right) + Lv(H20) + 30.092\cdot (TI - Tv) + 6.832514\cdot \frac{10^{-3}}{2}\cdot (TI^2 - Tv^2) - 6.793435\cdot \frac{10^{-6}}{3}\cdot (TI^3 - Tv^3) - 2.53448\cdot \frac{10^{-9}}{4}\cdot (TI^4 - Tv^4) - 0.082139\cdot 10^6\cdot \left(\frac{1}{TI} - \frac{1}{Tv}\right)\Big]$$

$$Ex_{HE1} = n_{H20}\Big[203.606\cdot (Tv - Tin) + 1523.29\cdot \frac{10^{-3}}{2}\cdot (Tv^2 - Tin^2) - 3196.413\cdot \frac{10^{-6}}{3}\cdot (Tv^3 - Tin^3) \quad + 2474.544\cdot \frac{10^{-9}}{4}\cdot (Tv^4 - Tin^4) - 3.855326\cdot 10^6\cdot \left(\frac{1}{Tv} - \frac{1}{Tin}\right) + Lv(H20) + 30.092\cdot (TI - Tv) + 6.832514\cdot \frac{10^{-3}}{2}(TI^2 - Tv^2) - 6.793435\cdot \frac{10^{-6}}{3}\cdot (TI^3 - Tv^3) - 2.53448\cdot \frac{10^{-9}}{4}\cdot (TI^4 - Tv^4) - 0.082139\cdot 10^6\cdot \left(\frac{1}{TI} - \frac{1}{Tv}\right)\Big]\cdot \left(1 - \frac{T0}{TI}\right)$$

A.4.2. Heat exchanger HE2

$$Q_{HE2} = n_{CuCl2}\Big[70.21882\cdot (TI - TIII) + 23.36132\cdot \frac{10^{-3}}{2}\cdot (TI^2 - TIII^2) - 14.86876\cdot \frac{10^{-6}}{3}\cdot (TI^3 - TIII^3) \quad + 4.053899\cdot \frac{10^{-9}}{4}\cdot (TI^4 - TIII^4) - 0.366203\cdot 10^6\cdot \left(\frac{1}{TI} - \frac{1}{TIII}\right)\Big]$$

$$Ex_{HE2} = n_{CuCl2}\Big[70.21882\cdot (TI - TIII) + 23.36132\cdot \frac{10^{-3}}{2}\cdot (TI^2 - TIII^2) - 14.86876\cdot \frac{10^{-6}}{3}\cdot (TI^3 - TIII^3) \quad + 4.053899\cdot \frac{10^{-9}}{4}\cdot (TI^4 - TIII^4) - 0.366203\cdot 10^6\cdot \left(\frac{1}{TI} - \frac{1}{TIII}\right)\Big]\cdot \left(1 - \frac{T0}{TI}\right)$$

A.4.3. Heat exchanger HE3

$$Q_{HE3} = n_{CuOCuCl2}\left[99.23243\cdot (TII - TI) + \frac{21.62162}{2000}\cdot (TII^2 - TI^2)\right]$$

$$Ex_{HE3} = n_{CuOCuCl2}\left[99.23243\cdot (TII - TI) + \frac{21.62162}{2000}\cdot (TII^2 - TI^2)\right]\cdot \left(1 - \frac{T0}{TII}\right)$$

A.4.4. Heat exchanger HE4

$$\begin{aligned} Q_{HE4} = {} & 32.12392\cdot (TIV - TI) - 13.45805\cdot \frac{10^{-3}}{2}\cdot (TIV^2 - TI^2) \\ & + 19.86852\cdot \frac{10^{-6}}{3}\cdot (TIV^3 - TI^3) \quad - 6.853936\cdot \frac{10^{-9}}{4}\cdot (TIV^4 - TI^4) \\ & + 0.049672\cdot 10^6\cdot \left(\frac{1}{TIV} - \frac{1}{TI}\right) \end{aligned}$$

$$\begin{aligned} Ex_{HE4} = n_{HCl}\Bigg[& 32.12392\cdot (TIV - TI) - 13.45805\cdot \frac{10^{-3}}{2}\cdot (TIV^2 - TI^2) \\ & + 19.86852\cdot \frac{10^{-6}}{3}\cdot (TIV^3 - TI^3) \quad - 6.853936\cdot \frac{10^{-9}}{4}\cdot (TIV^4 - TI^4) \\ & + 0.049672\cdot 10^6\cdot \left(\frac{1}{TIV} - \frac{1}{TI}\right)\Bigg]\cdot \left(1 - \frac{T0}{TIV}\right) \end{aligned}$$

A.4.5. Heat exchanger HE5

$$\begin{aligned} Q_{HE5} = {} & n_{H2O}\Bigg[203.606\cdot (TIII - TIV) + 1523.29\cdot \frac{10^{-3}}{2}\cdot (TIII^2 - TIV^2) \\ & - 3196.413\cdot \frac{10^{-6}}{3}\cdot (TIII^3 - TIV^3) \quad + 2474.544\cdot \frac{10^{-9}}{4}\cdot (TIII^4 - TIV^4) \\ & - 3.855326\cdot 10^6\cdot \left(\frac{1}{TIII} - \frac{1}{TIV}\right)\Bigg] \\ & + n_{CuCl2}\Bigg[70.21882\cdot (TIII - TIV) + 23.36132\cdot \frac{10^{-3}}{2}\cdot (TIII^2 - TIV^2) \\ & - 14.86876\cdot \frac{10^{-6}}{3}\cdot (TIII^3 - TIV^3) \quad + 4.053899\cdot \frac{10^{-9}}{4}\cdot (TIII^4 - TIV^4) \\ & - 0.366203\cdot 10^6\cdot \left(\frac{1}{TIII} - \frac{1}{TIV}\right)\Bigg] \end{aligned}$$

$$Ex_{HE5} = n_{H2O}\left[203.606\cdot (TIII - TIV) + 1523.29\cdot \frac{10^{-3}}{2}\cdot (TIII^2 - TIV^2)\right.$$
$$- 3196.413\cdot \frac{10^{-6}}{3}\cdot (TIII^3 - TIV^3) \quad + 2474.544\cdot \frac{10^{-9}}{4}\cdot (TIII^4 - TIV^4)$$
$$\left. - 3.855326\cdot 10^6\cdot \left(\frac{1}{TIII} - \frac{1}{TIV}\right)\right]\cdot \left(1 - \frac{T0}{TIII}\right)$$
$$+ n_{CuCl2}\left[70.21882\cdot (TIII - TIV) + 23.36132\cdot \frac{10^{-3}}{2}\cdot (TIII^2 - TIV^2)\right.$$
$$- 14.86876\cdot \frac{10^{-6}}{3}\cdot (TIII^3 - TIV^3) \quad + 4.053899\cdot \frac{10^{-9}}{4}\cdot (TIII^4 - TIV^4)$$
$$\left. - 0.366203\cdot 10^6\cdot \left(\frac{1}{TIII} - \frac{1}{TIV}\right)\right]\cdot \left(1 - \frac{T0}{TIII}\right)$$

A.4.6. Heat exchanger HE6

$$Q_{HE6} = n_{H2O}\left[203.606\cdot (TIV - TIII) + 1523.29\cdot \frac{10^{-3}}{2}\cdot (TIV^2 - TIII^2)\right.$$
$$- 3196.413\cdot \frac{10^{-6}}{3}\cdot (TIV^3 - TIII^3) \quad + 2474.544\cdot \frac{10^{-9}}{4}\cdot (TIV^4 - TIII^4)$$
$$\left. - 3.855326\cdot 10^6\cdot \left(\frac{1}{TIV} - \frac{1}{TIII}\right)\right]$$

$$Ex_{HE6} = n_{H2O}\left[203.606\cdot (TIV - TIII) + 1523.29\cdot \frac{10^{-3}}{2}\cdot (TIV^2 - TIII^2)\right.$$
$$- 3196.413\cdot \frac{10^{-6}}{3}\cdot (TIV^3 - TIII^3) \quad + 2474.544\cdot \frac{10^{-9}}{4}\cdot (TIV^4 - TIII^4)$$
$$\left. - 3.855326\cdot 10^6\cdot \left(\frac{1}{TIV} - \frac{1}{TIII}\right)\right]\cdot \left(1 - \frac{T0}{TIV}\right)$$

A.4.7. Heat exchanger HE7

$$Q_{HE7} = n_{CuCl}\left[66.944\cdot (Tf - TII) - 3.699628\cdot \frac{10^{-13}}{2}\cdot (Tf^2 - TII^2)\right.$$
$$+ 2.166748\cdot \frac{10^{-16}}{3}\cdot (Tf^3 - TII^3) \quad - 3.90046\cdot \frac{10^{-20}}{4}\cdot (Tf^4 - TII^4)$$
$$+ 9.813196\cdot 10^{-6}\cdot \left(\frac{1}{Tf} - \frac{1}{TII}\right) - Lf(CuCl) + 75.271\cdot (TIV - Tf)$$
$$- 26.83212\cdot \frac{10^{-3}}{2}\cdot (TIV^2 - Tf^2) + 25.69156\cdot \frac{10^{-6}}{3}\cdot (TIV^3 - Tf^3)$$
$$\left. - 7.357982\cdot \frac{10^{-9}}{4}\cdot (TIV^4 - Tf^4) + 1.847747\cdot 10^6\cdot \left(\frac{1}{TIV} - \frac{1}{Tf}\right)\right]$$

$$Ex_{HE7} = n_{CuCl}\Bigg[66.944\cdot (Tf - TII) - 3.699628\cdot \frac{10^{-13}}{2}\cdot (Tf^2 - TII^2) + 2.166748\cdot \frac{10^{-16}}{3}\cdot (Tf^3 - TII^3) \quad - 3.90046\cdot \frac{10^{-20}}{4}\cdot (Tf^4 - TII^4) + 9.813196\cdot 10^{-6}\cdot \left(\frac{1}{Tf} - \frac{1}{TII}\right) - Lf(CuCl) + 75.271\cdot (TIV - Tf) - 26.83212\cdot \frac{10^{-3}}{2}\cdot (TIV^2 - Tf^2) + 25.69156\cdot \frac{10^{-6}}{3}\cdot (TIV^3 - Tf^3) - 7.357982\cdot \frac{10^{-9}}{4}\cdot (TIV^4 - Tf^4) + 1.847747\cdot 10^6\cdot \left(\frac{1}{TIV} - \frac{1}{Tf}\right)\Bigg]\cdot \left(1 - \frac{T0}{TIV}\right)$$

A.4.8. Heat exchanger HE8

$$Q_{HE8} = n_{O2}\Bigg[30.03235\cdot (TO2 - TII) + 8.772972\cdot \frac{10^{-3}}{2}\cdot (TO2^2 - TII^2) - 3.988133\cdot \frac{10^{-6}}{3}\cdot (TO2^3 - TII^3) \quad + 0.788313\cdot \frac{10^{-9}}{4}\cdot (TO2^4 - TII^4) + 0.741599\cdot 10^6\cdot \left(\frac{1}{TO2} - \frac{1}{TII}\right) + 31.32234\cdot (T0 - TO2) - 20.2353\cdot \frac{10^{-3}}{2}\cdot (T0^2 - TO2^2) + 57.86644\cdot \frac{10^{-6}}{3}\cdot (T0^3 - TO2^3) - 36.50624\cdot \frac{10^{-9}}{4}\cdot (T0^4 - TO2^4) + 0.007374\cdot 10^6\cdot \left(\frac{1}{T0} - \frac{1}{TO2}\right)\Bigg]$$

$$Ex_{HE8} = n_{O2}\Bigg[30.03235\cdot (TO2 - TII) + 8.772972\cdot \frac{10^{-3}}{2}\cdot (TO2^2 - TII^2) - 3.988133\cdot \frac{10^{-6}}{3}\cdot (TO2^3 - TII^3) \quad + 0.788313\cdot \frac{10^{-9}}{4}\cdot (TO2^4 - TII^4) + 0.741599\cdot 10^6\cdot \left(\frac{1}{TO2} - \frac{1}{TII}\right) + 31.32234\cdot (Tex - TO2) - 20.2353\cdot \frac{10^{-3}}{2}\cdot (Tex^2 - TO2^2) + 57.86644\cdot \frac{10^{-6}}{3}\cdot (Tex^3 - TO2^3) - 36.50624\cdot \frac{10^{-9}}{4}\cdot (Tex^4 - TO2^4) + 0.007374\cdot 10^6\cdot \left(\frac{1}{Tex} - \frac{1}{TO2}\right)\Bigg]\cdot \left(1 - \frac{T0}{Tex}\right)$$